

Reduction of Whole-Body Vibration transmitted to test drivers performing complete vehicle durability testing at Hällered Proving Ground

Master's thesis in Applied Mechanics

AREZ MOHIDEEN

MASTER'S THESIS IN APPLIED MECHANICS

Reduction of Whole-Body Vibration transmitted to test drivers performing
complete vehicle durability testing at Hällered Proving Ground

AREZ MOHIDEEN

Department of Applied Mechanics
Division of Dynamics
CHALMERS UNIVERSITY OF TECHNOLOGY
Göteborg, Sweden 2017

Reduction of Whole-Body Vibration transmitted to test drivers performing complete vehicle durability testing at Hällered Proving Ground

AREZ MOHIDEEN

© AREZ MOHIDEEN, 2017

Technical report no 2017:21
ISSN: 1652-8557
Department of Applied Mechanics
Division of Dynamics
Chalmers University of Technology
SE-412 96 Göteborg
Sweden
Telephone +46 (0)31-772 1000

Cover:
Whole-body vibration test on manikin performed in hexapod

Chalmers Reproservice
Göteborg, Sweden 2017

Reduction of Whole-body vibration transmitted to test drivers performing complete vehicle durability testing at Hällerød Proving Ground
Master's thesis in Applied Mechanics
AREZ MOHIDEEN
Department of Applied Mechanics
Division of Dynamics
Chalmers University of Technology

ABSTRACT

The Vehicle Durability Division at Volvo Car Group is performing complete vehicle testing at Hällerød Proving Ground. The purpose is to verify the durability compliance of the car according to the Durability Vehicle Life Trustmark. However, the rough road conditions at Hällerød Proving Ground results in test drivers being exposed to Whole-body vibration. It has been proven that prolonged Whole-body vibration exposure may lead to muscle fatigue and weakening of the lumbar musculature, resulting in decreased spinal support and lower back pain. As a result, Swedish Work Environment Authority introduced directives according to AFS 2005:15, aimed to protect the employee from injuries due to vibration at work. These directives are based on the original regulations found in 2002/44/EC.

Hence, this thesis work has aimed to reduce Whole-body vibration transmitted to the test drivers as an effect of performing complete vehicle testing at Hällerød Proving Ground. A solution has been carried out based on material tests performed in a hexapod and transmissibility rig. Evident results confirm that there is a dependency between increased PUR foam thickness and extended drive time, before the daily exposure values are reached. Increased foam thickness appears to reduce the frequency at which resonance occurs, but yields higher transmissibility at amplification.

Keywords: Whole-body vibration, Hällerød Proving Ground, lower back pain, spinal injury, AFS2005:15, 2002/44/EC , PUR,

Examensarbete inom Tillämpad Mekanik
AREZ MOHIDEEN
Institutionen för Tillämpad Mekanik
Avdelningen för Dynamik
Chalmers tekniska högskola

SAMMANFATTNING

Avdelningen för livslängdsprovning på Volvo Personbilar utfärdar komplettbilsprovning på Hällered provbana. Syftet är att verifiera bilens livslängd enligt Durability Vehicle Life Trustmark. Dock resulterar de hårda vägförhållandena på Hällered provbana i att testförarna blir utsatta för helkropps vibrationer. Det har bevisats att långvarig exponering av helkropps vibrationer kan leda till muskelutmattning och försvagad ländryggsmuskulatur, vilket resulterar i sämre ryggradshållning och besvär i nedre rygg. Som ett resultat av detta, införde Arbetsmiljöverket direktiv enligt AFS 2005:15, som syftar till att skydda den anställda från skador på grund av vibrationer på jobbet. Dessa direktiv är baserade på originalbestämmelserna i 2002/44/EC

Därför, är målet med detta examensarbete att reducera helkropps vibrationer överförda till testförarna som en effekt av genomförda komplettbilsprovning på Hällered provbana. En lösning har verkställts baserat på materialtester genomförda i en hexapod och en transmissibilitetsrigg. Tydliga resultat bekräftar att det finns ett förhållande mellan ökad PUR-skumstjocklek och förlängd körtid, innan de dagliga exponeringsvärdena är uppnådda. Ökad skumtjocklek visar sig reducera frekvensen varvid resonans sker, men ger upphov till högre transmissibilitet vid resonans.

Nyckelord: Helkropps vibrationer, Hällered provbana, ryggbesvär, ryggradsskada, AFS2005:15, 2002/44/EC, PUR

LIST OF CONTENTS

ABSTRACT	I
SAMMANFATTNING	II
LIST OF CONTENTS	III
LIST OF TABLES	V
LIST OF FIGURES	VII
PREFACE	IX
NOTATIONS	X
1 INTRODUCTION	1
1.1 BACKGROUND	1
1.2 PROBLEM DEFINITION	1
1.3 OBJECTIVE	2
1.4 SCOPE AND LIMITATIONS	2
2 THEORY	3
2.1 VIBRATION DYNAMICS	3
2.1.1 DEFINITIONS	4
2.1.1.1 NATURAL FREQUENCY	4
2.1.1.2 AMPLITUDE	4
2.1.1.3 DISPLACEMENT, VELOCITY AND ACCELERATION	5
2.1.1.4 DEFLECTION	5
2.1.1.5 SPRING CONSTANT	5
2.1.1.6 DAMPING	5
2.1.1.7 HYSTERESIS DAMPING	5
2.1.1.8 VISCOUS DAMPING	5
2.1.1.9 VISCOUS DAMPING COEFFICIENT	5
2.1.1.10 CRITICAL DAMPING	6
2.1.1.11 DAMPING FACTOR	6
2.1.1.12 RESONANCE	6
2.1.1.13 TRANSMISSIBILITY	6
2.2 TRANSMISSIBILITY CURVES	7
2.2.1 HALF POWER BANDWIDTH METHOD	9
2.3 WHOLE-BODY VIBRATION	9
2.3.1 DAILY VIBRATION EXPOSURE VALUE	11
2.4 EFFECTS OF WHOLE BODY VIBRATIONS ON THE HUMAN BODY	13
2.4.1 HEALTH EXAMINATION AT VCC	15
2.5 COMPLETE VEHICLE TESTING	16
2.6 QUARTER CAR MODEL	18
3 SEAT SYSTEM	19
3.1 SEAT STRUCTURE VOLVO XC90	19
3.2 COMPLETE SEAT VOLVO XC90	20

3.3	CURRENT FOAM PAD SOLUTION	21
3.4	OPEN CELL POLYURETHANE FOAM	23
3.5	VIBRATION REDUCING ELEMENTS IN OPTIONAL PUR FOAMS	25
3.5.1	MECHANICAL LOSS FACTOR	25
4	METHODOLOGY	27
4.1	TEST 1 – HEXAPOD	29
4.2	TEST 2 – FIRST ROW - VIBRATION INSULATION TARGET LEVEL	31
4.3	TEST 3 – HÄLLERED PROVING GROUND	34
5	RESULTS	35
5.1	TEST 1 – HEXAPOD	35
5.1.1	PUR FOAM	35
5.1.2	PUR FOAM + GEL OVATIONS PAD	37
5.1.3	PUR + STAR STARLOCK	38
5.1.4	NATURAL AND BUTYL RUBBER	40
5.1.5	148 MM PUR	40
5.1.6	SEAT BACK REST INCLINATION	41
5.2	TEST 2 – FIRST ROW - VIBRATION INSULATION TARGET LEVEL	42
5.2.1	TEST 2 – SUMMARY	55
5.3	TEST 3 – HÄLLERED PROVING GROUND	56
6	DISCUSSION	57
6.1	INTEPRETATION OF RESULTS	57
6.2	SOURCES OF ERROR	60
6.3	WBV EXPOSURE	60
7	CONCLUSION	63
8	FUTURE WORK	65
	BIBLIOGRAPHY	67
	APPENDIX	73

LIST OF TABLES

TABLE 1: A(8) EXPOSURE LIMITS	13
TABLE 2: NATURAL FREQUENCIES OF DIFFERENT BODY PARTS	14
TABLE 3: MECHANICAL PROPERTIES OF FOAM MATERIAL IN VOLVO V526	21
TABLE 4: PROPERTIES OF THE CURRENT FOAM PAD	22
TABLE 5: THE TABLE SHOWS A NUMBER OF PRODUCTS THAT WERE SUPPLIED FROM DIFFERENT COMPANIES.....	28
TABLE 6: MATERIAL PROPERTIES SHOWN FOR REFERENCE V526, SYLOMER 11SR EN AND REGUFOAM VIBRATION 150 PLUS	28
TABLE 7: TRACK SEQUENCE AND RELATED VEHICLE SPEED	31
TABLE 8: MATERIAL CONFIGURATIONS TESTED	33
TABLE 9: THE TABLE SHOWS VALUES GAINED FROM TESTING PUR FOAMS, WITH SEAT BACK REST INCLINED 20° FROM THE Z-AXIS	36
TABLE 10: THE TABLE SHOWS VALUES GAINED FROM TESTING PUR FOAMS COMBINED WITH GEL OVATIONS PAD, WITH SEAT BACK REST INCLINED 20° FROM THE Z- AXIS	37
TABLE 11: THE TABLE SHOWS VALUES GAINED FROM TESTING STAR STARLOCK, BOTH SOLELY AND COMBINED WITH PUR FOAMS, WITH SEAT BACK REST INCLINED 20° FROM THE Z-AXIS	39
TABLE 12: THE TABLE SHOWS VALUES GAINED FROM TESTING NATURAL AND BUTYL RUBBER, WITH SEAT BACK REST INCLINED 20° FROM THE Z-AXIS	40
TABLE 13: THE TABLE SHOWS VALUES GAINED FROM TESTING 148 MM THICK PUR, WITH SEAT BACK REST INCLINED 20° FROM THE Z-AXIS	40
TABLE 14: THE TABLE SHOWS VALUES GAINED FROM TESTING 50 MM SYLOMER, WITH SEAT BACK REST ANGLE ALTERED.....	41
TABLE 15: THE CHART PROVIDES FREQUENCIES AND RELATED TRANSMISSIBILITY FOR 50 MM REFERENCE V526. DAMPING RATIO IS ALSO GIVEN	43
TABLE 16: THE CHART PROVIDES FREQUENCIES AND RELATED TRANSMISSIBILITY FOR 50 MM REFERENCE V526 COMBINED WITH GEL OVATIONS PAD. DAMPING RATIO IS ALSO GIVEN	43
TABLE 17: THE CHART PROVIDES FREQUENCIES AND RELATED TRANSMISSIBILITY FOR 12 MM REFERENCE V526. DAMPING RATIO IS ALSO GIVEN	44
TABLE 18: THE CHART PROVIDES FREQUENCIES AND RELATED TRANSMISSIBILITY FOR 50 MM REGUFOAM. DAMPING RATIO IS ALSO GIVEN	45
TABLE 19: THE CHART PROVIDES FREQUENCIES AND RELATED TRANSMISSIBILITY FOR 98 MM REGUFOAM. DAMPING RATIO IS ALSO GIVEN	46
TABLE 20: THE CHART PROVIDES FREQUENCIES AND RELATED TRANSMISSIBILITY FOR 50 MM REGUFOAM COMBINED WITH GEL OVATIONS PAD. DAMPING RATIO IS ALSO GIVEN	47
TABLE 21: THE CHART PROVIDES FREQUENCIES AND RELATED TRANSMISSIBILITY FOR RELAX EASY. DAMPING RATIO IS ALSO GIVEN	48
TABLE 22: THE CHART PROVIDES FREQUENCIES AND RELATED TRANSMISSIBILITY FOR STAR STARLOCK. DAMPING RATIO IS ALSO GIVEN.....	49
TABLE 23: THE CHART PROVIDES FREQUENCIES AND RELATED TRANSMISSIBILITY FOR 12,5 MM SYLOMER. DAMPING RATIO IS ALSO GIVEN.....	50
TABLE 24: THE CHART PROVIDES FREQUENCIES AND RELATED TRANSMISSIBILITY FOR 50 MM SYLOMER. DAMPING RATIO IS ALSO GIVEN.....	51
TABLE 25: THE CHART PROVIDES FREQUENCIES AND RELATED TRANSMISSIBILITY FOR 50 MM SYLOMER COMBINED WITH GEL OVATIONS PAD. DAMPING RATIO IS ALSO GIVEN	52
TABLE 26: THE CHART PROVIDES FREQUENCIES AND RELATED TRANSMISSIBILITY FOR 50 MM SYLOMER COMBINED WITH 50 MM REGUFOAM. DAMPING RATIO IS ALSO GIVEN.....	53
TABLE 27: THE CHART PROVIDES FREQUENCIES AND RELATED TRANSMISSIBILITY FOR 50 MM SYLOMER COMBINED WITH 98 MM REGUFOAM. DAMPING RATIO IS ALSO GIVEN.....	54
TABLE 28: SUMMARY OF RESULTS GAINED FROM TEST 2.....	55

TABLE 29: THE TABLE SHOWS VALUES GAINED FROM TESTING VARIOUS ADDITIVE
PADS IN COMPLETE VEHICLE. THE SEAT BACK REST IS INCLINED 20° FROM THE Z-
AXIS 56

LIST OF FIGURES

FIGURE 1: MASS, SPRING AND VISCOUS DAMPER CONFIGURATION, CONNECTED TO A MOVING BASE	4
FIGURE 2: TRANSMISSIBILITY CURVE SHOWING REGION OF AMPLIFICATION AND REGION OF ISOLATION	7
FIGURE 3: TRANSMISSIBILITY CURVES FOR DIFFERENT DAMPING RATIOS (BARRY CONTROLS, 1999).....	8
FIGURE 4: TRANSMISSIBILITY CURVE FOR ESTIMATING DAMPING RATIO, USING HALF POWER BANDWIDTH METHOD.....	9
FIGURE 5: SIX DEGREES OF FREEDOM OF THE BODY OCCURRING IN WBV (KLOOSTER, 2004).....	11
FIGURE 6: THE IMAGE SHOWS THE MEASURING EQUIPMENT. THE GREY DEVICE BELOW THE STEERING WHEEL IS THE VIBRATION ANALYZER AND THE BLACK DISC ON THE SEAT CUSHION IS THE ACCELEROMETER.....	12
FIGURE 7: GRAPHICAL REPRESENTATION OF EXPOSURE TIME RECOMMENDED BASED ON VIBRATION MAGNITUDE	13
FIGURE 8: SCHEMATIC PRESENTATION OF A DRIVE CYCLE	17
FIGURE 9: A) BELGIAN PAVE (LEFT) B) SILVER CREEK (MIDDLE) C) CORRUGATION (RIGHT)	17
FIGURE 10: FFT ON CHASSIS RESPONSE FROM SILVER CREEK (LEFT) AND FFT ON CHASSIS RESPONSE FROM BELGIAN PAVE ANTI-CLOCKWISE (RIGHT). AMPLITUDES ARE GIVEN IN $[M/S^2]$	17
FIGURE 11: 4 DOF QUARTER CAR MODEL	18
FIGURE 12: A) ILLUSTRATION OF SEAT BEAMS, RAISER AND RAILS (LEFT) B) SEAT FRAME SPRINGS AND METAL PAN COVERING THE FRONT END AREA OF THE FRAME (RIGHT).....	20
FIGURE 13: A) 3D MODEL OF COMPONENTS BENEATH THE FRONT SEAT (LEFT) B) ACTUAL PICTURE OF THE ENVIRONMENT BENEATH THE FRONT SEAT (RIGHT)....	20
FIGURE 14: COMPLETE SEAT MODEL OF VOLVO V526 (ADIANT, 2016)	21
FIGURE 15: THE DRIVER IS CLASHING WITH THE ROOF WHEN SITTING ON THE FOAM PAD	22
FIGURE 16: A) THREE LAYERS OF PUR B) COMPLETE DESIGN READY TO BE INSTALLED ON THE SEAT C) THE PAD IS INSTALLED ON THE SEAT	22
FIGURE 17: SQUARE PRISM MODEL FOR OPEN CELL FOAM (ZHANG, 2014).....	24
FIGURE 18: STRESS-STRAIN CURVE SHOWING BEHAVIOR OF PUR IN THREE DIFFERENT REGIONS BASED ON COMPRESSION MECHANISMS (ZHANG, 2014)	24
FIGURE 19: REFERENCE V526 (LEFT) REGUFOAM VIBRATION 150 PLUS (MIDDLE) SYLOMER SR11 EN (RIGHT).....	29
FIGURE 20: BUTLY RUBBER (LEFT) AND NATURAL RUBBER (RIGHT).....	29
FIGURE 21: GEL OVATIONS PAD (LEFT) RELAX EASY (MIDDLE) STAR STARLOCK (RIGHT)	29
FIGURE 22: THE FIXTURE IS INSTALLED ON THE HEXAPOD AND THE SEAT IS ATTACHED TO THE FIXTURE	30
FIGURE 23: A) ACCELEROMETER PLACED ON TEST MATERIAL B) MANIKIN STRAPPED TO THE BACKREST C) MANIKIN FEET STRAPPED TO THE FOOTREST.....	31
FIGURE 24: PICTURE OF TEST SETUP.....	32
FIGURE 25: ARRANGEMENT FOR PLACING THE DUMMY IN THE MIDDLE OF THE TEST MATERIAL.....	32
FIGURE 26: SIGNAL SWEEP SHOWING AMPLITUDE [MM] ON THE VERTICAL AXIS AND TIME [S] ON THE HORIZONTAL AXIS	33
FIGURE 27: RELATION BETWEEN INCREASED MATERIAL THICKNESS AND DRIVE TIME, UNTIL DAILY EXPOSURE ACTION AND EXPOSURE LIMIT VALUE ARE SURPASSED	36
FIGURE 28: RELATION BETWEEN INCREASED MATERIAL THICKNESS AND DRIVE TIME, UNTIL DAILY EXPOSURE ACTION AND EXPOSURE LIMIT VALUE ARE SURPASSED	38

FIGURE 29: RELATION BETWEEN INCREASED MATERIAL THICKNESS AND DRIVE TIME, UNTIL DAILY EXPOSURE ACTION AND EXPOSURE LIMIT VALUE ARE SURPASSED	39
FIGURE 30: TRANSMISSIBILITY PLOT FOR 50 MM REFERENCE V526.....	42
FIGURE 31: TRANSMISSIBILITY PLOT FOR 50 MM REFERENCE COMBINED WITH GEL OVATIONS PAD.....	43
FIGURE 32: TRANSMISSIBILITY PLOT FOR 12 MM REGUFOAM.....	44
FIGURE 33: TRANSMISSIBILITY PLOT FOR 50 MM REGUFOAM.....	45
FIGURE 34: TRANSMISSIBILITY PLOT FOR 98 MM REGUFOAM.....	46
FIGURE 35: TRANSMISSIBILITY PLOT FOR 50 MM REGUFOAM COMBINED WITH GEL OVATIONS PAD.....	47
FIGURE 36: TRANSMISSIBILITY PLOT FOR RELAX EASY.....	48
FIGURE 37: TRANSMISSIBILITY PLOT FOR STAR STARLOCK.....	49
FIGURE 38: TRANSMISSIBILITY PLOT FOR 12,5 MM SYLOMER.....	50
FIGURE 39: TRANSMISSIBILITY PLOT FOR 50 MM SYLOMER.....	51
FIGURE 40: TRANSMISSIBILITY PLOT FOR 50 MM SYLOMER COMBINED WITH GEL OVATIONS PAD.....	52
FIGURE 41: TRANSMISSIBILITY PLOT FOR 50 MM SYLOMER COMBINED WITH 50 MM REGUFOAM.....	53
FIGURE 42: TRANSMISSIBILITY PLOT FOR 50 MM SYLOMER COMBINED WITH 98 MM REGUFOAM.....	54

PREFACE

This Master's thesis is written during the spring 2017 as a final part of the Applied Mechanics program at Chalmers University of Technology. The origin of this task was formed by Volvo Car Group, Hällered, Sweden, where the project also carried out. Parts of the task have been completed at Volvo Car Group, Torslanda, Sweden.

I would like to gratefully acknowledge Volvo Car Group for giving me the privilege to complete this task. A special thanks to my supervisors at Volvo Car Group, Stefan Magnusson and Carolina Peters for their assistance through the whole project. I would also like to thank my supervisor and examiner at Chalmers, Mr. Thomas Abrahamsson.

I would especially like to thank following people at Volvo Car Group whom I had the pleasure to work with, Tommy Apell, Anders Wirje, Malin Bodfors, Mikael Holmström, Jonas Hagberg.

I would also like to acknowledge Adient, Christian Berner, Vibratex Akustikprodukter, Salubrious AB and The Trelleborg Group for providing material during this project.

Gothenburg, June 2017

Arez Mohideen

NOTATIONS

ABBREVIATIONS

BMI	Body Mass Index
FFT	Fast Fourier Transform
HPG	Hällered Proving Ground
LBP	Low back pain
PSD	Power Spectrum Density
PUR	Polyurethane
RMS	Root mean square
SWEA	Swedish Work Environment Authority
VCG	Volvo Car Group
VDV	Vibration Dose Values
WBV	Whole-body vibration

VARIABLES

$A(8)$	Vibration exposure value [m/s^2]
T	Transmissibility [dB]
T	Period time [s] or Exposure time [h]
W	Frequency weighing factor [dB]
a	Acceleration [m/s^2]
c	Viscous damping coefficient [Ns/m]
f	Frequency [Hz]
k	Spring coefficient [N/m]
m	Mass [kg]
z	Vertical displacement [m]
ω	Angular frequency [rad/s]

DIMENSIONLESS CONSTANTS

ζ	Damping ratio
---------	---------------

INDEX

x	Longitudinal direction
y	Lateral direction
z	Vertical direction

1 INTRODUCTION

This chapter is an introduction to this thesis work. The aim is to guide and acquire the reader with this study by presenting an overview of the issue. In addition, objective, scope and limitations are also found in this section.

1.1 BACKGROUND

The Vehicle Durability Division at Volvo Car Group is performing complete vehicle testing at Hällered Proving Ground. The purpose is to verify the durability compliance of the car according to the Durability Vehicle Life Trustmark. The requirement states that the vehicle shall comply with the corporate guidelines for a minimum of total vehicle durability of 240 000 customer equivalent kilometers. This applies for failure modes that are mileage based for the designated severe case, assuming 90th percentile customer, in the most severe market in which the vehicle is to be sold (Volvo Car Group, 2012). Thus, the requirement is verified by achieving 400 drive cycles for a specified circuit at Hällerd Proving Ground. Each cycle involves driving on different durability challenging road surfaces, but also inclined driving, brake testing etc. The drive cycle is further explained in Chapter 2.5.

The rough road conditions at HPG results in test drivers being exposed to Whole-body vibration. The European Union has since year 2002 introduced new directives according to 2002/44/EC, referring to accepted vibration exposure levels transmitted to employees (2002/44/EC, [2002]). The directives define daily maximum exposure limit values that prevent health and safety risks of each individual. As a result, the Swedish Work Environment Authority introduced directives according to AFS 2005:15, aimed to protect the employee from injuries due to vibration at work (AFS 2005:15, [2015]). These directives are based on the original regulations found in 2002/44/EC.

1.2 PROBLEM DEFINITION

It has been proven that prolonged WBV exposure may lead to muscle fatigue and weakening of the lumbar musculature, resulting in decreased spinal support and lower back pain. Hence, the amount of allowed complete vehicle testing time at HPG has been limited to 1.5 – 2 hours per day for each driver. Assuming 30 minutes per cycle, this corresponds to 3 – 4 cycles per operator. Amount of cycles depends mainly on which car model that is being tested. Therefore, in order to increase the test time for the same vehicle, the drivers operate in shifts of four hours in total. Thus, assuming eight-hour workday, there is still four hours to spare, which can increase the efficiency for completing 400 drive cycles.

1.3 OBJECTIVE

The aim of this thesis work is to reduce WBV transmitted to test drivers performing complete vehicle durability testing at HPG, by using theoretical fundamentals and practical experiments.

1.4 SCOPE AND LIMITATIONS

This thesis is limited to low frequency vibrations. In the studies of WBV, oscillations in the frequency range 2 – 20 Hz are investigated. Frequencies excluded from this range will therefore not be considered. In addition, only vertical transmissions will be considered, since these cause highest exposure values. Furthermore, Vibration Dose Values will not be taken into consideration, due to preferences given by VCG. When developing a solution, a requirement is to keep the seat frame design unchanged. Since this thesis work is related to durability testing of vehicles at HPG, a potential solution will only be implemented in complete car testing. Moreover, the solution will be derived for the latest Volvo XC90 (year model 2014 – present). However, it should be applicable on every current car model manufactured by VCG.

2 THEORY

This chapter includes fundamental facts, including equations, explanations of physical behaviors, figures, tables etc. needed to understand the analysis and calculations made in this report. The reader is initially introduced to basic vibration dynamics, followed by the possible effects of WBV.

2.1 VIBRATION DYNAMICS

Mechanical vibrations are instantaneous mechanical oscillations in solids deviating from a point of equilibrium. These mechanical oscillations are often complex, containing different frequencies, appearing in several directions and changes over time (ISO 2631-1, [1997]). Vibrations are commonly expressed in terms of frequency and amplitude. Frequency is number of cycles per second, while the amplitude defines the magnitude of the force, displacement or acceleration. Normally oscillations in mechanical systems are unwanted since they result in wasted energy, reduced efficiency and may even lead to structural failure. Vibrations occur due to two physical properties: elasticity and inertia. When the system fluctuates around its point of equilibrium, the elasticity provides a restoring force in order to bring the system back to its equilibrium. Inertia on the other hand, causes the system to deviate from equilibrium. When discussing vibration protection, it is beneficial to discuss three basic fundamentals of dynamic systems; the equipment, the support structure and the resilient member (Barry Controls, 1999). Equipment refers to components, machines, motors, instruments etc. A support structure is often referred to as floor, road, and baseplate, while a resilient member is an isolator or mount. This member is found between the equipment and the support structure. In this thesis, only vibrations caused by oscillations in supporting structures (base excitation) will be discussed. The basic idea is to reduce the dynamic disturbance transmitted from the support structure to the operator, which in this case is the driver.

Figure 1 shows a common problem in the study of vibrations. The figure illustrates a mass, spring and damper systems, connected to a moving base. An example of this is a working automobile suspension or the sprung mass. Horizontal and rotational movements are neglected, since these are small compared to vertical motion (Volvo Car Group, 2016). The arrangement presented in Figure 1 is said to be a single degree-of-freedom system. The reason is that the system at any time can be specified by a sole coordinate; e.g. the acceleration of the mass with the respect to the acceleration of the base. The base may have undesired characteristic motion, which can damage the mass or even cause failure.

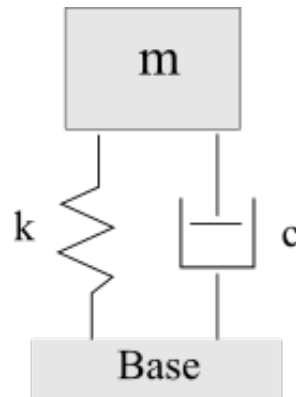


Figure 1: mass, spring and viscous damper configuration, connected to a moving base

There are three fundamental ways of reducing vibrations in a system; eliminating, isolating or damping the vibrational energy (Sharma and Peel, 2004). Due to self-evident reasons, the source (road surface) cannot be eliminated in this case. The second option refers to isolating the vibration. In today's commercial car seats, isolation is primarily achieved through the cushion. Hence, changing the mechanical properties of the cushion could result in improved isolation. Chapter 2.1.1 presents basics and important definitions that will help the reader understand the root of the problem. These are the parameters, which must be considered when creating a solution within the scope of this thesis.

2.1.1 DEFINITIONS

To make the report more structured and easier to follow, different notions will be presented as subsections to this chapter.

2.1.1.1 NATURAL FREQUENCY

The natural frequency is the frequency at which the system will vibrate freely, when displaced from its equilibrium. This results in oscillations despite the absence of any driving or damping force. The frequency, at which a system will vibrate freely, depends on stiffness k and mass m . This is presented in Equation (1) (Barry Controls, 1999).

$$f_n = \frac{1}{2\pi} \sqrt{\frac{k}{m}} \quad \text{Equation (1)}$$

2.1.1.2 AMPLITUDE

The amplitude of an oscillation defines the zero to peak value of a displacement, velocity or acceleration. This corresponds to the maximum magnitude of the harmonic motion.

2.1.1.3 DISPLACEMENT, VELOCITY AND ACCELERATION

The displacement is a distance, which expresses how much a body has been dislocated from the mean position or equilibrium position. Velocity however, gives time dependent change of the displacement with respect to a frame of reference. Likewise, the acceleration is the time rate change of the velocity in regarding to a frame of reference.

2.1.1.4 DEFLECTION

Consider a spring that is either compressed or extended due to a static or dynamic force. The distance, which the spring is moved, is defined as the deflection.

2.1.1.5 SPRING CONSTANT

One of the main tasks of the spring is to store the energy in a vibrating system. Hence, the spring constant is given as the ratio between increased forces to corresponding deflection increment of the spring.

2.1.1.6 DAMPING

Damping is measure of how much energy a vibrating system dissipates. More energy dissipated, is a result of better damping ability. Three different cases of damping can be encountered; coulomb, hysteresis and viscous. However, this report will only discuss the two latter.

2.1.1.7 HYSTERISIS DAMPNIG

This is a form of frictional damping due to molecular structure of a material when the object is set in motion. Materials with viscoelastic properties are good examples where hysteresis damping can be seen. This will be discussed further in Chapter 3.4.

2.1.1.8 VISCOUS DAMPING

Viscous damping is said to be present if any particle in a vibrating body encounters a force, whose magnitude is proportional to the magnitude of the particle's velocity. In addition, the damping force is opposing the direction of motion. Thus, the damping force is a linear function of the velocity.

2.1.1.9 VISCOUS DAMPING COEFFICIENT

Damping in linear materials is quantified by its damping coefficient. This is mathematically defined as the ratio between damping force and velocity. The expression is given by Equation (2) (Barry Controls, 1999).

$$c = \frac{F}{v} \quad \text{Equation (2)}$$

2.1.1.10 CRITICAL DAMPING

A system that is set in motion is critically damped, when it returns most rapidly to static position without any over-oscillation. The critical damping coefficient is dependent on mass and stiffness. The expression can be seen in Equation (3) (Grahn and Jansson, 1997).

$$c_c = 2\sqrt{km} \quad \text{Equation (3)}$$

2.1.1.11 DAMPING FACTOR

This is a dimensionless factor, defining amount of damping in a system. The ratio is given by viscous damping constant over critical damping, which can be found in Equation (4) (Grahn and Jansson, 1997)

$$\zeta = \frac{c}{c_c} \quad \text{Equation (4)}$$

2.1.1.12 RESONANCE

In cases when the input frequency f_d , i.e. disturbing frequency, coincides with the natural frequency, resonance is attained. Resonance is undesirable since the transmissibility is amplified where it acts.

2.1.1.13 TRANSMISSIBILITY

This is given by the ratio between dynamic output over dynamic input. The transmissibility is usually visualized in a plot that, showing where the system is amplified and where it is isolated. However, transmissibility is mathematically presented in Equation (5) (Barry Controls, 1999).

$$T = \sqrt{\frac{1 + \left(2\zeta \frac{f_d}{f_n}\right)^2}{\left(1 - \frac{f_d^2}{f_n^2}\right)^2 + \left(2\zeta \frac{f_d}{f_n}\right)^2}} \quad \text{Equation (5)}$$

2.2 TRANSMISSIBILITY CURVES

Prior to designing a vibration attenuating mechanism, both disturbing and natural frequencies must be known. This will determine whether the system should isolate or damp the oscillation. In addition, as seen in Equation (5), the viscous damping coefficient must be known, in order to theoretically determine the transmissibility. Figure 2 shows an example when amount of desired damping cannot be obtained and resonance occurs. Thus, the disturbing frequency is amplified, which happens when it coincides with the natural frequency of the object. While there is lack of damping, a more preferred solution is to isolate the vibration, in order to decrease the transmissibility. The vibration is isolated whenever the ratio between disturbing and natural frequency is greater than $\sqrt{2}$. This can be achieved either by increasing the disturbing frequency or decreasing the natural frequency.

Knowing the spectra of the disturbing frequencies exiting the chassis and entering the seat makes it easier to develop a vibration reducing system. The system should be designed to isolate the lowest frequency entering the seat. Isolating the lowest excitation value will also isolate all higher frequencies, according to the frequency ratio.

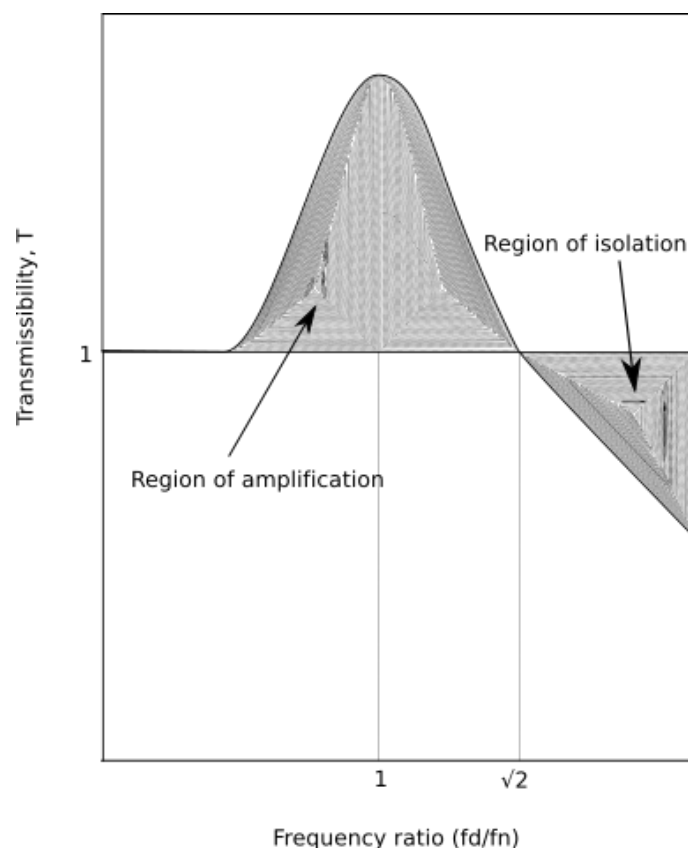


Figure 2: transmissibility curve showing region of amplification and region of isolation

Amplification of the disturbing frequency, which leaves the sprung mass, implies a different spring-damper characteristic of the system. Hence, taking the project limitations into consideration, changing chassis dynamics only for complete vehicle testing at HPG is costly, time craving and thus unrealistic. Consequently, possible vibration reducing improvements in the cushion would be less expensive, probably easier to implement and therefore more preferred. Equation (1) shows that reducing the stiffness or increasing the mass of the cushion can decrease the natural frequency. However, it is important to remember that a softer system results in increased travel, since it becomes easier to move the mass relative the base. Thus, the same input force will cause larger mass displacements. This can in many cases be an issue since systems are generally designed to occupy minimum space. Too much travel could consequently lead to an impact with other structures or systems. Hence cushions with different properties and desired natural frequencies must be investigated.

Figure 3 shows a schematic representation of the relation between damping ratio and transmissibility. As the ratio increases, the system becomes less underdamped and hence less susceptible for resonance. However, by increased damping follows less effective isolation in the isolation region.

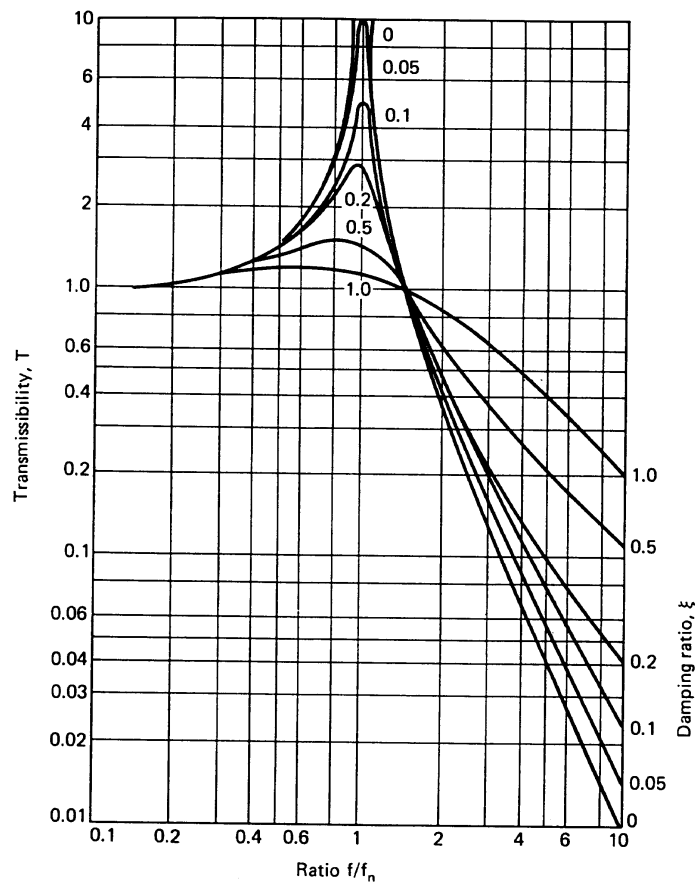


Figure 3: Transmissibility curves for different damping ratios (Barry Controls, 1999)

2.2.1 HALF POWER BANDWIDTH METHOD

The amount of damping in different systems is not always quantified or given. In these cases, information can be extracted from the transmissibility curve, using the half power bandwidth method and used inserted in Equation (6). Thus, from Equation (6) a fair approximation of the damping ratio can be obtained. Figure 4 presents three relevant angular frequencies, ω_1, ω_n and ω_2 , on the horizontal axis. Peak transmissibility is given at the resonance angular frequency ω_n . The two other angular frequencies, ω_1 and ω_2 , yield the transmissibility, which is attained by subtracting 3 dB from the peak transmissibility value, $T(\omega_n)$ (Papagiannopoulos and Hatzigeorgiou, 2011).

$$\zeta = \frac{1}{2} \frac{(\omega_2 - \omega_1)}{\omega_n} \quad \text{Equation (6)}$$

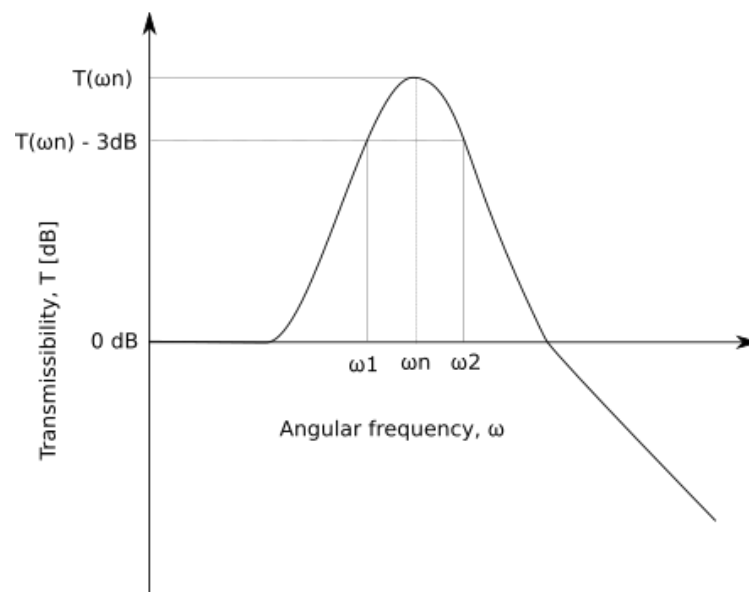


Figure 4: Transmissibility curve for estimating damping ratio, using half power bandwidth method

2.3 WHOLE-BODY VIBRATION

Transportation in car exposes human bodies to whole-body vibrations, especially when the vehicle is driving over speed bumps, potholes and other road surface irregularities. Most of the vibrations are blocked by the car suspension but also the seat is suppressing some. However, these systems are not capable of isolating low frequency vibrations, from given design requirements. Hence, bigger parts of these harmful frequencies are transferred to the driver, causing a complex distribution of oscillatory motions and forces within the body (Hägglund and Danielsson, 2015). ISO

2631-1:1997 is a governmental standard that defines methods for measuring periodic, random and transient WBV (AFS 2005:15, [2015]). The standard indicates to which RMS acceleration magnitudes that daily vibration exposure will be allowed. Two frequency ranges are regulated considered: 0.5 – 80 Hz for health, comfort and perception and 0.1 – 0.5 Hz for motion sickness (ISO 2631-1, [1997]). Since the frequencies in the range 2 – 20 Hz are most critical when studying WBV in cars, only this span is considered in this thesis (Hägglund and Danielsson, 2015).

WBV can occur in any of the human body's six degrees of freedom, illustrated in Figure 5. However, for a person in sitting posture, RMS weighing accelerations are measured on the seat pan, in the three translational axes. These values measure the effective acceleration, as a summary of the peak amplitudes. The weighed magnitudes are by definition coupled with duration T , from an initial time T_1 to end time T_2 (Pauschke and Krishnamurty, 1985). T in this case should not be understood as transmissibility. The RMS accelerations are calculated using the formula, presented in Equation (8) (ISO 2631-1, [1997]).

$$a_{RMS} = \left[\frac{1}{T} \int_0^t a^2(t) dt \right]^{1/2} \quad \text{Equation (8)}$$

The way vibrations have an impact on health, comfort, perception and motion sickness is a result of vibration frequency content (ISO 2631-1, [1997]). Equation (8) does not consider the content and thus frequency weighing are required, for each axis where the vibration is present (Albin and Bohgard, 2015). Two principal frequency weighing are relevant, W_d for x- and y-directions and W_k for z-direction. The weighing factors for W_d and W_k are presented in Appendix A2. The frequency- weighed acceleration, a_w , is calculated by using Equation (9).

$$a_{wi} = \sqrt{\sum (W_i a_i)^2} \quad i = x, y, z \quad \text{Equation (9)}$$

Note that $W_d = W_x = W_y$ and $W_k = W_z$, while a_i is the RMS acceleration. As Equation (9) shows, the frequency- weighed acceleration is computed as the sum of the RMS accelerations multiplied with each weighing factor. Testing data results obtained from HPG show that vibrations in vertical direction has greatest influence on the daily vibration exposure (Volvo Car Group, 2016). Therefore, only this direction is studied henceforth.

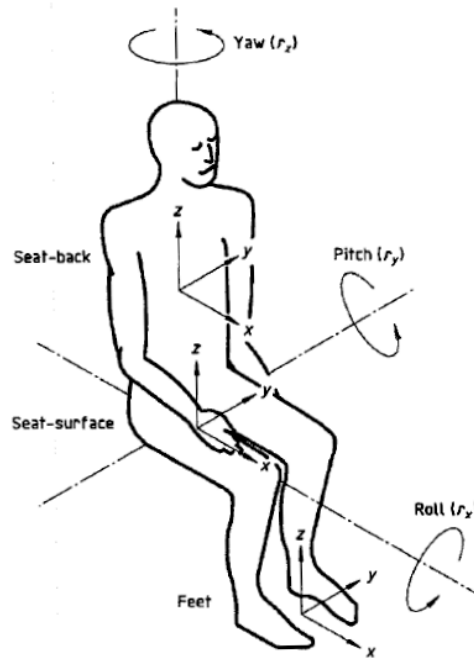


Figure 5: Six degrees of freedom of the body occurring in WBV (Klooster, 2004)

2.3.1 DAILY VIBRATION EXPOSURE VALUE

The vibration exposure value, $A(8)$, defines daily recommended transmissibility and is highly influenced by the frequency-weighted accelerations. According to the provision introduced by SWEA, the quantity is counted for an eight-hour workday. Equation (10) presents the formula, which is applied for estimation of the exposure value (Albin and Bohgard, 2015).

$$A_z(8) = \sqrt{\frac{1}{8} \sum_{i=1}^n a_{wzi}^2 T_i} \quad \text{Equation (10)}$$

As the exposure usually consists of a vector of magnitudes, T_i is the time interval of the different acting frequency-weighted accelerations (Albin and Bohgard, 2015). Equation (11) can be applied if the driver is only subjected to one time specific frequency-weighted acceleration.

$$A_z(8) = a_{wz} \sqrt{\frac{T}{8}} \quad \text{Equation (11)}$$

where, T denotes the exposure time in hours. Appendix A3 calculated example of the A(8) value.

A common way to estimate the daily exposure values is to use a measuring instrument that fulfills the requirements defined in ISO 8041:2005 (ISO 8041:2005, [2005]). The instrument is composed of a vibration analyzer, which is connected to an accelerometer. The accelerometer is thenceforth installed between the operator and the seat cushion. This configuration is illustrated in Figure 6.

Two regulated limits are encountered when discussing A(8) levels, the action value and the limit value (2002/44/EC, [2002]). The action value is a limit, after which the employer is responsible to make an assessment if exceeded. The daily exposure limit value on the other hand, is a upper limit, which shall not be exceeded during any circumstances (AFS 2005:15, [2015]). Table 1 presents the magnitudes, after which these two thresholds are surpassed (AFS 2005:15, [2015]). A more detailed illustration is given in Figure 7. The figure shows recommended exposure time dependent on frequency-weighted acceleration. An important conclusion is that extended exposure time follows with decreased acceleration magnitude. As it has been mentioned, the definition of A(8) is based on an eight-hour workday and thus the exposure limit magnitudes specified in Table 1 are reached after eight hours. However, an assesment is required after 1.7 hours, if the acceleration content corresponds to the daily exposure limit value.

The VDV value is an alternative method for quantifying potential health risks due to vibration exposure. However, since the A(8) value is primarily driving daily allowed complete vehicle testing time at HPG, the VDV value is henceforth not discussed. Thus, the reader is referred to EN ISO 2631-1:1997 for further information about this method (ISO 2631-1, [1997]).



Figure 6: The image shows the measuring equipment. The grey device below the steering wheel is the vibration analyzer and the black disc on the seat cushion is the accelerometer

Table 1: A(8) exposure limits

Whole-body vibration	Daily exposure action value	Daily exposure limit value
A(8)	0.5 m/s ²	1.1 m/s ²

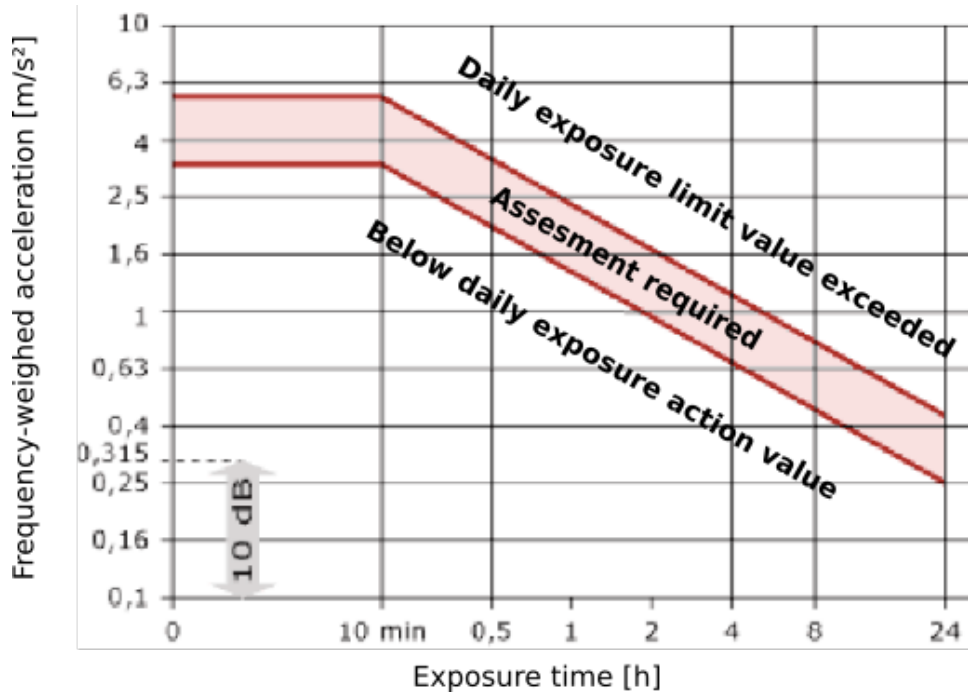


Figure 7: Graphical representation of exposure time recommended based on vibration magnitude. Higher magnitudes decrease in allowed exposure time

2.4 EFFECTS OF WHOLE BODY VIBRATIONS ON THE HUMAN BODY

The human body is a complex and unique dynamic system, built of an uncertain structure with inconsistency between, as well as within subjects. Prolonged exposure to WBV can cause adverse health risks, muscle fatigue and discomfort (Makhsous et al., 2005). An overview of the literature indicates that WBV causes lower back pain and damage on the spinal column (Slota, 2008). The reason why WBV can have harmful effects to individuals is because the vibrations excite natural frequencies of different body parts, allowing free vibration (Klooster, 2004). Therefore, human body dynamics have been studied to conclude which frequencies that are most injurious. Table 2 presents various body parts with related natural frequencies (Albin and Bohgard, 2015). As the table shows, the ranges of natural frequencies coincide with the disturbing frequencies entering the seat, which leads to amplification of the vibration. The theories about resonance are already introduced in chapter 2.1 and the ideas that are presented in this section; also apply to the human body. This implies that the total human body or individual parts will oscillate at a level greater than at the source (Siddha Y and Kumbhar B, 2013). Chapter 2.5.1 will further clarify how the

biomechanics of the abdominal and spinal region can be changed due to WBV and thus mediate the importance of why this phenomenon should be eliminated.

LBP is in literature described as pain, muscle tension or stiffness of the lumbar spine (Slota, 2008). However, in approximately 90 % of LBP cases, health care professionals classify the issue as nonspecific, due to having no detectible physiological cause (Slota, 2008). There are many different researches that discuss the cause of LBP. However, this thesis will only bring up possible individual risk factors. Since LBP is not necessarily an effect of WBV, these aspects must be discussed in order to confidently provide further recommendations, presented in this report.

Individual risk factors include age, gender, overall health, spinal anatomy, anthropometrics, socioeconomic status and education level. LBP is plausible to initially appear during the first four decades of life. However, the probability for LBP to happen increases with age and is most likely to occur between ages of 35 – 55 years (Slota, 2008). It has also been discussed whether gender has any significance for being subjected to LBP (Bressler, Keyes, Rochon and Badley, 1999). There is yet no consensus shared in this question and the general conclusion is that LBP is problematic for both sexes.

Anthropometric factors in this study are limited to body proportions, as height and weight. Correlations between these properties and LBP have been noted (Mellin, 1987). The chance for LBP to occur grows with increased height and weight, likely due to higher moment-loads on the spinal column. In addition, herniated discs and thus LBP are said to be associated with body mass index (Slota, 2008). In a study, it has been claimed that obesity (BMI > 30) is an independent contribution for development of LBP (Webb et al., 2003).

As it has been mentioned, an individual's health status is also relevant when studying individual risk factors of LBP. One of the topics to this subject is smoking habits. Smoking influences the musculoskeletal system, increasing the risk of osteoporosis, fractures, reducing bone density and conducting degenerative changes in the spine (Rubin, 2007). Consequently, these health drawbacks can lead to LBP and low back disorders, which are anatomical and neuromuscular deviations. Deformations in the spine can earlier develop degenerative alternations in the disc (Noren, Trafimow, Andersson and Huckman, 1991). The incident is even more severe when mechanical stress is applied to the spine, since it accelerates these undesired deviations in the disc (Biering-Sørensen, Hansen, Schroll and Runeborg, 1985).

Table 2: Natural frequencies of different body parts

Body part	Natural frequency [Hz]
Shoulder	4 – 6
Abdominal	4 – 8
Spinal column	10 – 20
Head	10 – 20

A properly functioning disc is essential for motions of the vertebrae, since the disc acts as a spacer and cushion. Therefore, a disc with reduced working capability can cause stenosis and nerve pinching and thus LBP. One should also consider how dietary habits and fitness condition of an individual influence LBP. Chronic LBP is defined as pain that has been lasting for more than three months (Slota, 2008). A regularly exercising person has most likely lesser risk of gaining chronic LBP (Slota, 2008). However, research has also shown that disc degeneration is more common in people who do heavy lifting (Andersson, 1981).

Even though it has been largely accepted to associate WBV with LBP, there is not entirely evident that this phenomenon solely raises LBP (Maeda and Mansfield, 2005). Furthermore, there is no general method for predicting individuals who are most receptive to the outcomes of WBV (Mansfield, 2005). WBV may lead to LBP if deviations occur in the spinal stability control system, since dynamic loads on the spine can be amplified (Slota, 2008; Eklundh, 2015b). Spinal stability is controlled by the neuron musculoskeletal system, which describes the interaction between nerves, muscles and skeleton in the body. The system involves three networking functions: passive tissue stiffness, active muscle stiffness and neuromuscular reflexes (Panjabi, 1992). Presence of WBV can interfere any of these systems, which can cause disturbance of spinal stability and LBP. In the system of passive tissue not only ligaments and tendons that support the spine are included, but also the vertebrae and in vertebral discs. An important function of these tissues is to defy forces and moments. However, creep deformation due to WBV exposure has been proven, which can lead to tissue failure (Wilder, Pope and Frymoyer, 1988). Besides this, reports have also shown that vibration exposure damages vascular tissues (Curry et al., 2002) and nerve tissues (Govindaraju, Curry, Bain and Riley, 2006).

2.4.1 HEALTH EXAMINATION AT VCC

In order to truly advance the discussion regarding the relation between WBV and LBP, the health development among the operating drivers at HPG must be reviewed. As it is indicated in the directives written by SWEA, the employer has to offer medical examinations, if the employee is exposed to WBV values that exceed the daily exposure action value. In addition, health inspections must also be made available if there are other motives to suspect health risks at the workplace (AFS 2005:15, [2015]). Since the reforms concerning WBV were introduced 2005, two health inspections have been made at HPG, 2007 and 2010 – 2011. In addition, these two examinations were followed up during 2014 – 2015 (Eklundh, 2015b).

The follow-up focused on pain in lower back, neck and shoulders and was made on 72 test drivers, 16 women and 56 men. 21 drivers who participated in the inspection from 2010 – 2011 were not any longer employed, while 10 new operators had supervened. In addition, one person participated both 2007 and 2014 – 2015 but not 2010 – 2011. Both mean and median ages among the drivers were 44 years, which was a two-year decrease since last health inspection. Furthermore, average and median time length operating as a test driver were 13.6 and 12.5 years respectively. This was increased with one year since the previous examination (Eklundh, 2015b).

Even though 43 people confirmed to experience temporary pain, they declared being well conditioned. 29 people experienced pain continuously, but also these declared to having good health. However, even if a majority of the partakers experienced an increase in pain during testing, it was confirmed that the discomfort has not initially been developed from the tests (Eklundh, 2015b). The most common issue was distress in the lumbar region, which was found in 32 drivers. Second most common concern was neck pain that was found in 15 persons, while 11 drivers confirmed spinal pain. Five drivers experienced pain in all three regions. Lastly, despite all these health issues, work comfort were verified among all participating drivers (Eklundh, 2015b).

2.5 COMPLETE VEHICLE TESTING

The average time required to complete one drive cycle is 30 minutes. Driving without current foam pad solution, allows the operator to perform three cycles, before exceeding the action value. On the other hand, implementing the pad, allows the driver to complete four cycles. The pad is further mentioned in Chapter 3.3. In Figure 8, a schematic demonstration of one drive cycle is seen. However, it has been shown that Belgian pave, Silver creek and the Corrugation have greatest impact on WBV transmission. Therefore, only these three obstacles are of interest henceforth in this thesis.

Figure 9 presents captured pictures of each hindrance. Figure 9a) shows Belgian pave, which is supposed to challenge vehicle durability on paving stones. Silver creek is aimed to challenge the vehicle in off-road environments and is only applied to cars from Volvo in the XC-series. However, during real testing, Silver creek is appearing every fourth cycle. The obstacle is shown in Figure 9b). The Corrugation characterizes a repetitive wavy surface, shown in Figure 9c).

A study of simulated data in ADAMS yields desirable information regarding which specific frequency domains that exit the chassis and enters the seat. The simulations provide time-based data that need to be translated into the frequency domain. This is achieved by doing a Fast Fourier Transform. In addition, the power contain in a frequency range $f + df$ is given by the power spectral density. Two obstacles from the track are studied, Silver creek and Belgian pave, both clockwise and anti-clockwise. The FFTs on chassis response for Silver Creek and Belgian Pave anti-clockwise driven are presented in Figure 10, while FFT for the clockwise driving case on Belgian pave is found in Appendix A4. The vertical axes in these figures measure the acceleration amplitude per Hz. Moreover, the transformed data corresponds to a signal, which is 155.6 seconds long. In Figure 10, it can be seen that while driving on Silver creek, the major amplification during studied time interval is given at 11 Hz. There are also minor peaks at frequencies 2 – 3 Hz, 5 Hz and 13 Hz. For the Belgian pave, driven anti-clockwise, the main peak is seen at 10 – 11 Hz, while minor amplifications are shown at 2 – 4 Hz and 13 Hz.

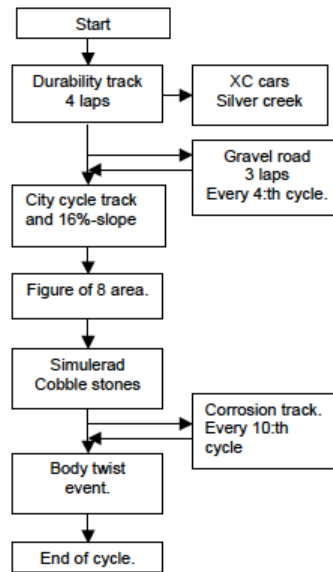


Figure 8: Schematic presentation of a drive cycle



Figure 9: a) Belgian pave (left) b) Silver creek (middle) c) Corrugation (right)

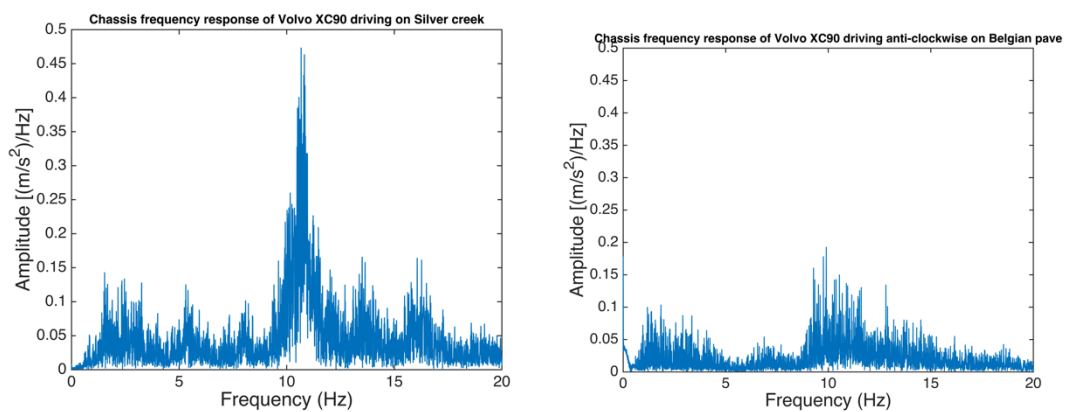


Figure 10: FFT on chassis response from Silver creek (left) and FFT on chassis response from Belgian pave anti-clockwise (right).

2.6 QUARTER CAR MODEL

In order to reduce or eliminate WBV in vehicles, it is in many cases useful to create a quarter car model, which is moving over an uneven surface. The model is a simplified representation of reality by presenting interconnections of masses, springs and dampers (Dowds and Dwyer, 2005). In this context, the aim is to investigate where changes can be made, in order to obtain a less vibrating system. Even though this thesis is not focused on every system shown in the model, visualizing the whole system is useful for further studies.

Figure 11 presents a 4 degree-of-freedom quarter car model. The unsprung mass, which represents the wheel assembly, is denoted m_u (m_u). The mechanical attachment between the sprung mass and the seat frame is assumed to be rigid. This implies no relative motion among the systems and the corresponding mass is m_{ss} . Seat cushion and driver masses are denoted m_c and m_d respectively. Furthermore z_u, z_{ss}, z_c and z_d define displacements of the masses correspondingly. The offset from equilibrium due to road roughness is z_r . The stiffness constant of the pneumatic tire is k_t , while k_s and k_c are stiffness constants of the car suspension and seat cushion respectively. k_t denotes the internal biodynamic stiffness of the driver. Similarly, c_s, c_c and c_d are associate damping coefficients. Furthermore, assuming that the displacements are equal to zero at static equilibrium, allows gravity force to be neglected. In essence, this means that the masses are there but are offset by the force generated by static deflection of the springs. The tire is assumed to be purely elastic with negligible damping. In order to use this model linear constants for the seat cushion and the driver body must be found. Since these systems are nonlinear, standardized table data, material data or computed aided linearization is necessary to apply.

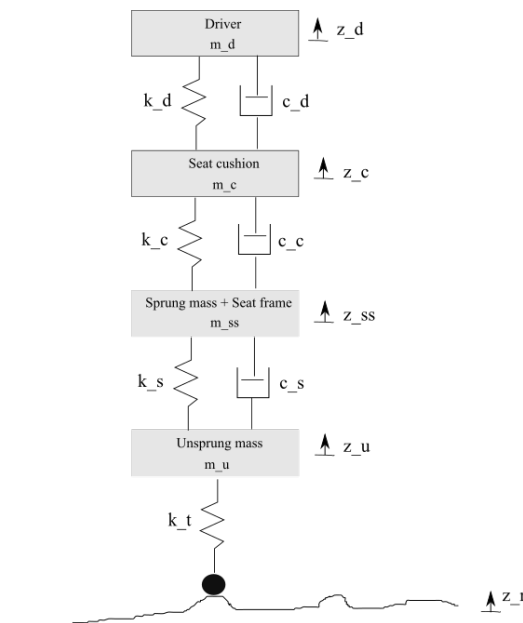


Figure 11: 4 DOF quarter car model

3 SEAT SYSTEM

This section is a continuation of Chapter 2. Instead, the main focus of this chapter is to present components in the seat, which are essential when studying WBV. In addition, the current WBV reducing foam pad used during complete vehicle testing is introduced. In order to gain knowledge regarding how this pad can be optimized, nonlinear behavior of PUR foams is stressed.

3.1 SEAT STRUCUTRE VOLVO XC90

The seat is an important system, since it both provides comfort but also limited protection from vibration. This is a complex system including many electrical components but also safety features, such as airbag. Figure 12 shows the seat at its simplest form. As it can be seen, only metal parts are shown. Figure 12a) illustrates how the frame is attached to two parallel beams, which are bolted to the chassis floor. The attachment mechanism is however not presented in the figure. As the frame is rigidly mounted, it can be assumed that there is no relative motion between seat and cabin floor. In addition, a seat raiser is in Volvo XC90 placed between the beams and the seat rails. The seat raiser provides increased SUV experience by adding 40 mm to the seat height. The seat raiser is indicated by the dark grey component in Figure 12a).

Due to the safety aspects, the seat construction is asked to remain unchanged. This limits the amount of changeable variables in the seat, seen from a vibration reducing point of view. The Z-thud internal seat requirement, which is a design regulation, refers to safety of individuals in case of a front collision. The metal pan, seen in Figure 12b), is designed to prevent sever injuries to the spine if a collision occurs. In addition, the same figure shows the seat frame springs. The current seat springs are soft enough that if a heavy impact occurs, the springs are allowed to deform without plasticity, until the chassis floor is hit.

Restricted space beneath the seat, challenges modifications and other size changes. Figure 13a) presents a 3D model of typical components found beneath the front seat. As the figure shows, cables and motors for seat adjustment mainly occupy the space. The seat length motor, indicated by the black shaft in Figure 13a), is placed vertically under the driver's button. Space limitation may be even clearer when looking at Figure 13b), which presents an actual picture of the environment beneath the seat. The vertical distance between the chassis floor and the lowest point on the seat frame springs unloaded are approximately 135 mm. This is measured in real life, with the seat installed on the lowest height and in the foremost rear position.

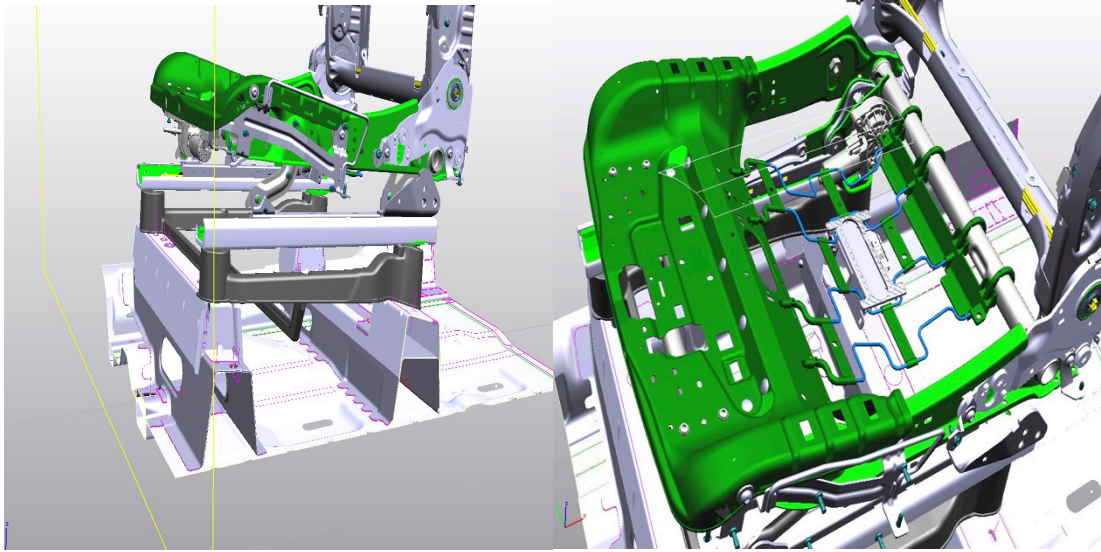


Figure 12: a) Illustration of seat beams, raiser and rails (left) b) Seat frame springs and metal pan covering the front end area of the frame (right)

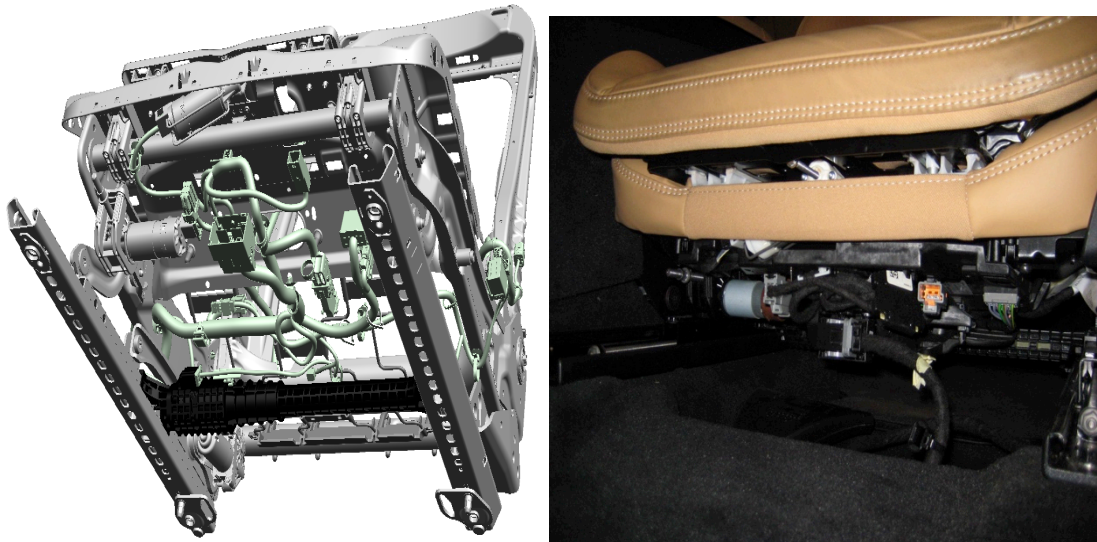


Figure 13: a) 3D model of components beneath the front seat (left) b) Actual picture of the environment beneath the front seat (right)

3.2 COMPLETE SEAT VOLVO XC90

Foam manufacturing processes include shape molding. This is an advantage since the technique allows high degree of freedom when complex shapes are desired. The foam is covered with protecting upholstery, which are available in varied fabrics. Unfortunately, there is a great limitation in provided material data for the seat cushion. However, the known properties are presented in Table 3. In addition, a complete front seat model of Volvo XC90 is found in Figure 14. As this figures shows, the seat is shaped to embrace the driver, for maximum comfort and stability. The side bolsters for the back support and seat pad provide increased side stability, particularly when the driver is dislocated sideways. The foam thickness, for the area at which the driver's button and the cushion is in contact, is 86 mm.

Table 3: Mechanical properties of foam material in Volvo XC90

Mechanical property	Value
Density	60 kg/m ³
Hardness	6 kPa



Figure 14: Complete seat model of Volvo XC90 (Adient, 2016)

3.3 CURRENT FOAM PAD SOLUTION

VCG is currently using an extra foam pad on top of the conventional seat design, to reduce WBV transmitted to the operating driver. Even though this implementation has increased allowed driving time with 72 % (from 87 to 150 minutes per driver) before the daily exposure action value is reached, the foam design disfavors some drivers (Magnusson, 2015). The pad consists of 3 layers of 19 mm PUR foam, covered with trim and a dimension of 440 x 480 mm. The design is presented in Figure 16 a) – c). This additional thickness added to the seat cushion is a disadvantage in terms of that cab space restrictions are challenged. This refers to the fact that there is a clash between the head of the tall drivers and the roof, during vibrating circumstances. The issue is seen in Figure 15. “Tall” in this case is abstractly used, since not only the driver height is an influencing factor but also the driver mass. By taking Newton’s second law of motion into consideration, lighter objects achieve greater acceleration magnitudes and thus greater displacement, when subjected to the same force. Furthermore, the increased height in sitting posture can result in reduced support for the lower back, since the driver’s back is dislocated from the lumbar support in the seat. Relevant properties for the foam are presented in Table 4.



Figure 15: The driver is clashing with the roof when sitting on the foam pad



Figure 16: a) Three layers of PUR b) Complete design ready to be installed on the seat c) The pad is installed on the seat

Table 4: Properties of the current foam pad

Mechanical property	Value
Density	31 – 34 kg/m ³
Hardness	150 ± 15 % N
Dimension	440 x 480 mm
Thickness	3 x 19 mm

3.4 OPEN CELL POLYURETHANE FOAM

Understanding how vibrations are transmitted through the cushion to the seated human body can ease the comprehension of how cushion material characteristics will affect human body response to external disturbances. Depending on properties required, different variations of PUR foams are widely used in conventional car seat cushions. However, in the Volvo XC90, the choice of foam is primarily based on maximum ride comfort experienced. Maximum ride comfort is in this case a subjective experience, which is based on a practical study performed at HPG. The study includes driving on a predetermined circuit to evaluate different seat material concepts, after which the participants answer a survey regarding ride comfort of the different materials.

The geometric structure of open cell foams exhibits a repetitive three-dimensional structure, as seen in Figure 17. By varying geometric shapes and cell edge sizes, foams are given different mechanical properties. A general manufacturing process is casting, by adding a gassing agent to a mixture of polymer resin and hardener. The foaming procedure is then initiated after which the mixture expands and rises. This generates random sized and shaped cells, which are elongated in the direction of the growth. Gravity may affect cells to have different sizes in certain directions, which can lead to anisotropy in foam properties in the elongated direction (Hansen, Hopperstad, Langseth and Ilstad, 2002). Advances in technology concerning foam manufacturing are making it possible to customize the mechanical properties of foam materials (Zhang, 2014). This is a helpful tool in seat optimization, since the foam influences static and dynamic performance of the seat. There are two kinds of PUR, open cell foams and closed cell foams. Open cell foams are broadly used in car seat cushions. These foams have a cell arrangement that makes the material more flexible and soft, while vibration elimination within specific range of frequencies can be attained. Closed cell foams are less suitable in car cushion applications, since they are usually too stiff and used in application where higher forces are present. Therefore, this report will henceforth focus on open cell foams. Open cell PUR foam consists of a polymer matrix with air entrapped in the cell matrix. When the material is exposed to a load, the gas is able to flow through the polymer matrix and thus affect mechanical properties of the foam. One of the reasons why PUR foams have been a more preferred material in automotive seats instead of traditional steel springs is because of its weight to performance ratio. Also, another motive is that it makes it possible to construct a seat at a reduced cost compared to previous used materials (Patten, Sha and Mo, 1998).

The non-linear elastic compliance and damping of PUR materials make the modeling difficult. PUR foams show to behave characteristically in three different regions, illustrated in Figure 18. The figure provides stress-strain relation based on the size of the imposed compressive load. The material is shown to behave linearly during relatively small compressions, which is seen in region A. In this region, Young's modulus is obtained as the slope of the stress-strain curve. The non-linear elasticity appears in the plateau phase, presented as region B in the same figure. Buckling of the cell elements occur in this region. Lastly, as the compressive load increases, plastic collapse and densification take place in region C. As the figure shows, the material also stiffens in this region (Zhang, 2014).

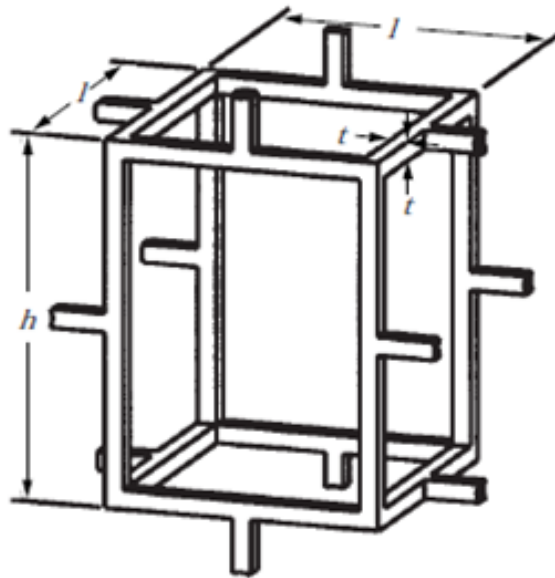


Figure 17: Square prism model for open cell foam (Zhang, 2014)

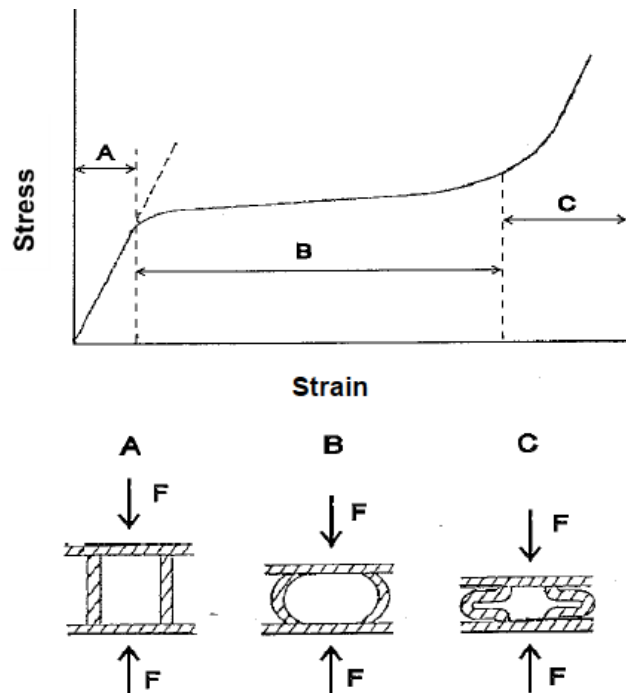


Figure 18: Stress-strain curve showing behavior of PUR in three different regions based on compression mechanisms (Zhang, 2014)

The plot characteristics provided in Figure 17 is typical for viscoelastic materials, as PUR foam. As one can tell from the name, a viscoelastic material exhibits both viscous and elastic characteristics when enduring deformation. In addition, it is also known that a deformed elastic material instantly return to its original state once unstressed. Furthermore, viscosity in materials opposes shear flow and strain linear

with time when stressed. Hence, since both these attributes are found in viscoelastic fabrics, PUR foams yields a slower recovering process in the cell structure when unloaded to conventional state (Nandini, Venkatesh and Nair, 2008). Since elastic materials return to ordinary state instantly, no energy is dissipated. Unlike elastic materials, parts of the mechanical energy absorbed in viscoelastic subjects are finally dissipated as heat. This phenomenon is known as hysteresis. The hysteresis characteristics are generally illustrated in stress-strain curves, where the area of each loop presents the energy dissipated during one loading cycle (Özkaya, Leger, Goldsheyder and Nordin, 1991).

3.5 VIBRATION REDUCING ELEMENTS IN OPTIONAL PUR FOAMS

Studies have been carried out in order to understand how changes in properties affect damping and or isolation abilities of PUR foams. Some of the investigations are based on material data, derived from previous experiments, rather than theoretical knowledge. The reason is that there is a lack of relevant studies that confirms how nonlinear mechanical properties might be affected, when foam thickness is changed. Therefore, the current conventional foam used in XC90 is compared to two other PURs, Sylomer 11SR EN and Regufoam Vibration 150 Plus. Unfortunately, properties like mechanical loss factor, natural frequency and stiffness are only presented for Sylomer 11SR EN and Regufoam Vibration 150 Plus, since the same data is inaccessible for the XC90. For material data, see Appendix A5.

3.5.1 MECHANICAL LOSS FACTOR

Mechanical loss factor, also denoted $\tan \delta$, is a measure of mechanical damping or internal friction in viscoelastic materials. Briefly, the property is given as the ratio between loss and storage modulus. The loss modulus provides the energy dissipated during one loading cycle, while the storage modulus defines the viscoelastic stiffness, which is proportional to the stored energy during the same cycle (ISO 6721-1, [2011]). The factor is derived experimentally by performing Dynamic Mechanical Analysis (Nandini, Venkatesh and Nair, 2008). However, the test methodology will not be explained further and the reader is thus referred to DIN 53513 for additional knowledge (DIN 53513, [1990]).

The phase angle δ can vary between $0^\circ - 90^\circ$ and as delta reaches 0° the material becomes purely elastic, while delta at 90° gives purely viscous behavior. However, $\tan \delta$ is dependent on several inputs, as frequency, amplitude, temperature etc. Therefore, the property is unique and may alter significantly (Rasa, 2014).

4 METHODOLOGY

Due to the complex characteristics of nonlinear materials, three practical tests had to be made. The first test was performed in a hexapod, a six degree-of-freedom (lateral, longitudinal, vertical, pitch, roll and yaw) moving platform. However, the test was limited to vertical movements. The second test was a vibration requirement test according to REQ-021956/1 First Row-Vibration Insulation Target Level (Hägglund and Danielsson, 2015). Lastly, the third test was performed at HPG.

The aim of the first test was to find a product that potentially can reduce the A(8) value. Furthermore, also materials that hypothetically could reduce the transmission of vibrations were investigated, both solely but also combined with PUR foams. A combination with PUR could potentially increase the seat comfort aspect and still also reduce the exposure. However, in either cases, even if the A(8) would be decreased, this value does not specify how the material behave when exposed to different input frequencies. Therefore, in order to gain knowledge about the material's natural frequency, the first row-vibration insulation target level test was essential. However, in order to increase test efficiency, this methodology was only applied on materials and material combinations that indicated promising results in the first test. In the last test performed at HPG, three products were compared to the existing foam pad, which was introduced in Chapter 3.3. The aim in this test was to examine if using an additive pad, which is thinner than the current foam pad solution, still can reduce the exposure.

To minimize costs and delivery times in both tests, block shaped materials with a dimension of 300 x 300 mm were used. The dimension was chosen accordingly existing material data, which is based on the same size. However, not all suppliers could satisfy the requested dimension. Hence this caused size deviations among the materials. In addition, neither consistency in material thickness could be gained due to the suppliers. Therefore, there are also alterations in material thickness. Table 5 shows eight materials that were studied. Current foam used in Volvo XC90 was set as reference. By stacking several layers of Sylomer SR11 EN and Regufoam Vibration 150 Plus respectively, a comparison against the reference material could be performed, for equivalent thicknesses. Mechanical properties of these foams are presented in Table 6. Note that there is no hardness defined for Sylomer SR11 EN, due to unavailability. In addition, the rubbers were delivered in two thicknesses; 5 mm and 10 mm. By stacking each of these yielded a maximum thickness of 15 mm. The three different PUR foams are shown in Figure 19, while the two rubber types are presented in Figure 20. Butyl rubber is generally known for having high damping ability (Trelleborg Elastomer Laminates, 2015). However, research did not prove at which conditions (frequencies, vibration magnitudes, temperatures etc.) that the material operates ideally. Testing of this fabric was therefore of an interest. A greater skeptical attitude was put towards natural rubber and its ability to damp oscillation. However, in an oral discussion with the company, it was stated that this rubber type has performed well in previous vibration tests.

Table 5: The table shows which products that were tested

Product name	Company	Material	Thickness [mm]	Dimension [mm]
Reference	Adient	PUR	37.5	300 x 300
Reference	Adient	PUR	50	300 x 300
Reference	Adient	PUR	86	300 x 300
Sylomer SR11 EN	Christian Berner	PUR	12.5	300 x 300
Regufoam Vibration 150 Plus	Vibratec	PUR	12	300 x 300
Regufoam Vibration 150 Plus	Vibratec	PUR	50	300 x 300
Gel ovations pad	Salubrious	Silicon	13	360 x 360
Relax Easy	Salubrious	Silicon + absorbing foam	60	360 x 400
Star Starlock	Salubrious	Silicon	50	340 x 390
Butyl rubber	Trelleborg	IIR	5	300 x 300
Butyl rubber	Trelleborg	IIR	10	300 x 300
Natural rubber	Trelleborg	NR	5	300 x 300
Natural rubber	Trelleborg	NR	10	300 x 300

Table 6: Material properties shown for the Reference, Sylomer 11SR EN and Regufoam Vibration 150 plus

Material	Density [kg/m ³]	Hardness [kPa]
Reference V526	60	6
Sylomer SR 11 EN	170	Unknown
Regufoam Vibration 150 Plus	150	14

The products from Salubrious are commonly recommended for rehabilitation and improved comfort. Gel ovations pad is widely used in wheel chairs since it provides enhanced pressure distribution between the seated individual and the chair (Salubrious Good Medical, 2016). The improved pressure distribution is thanks to high viscosity silicon, which is encapsulated in the pad. Relax Easy is purposed for individuals who experience pain and desires more stable sitting posture. The cushion does also prevent deformation in shear (Salubrious Good Medical, 2016). Star Starlock is more technically advanced compared to the two last mentioned products. It utilizes individual pressure adjusted pockets, which allows airflow between the cells. Since the area where the air is allowed to flow is limited, the cushion stiffens and provides improved stability (Salubrious Good Medical, 2016). The products from Salubrious are shown in Figure 21. Chapters 4.1, 4.2 and 4.3 will explain each test methodology more in detail.



Figure 19: Reference (left) Regufoam Vibration 150 Plus (middle) Sylomer SR11 EN (right)

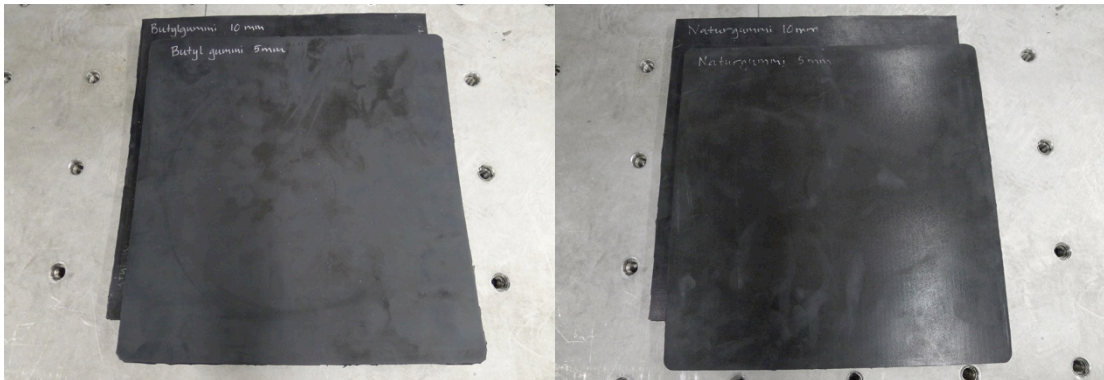


Figure 20: Butyl rubber (left) and natural rubber (right)



Figure 21: Gel ovals pad (left) Relax Easy (middle) Star Starlock (right)

4.1 TEST 1 – HEXAPOD

To provide the correct seat rail inclination found in a Volvo XC90, a seat fixture was rigidly installed on the hexapod. A seat frame was attached to the fixture. Since the test aimed to study vibration reduction among the materials, foam and trim from the installed seat were removed, in order to eliminate the contribution from current cushion. The seat rail angle was 3° in relation to the x-axis, illustrated in Figure 5. The arrangement is shown in Figure 22. Each test was prepared by placing the materials directly on the seat frame springs. The accelerometer was then positioned on top of the materials. Due to restrictions, the accelerations were measured on a sitting manikin weighing 75 kg, which was placed on the accelerometer. In addition, to ensure vertical displacement, the manikin was strapped to the seat back support, at two body

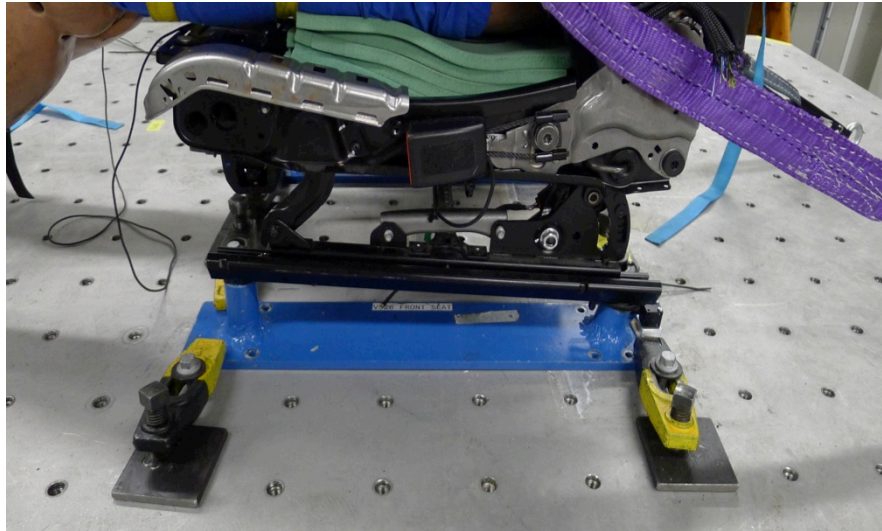


Figure 22: The fixture is installed on the hexapod and the seat is attached to the fixture

locations; the waist and the neck. The strapping force was chosen arbitrary. Lastly the manikin's feet were fastened to a footrest, which was intended to represent a pedal box. The procedure is shown in Figure 23 a) – c). The seat back rest was inclined 20° in relation to the z-axis, shown in Figure 5. Furthermore, seat elevation was set to the highest position, in order to avoid clashes between the materials and other components. Since it is already proven that the Belgian pave, Silver creek and the Corrugation have greatest impact on WBV, the tests only contained vibrations from these obstacles. Since similar velocity amplitudes are gained from FFT for clockwise and anti-clockwise driving on Belgian pave, the choice of direction is unimportant. Thus, anti-clockwise driving was chosen. In contrast to Belgian Pave and Silver creek, the vehicle velocity on the Corrugation alters. Hence, in order to expose the materials for maximum vibration magnitudes, the highest velocity lap was chosen. The velocity for each obstacle is specified in Table 7.

The test was initiated by sending the requested signal to the hexapod, by using a software called RPCPro. The platform motion was based on accelerometer data measured on the front seat rails during complete vehicle testing at HPG. However, the signal for Belgian pave was extracted from accelerometers positioned near the left front wheel. The total signal time for the three track sequences was 132 seconds. The signals for each track sequence are found in Appendix A5. After each finished test, the same preparation process mentioned in the previous section was iterated for the following experiment. A note is that there was no material recovery time specified and the average time between each test was approximately four minutes. The experiments were performed in descending order according to the test plan, which is given in Appendix A6. When all analysis were completed, three experiments on 50 mm thick Sylomer SR11 EN were performed. The aim was to investigate if seat back rest inclination has any contribution on the A(8) value. The angles studied were 10° , 30° and 40° .



Figure 23: a) Accelerometer placed on test material b) Manikin strapped to the backrest c) Manikin feet strapped to the footrest

Table 7: Track sequence and related vehicle speed

Track sequence	Belgian Pave	Silver creek	Corrugation
Vehicle velocity	40 km/h	30 km/h	50 km/h

4.2 TEST 2 – FIRST ROW - VIBRATION INSULATION TARGET LEVEL

The components that were used in this test are shown in Figure 24. A measuring plate was mounted on a hydraulic cylinder. A test fixture was then installed on the hydraulic cylinder. The test fixture was set to the correct rail angle and seat height. An exact rail angle was secured by using a digital protractor. Both angle and height were based on preferences chosen in TEST 1. An aluminum plate (EN AW 5754 h111) was installed on the fixture. The properties of the plate were chosen to prevent occurrence of resonance. The test material was then placed on the aluminum. A dummy weighing 53 kg was positioned on the cushion. The dummy was mounted to a measure arm, which was topped with weights with a mass of 35 kg. In addition, it was assured that the arm did not rest on the material before the test was initiated, to avoid pre-compression. To place the dummy in the middle of the test material, the arm was adjusted, using a measure arm hinge. To assure high accuracy, a laser instrument and a fixture were used to localize the middle point, which is shown in Figure 25. Lastly, accelerometers were mounted on the measuring plate and on the weights. Thus the transfer function between the material and the measuring plate could be calculated and the transmissibility was obtained. A list of hardware and software that were used during the tests are attached in Appendix A7.

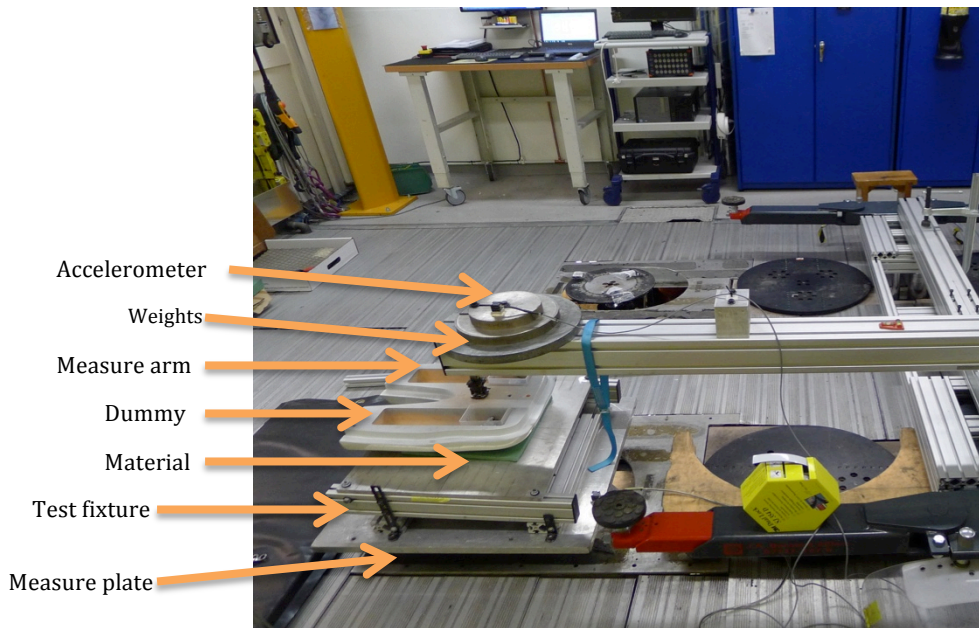


Figure 24: Picture of test setup

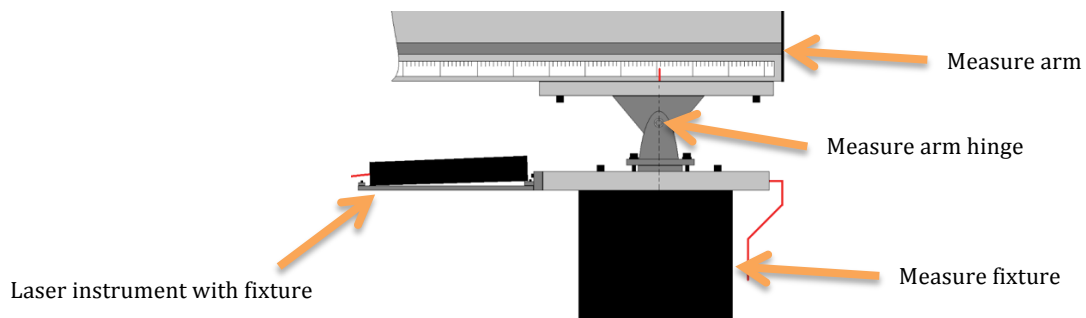


Figure 25: Arrangement for placing the dummy in the middle of the test material

As it already has been stated, only materials and material combinations that yielded promising results from TEST 1 were examined in TEST 2. This is partly true. Regardless result given in TEST 1, some materials had to be examined in TEST 2 for thickness comparison. Material configurations studied in TEST 2 are given in Table 8. As the table shows, some tests involved two materials. In these experiments, the material at the left of the addition was placed bottommost. The actual test time of each configuration was 17.5 minutes. A signal with constant acceleration was swept from 2 Hz to 25 Hz. The corresponding amplitudes descended from 6.2 mm to 0.1 mm respectively. This is illustrated in Figure 26. Note that in this figure, the amplitude in millimeters is given by the vertical axis, while the horizontal axis provides the time in seconds. Each experiment was performed three times, after which the average transmissibility was calculated. However, between each iteration, there was a material recovery time of 25 – 30 minutes.

Table 8: Material configurations tested

Material configuration	Thickness [mm]
Reference	50
Reference + Gel ovations pad	50 + 13
Regufoam Vibration 150 Plus	12
Regufoam Vibration 150 Plus	50
Regufoam Vibration 150 Plus	98
Regufoam Vibration 150 Plus + Gel ovations pad	50 + 13
Relax Easy	60
Star Starlock	50
Sylomer SR11 EN	12,5
Sylomer SR11 EN	50
Sylomer SR11 EN + Gel ovations pad	50 + 13
Sylomer SR11 EN + Regufoam Vibration 150 Plus	98
Sylomer SR11 EN + Regufoam Vibration 150 Plus	148

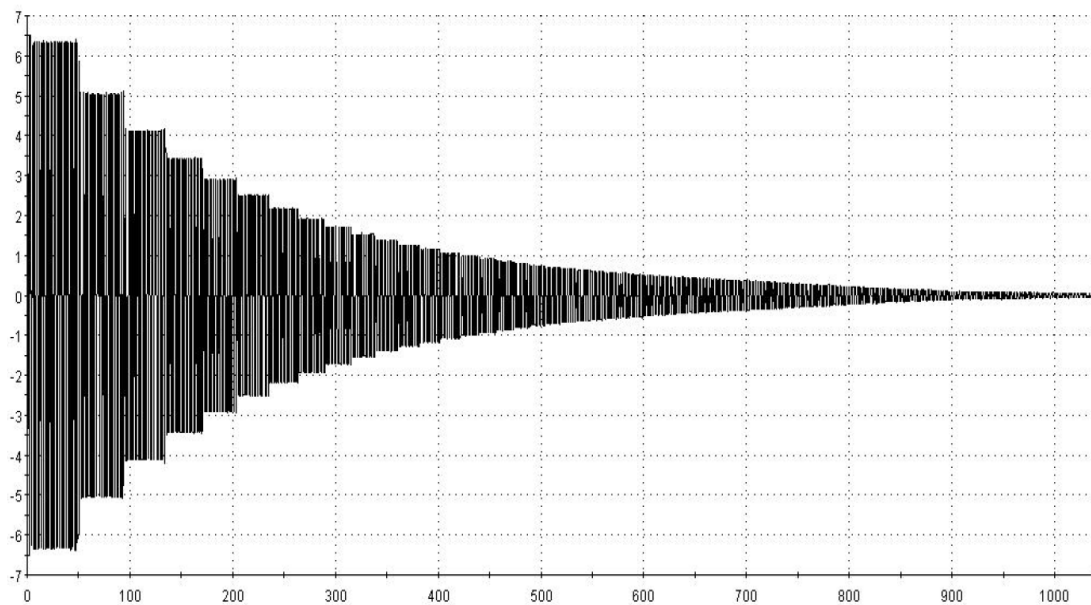


Figure 26: Signal sweep showing amplitude [mm] on the vertical axis and time [s] on the horizontal axis

4.3 TEST 3 – HÄLLERED PROVING GROUND

In order to validate the performance of the current foam pad, four tests were completed at HPG. In two of the tests, Gel oventions pad and Star Starlock were placed on the seat cushion. In addition, a third test was done with the seat in original formation, i.e. without any foam pads installed. Since TEST 1 was simplified in relation to reality, performing additional tests in complete car, could also confirm the results that were finalized in the hexapod. Similar to the tests completed in the hexapod, the drive cycle involved Belgian pave, Silver creek and the Corrugation. For each obstacle, the vehicle was driven at the velocities seen in Table 7. A driver weighing 75 kg was used in the experiments. The WBV transmitted to the driver was measured with the accelerometer shown in Figure 23 a). This was placed between the operator's buttock and the cushion. Lastly, the seat back rest inclination was set to 20°.

5 RESULTS

This section presents results from TEST 1, TEST 2 and TEST 3. Thus the outcomes are based on practical tests only. Solely results from TEST 1, which highest and lowest A(8) values are presented. The reader is referred to Appendix A6 for all numbers.

5.1 TEST 1 – HEXAPOD

This subchapter delivers results that are given from experiments in the hexapod.

5.1.1 PUR FOAM

Table 9 presents results obtained for tests performed on the PUR foams. The third column from left yields frequency-weighted accelerations, while fourth and fifth column show the daily exposure action and the exposure limit values respectively. As the table shows, a pattern is seen between increased foam thickness and drive time. A comparison in foams at a thickness of 50 mm indicates that Sylomer yields highest drive time, before exceeding the exposure values. Furthermore, a remarkable difference in drive times is seen between Sylomer and Regufoam when comparing the thinnest blocks. The results for 86 mm confirm that the drive time can be increased with 35 %, only by changing the material. Figure 27 illustrates plotted graphs for Regufoam. This material is used in this example since more plotting points are available. The figure displays how time rate deviates with increased foam thickness. Both plots confirm similar behavior as the thicknesses grow, indicating that the time derivatives decrease in three segments. The highest rate is yielded initially, while no change or degradation is given as the thickness increases from 86 – 98 mm.

Table 9: The table shows values gained from testing PUR foams, with seat back rest inclined 20° from the z-axis

Material	Thickness [mm]	a_w [m/s ²]	A(8)_action [min]	A(8)_limit [min]
Reference	37.5	2.69	16	87
Reference	50	2.98	13	71
Reference	86	2.44	20	106
Sylomer	12.5	2.59	17	94
Sylomer	25	2.59	17	94
Sylomer	37.5	2.28	23	122
Sylomer	50	2.24	23	126
Regufoam	12	2.84	14	78
Regufoam	24	2.64	17	91
Regufoam	36	2.39	21	111
Regufoam	50	2.32	22	118
Regufoam	86	2.1	27	143
Regufoam	98	2.11	27	142

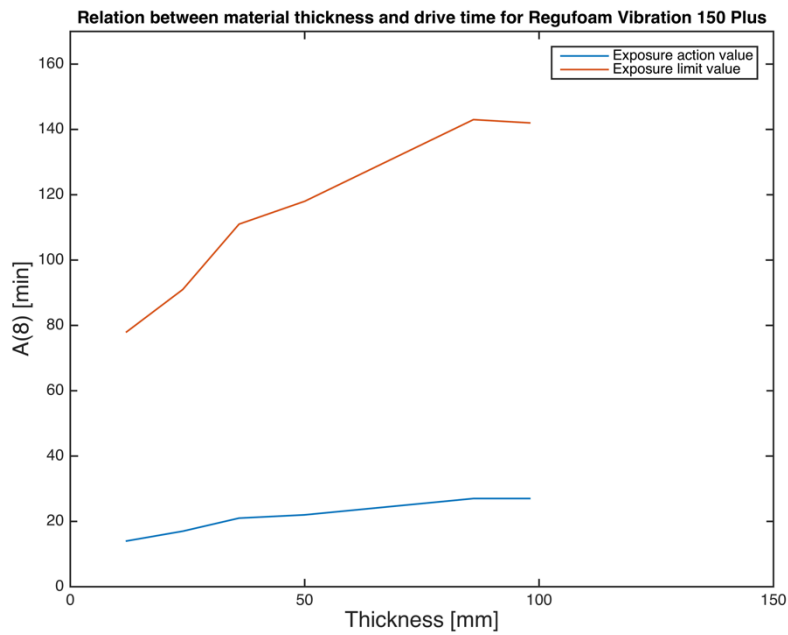


Figure 27: Relation between increased material thickness and drive time, until daily exposure action and exposure limit value are surpassed

5.1.2 PUR FOAM + GEL OVATIONS PAD

Table 10 presents results from experiments involving material combinations of PUR foam and Gel oventions pad. The exposure times indicate that this kind of material arrangement decreases the drive time compared to results yielded in Table 9. Sylomer and Regufoam, provides fairly similar performance at 50 mm thickness. In addition, the thinnest blocks of these two materials yield exposure values, related to the reference material at 37.5 mm thickness. A decrease in drive time is obtained for Sylomer, while the thickness increases from 12.5 – 25 mm. Note that there is no test result presented for the reference material and Regufoam at 86 mm thickness.

A comparison of increased material thickness and drive time is shown in Figure 28, which illustrates the behavior when Regufoam and Gel oventions pad are stacked. The figure shows an iterative pattern, where the drive time initially increases with raised PUR thickness. However, the gradient becomes constant while the foam thickness is increased from 36 – 50 mm and thus same drive time is obtained. The same pattern is repeated as the thickness grows additionally.

Table 10: The table shows values gained from testing PUR foams combined with Gel oventions pad, with seat back rest inclined 20° from the z-axis

Material	Thickness [mm]	a_w [m/s ²]	A(8)_action [min]	A(8)_limit [min]
Reference + Gel oventions pad	37.5 + 13	2.80	15	80
Reference + Gel oventions pad	50 + 13	2.61	17	92
Sylomer + Gel oventions pad	12.5 + 13	2.66	16	89
Sylomer + Gel oventions pad	25 + 13	2.74	15	84
Sylomer + Gel oventions pad	37.5 + 13	2.47	19	103
Sylomer + Gel oventions pad	50 + 13	2.36	21	113
Regufoam + Gel oventions pad	12 + 13	2.79	15	81
Regufoam + Gel oventions pad	24 + 13	2.64	17	91
Regufoam + Gel oventions pad	36 + 13	2.64	17	91
Regufoam + Gel oventions pad	50 + 13	2.32	22	117
Regufoam + Gel oventions pad	98 + 13	2.29	22	121

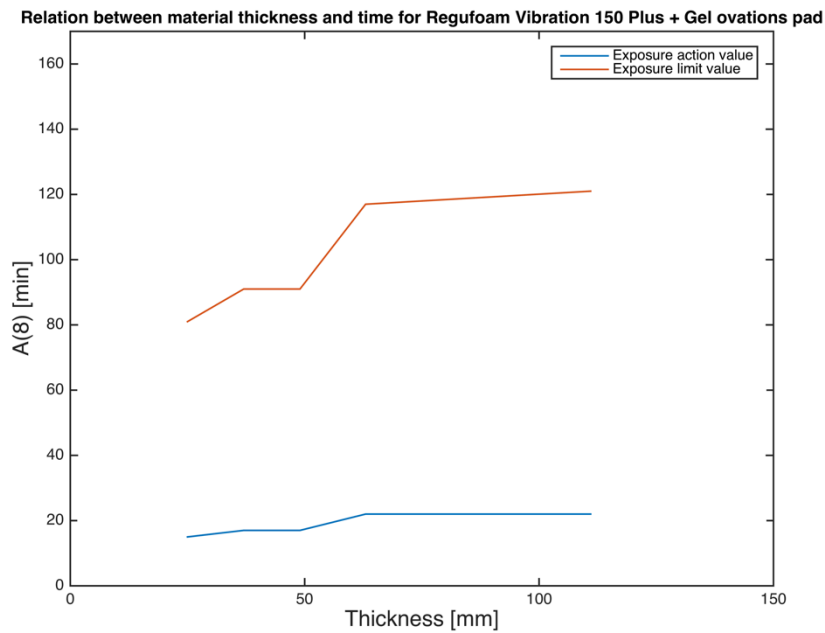


Figure 28: Relation between increased material thickness and drive time, until daily exposure action and exposure limit value are surpassed

5.1.3 PUR + STAR STARLOCK

Results from seven experiments involving Star Starlock are displayed in Table 11. From the table, it can be concluded that highest drive time is achieved by using the material alone. The exposure values are gained within less time, as soon as it is joined with presented PUR foams. However, when combined with Reference, the drive time increases, as the foam gets thicker. There are no significant changes confirmed in the tests with Sylomer. Thus, the same drive time remains even when foam thickness develops. Referring to Table 8, another observation is that merging Sylomer 12.5 mm and Sylomer 25 mm respectively with Star Starlock, delays the action value compared to when these thicknesses of Sylomer are used solely. However, this is not true for Sylomer thicker than 25 mm. Figure 29 shows how time rate stagnates when using both Star Starlock and Sylomer. Note that Regufoam is excluded from this particular study.

Table 11: The table shows values gained from testing Star Starlock, both solely and combined with PUR foams, with seat back rest inclined 20° from the z-axis

Material	Thickness [mm]	a_w [m/s ²]	A(8)_action [min]	A(8)_limit [min]
Star Starlock	50	2.08	27	146
Reference + Star Starlock	37.5 + 50	2.3	22	119
Reference + Star Starlock	50 + 50	2.66	24	131
Sylomer + Star Starlock	12.5 + 50	2.36	21	113
Sylomer + Star Starlock	25 + 50	2.44	20	106
Sylomer + Star Starlock	37.5 + 50	2.40	20	109
Sylomer + Star Starlock	50 + 50	2.45	20	105

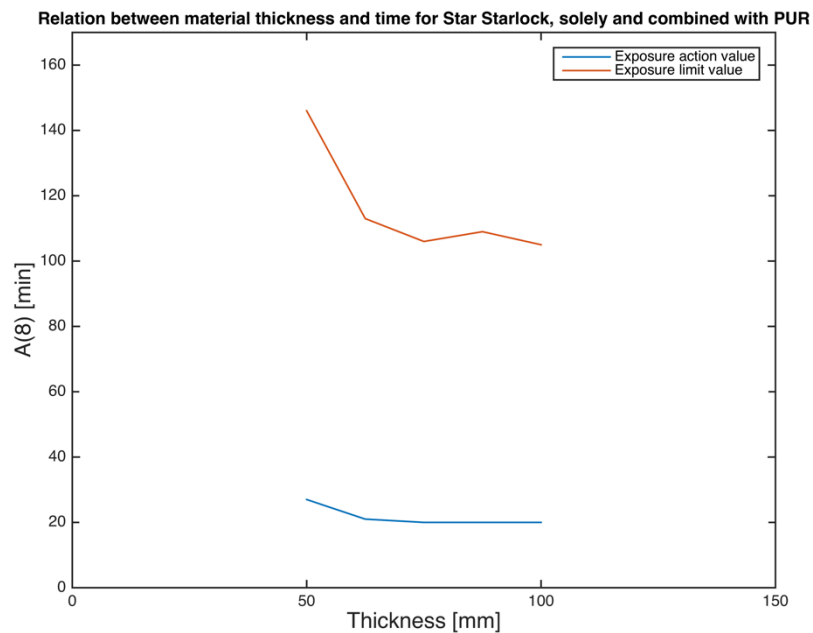


Figure 29: Relation between increased material thickness and drive time, until daily exposure action and exposure limit value are surpassed

5.1.4 NATURAL AND BUTYL RUBBER

Table 12 presents results gained from tests for natural rubber and butyl rubber. It is confirmed that both rubber types provide analogous results, even though the thickness is altered. Hence, there is no need to graphically present the drive time as function of the thickness. There are no significant improvements when the rubbers pads are stacked with PUR foams. Therefore these results are not presented and the reader is thus referred to Appendix A6 for further studies.

Table 12: The table shows values gained from testing natural and butyl rubber, with seat back rest inclined 20° from the z-axis

Material	Thickness [mm]	a_w [m/s ²]	A(8)_action [min]	A(8)_limit [min]
Natural rubber	5	3.10	12	65
Natural rubber	10	3.11	12	65
Natural rubber	15	3.19	11	62
Butyl rubber	5	3.33	10	57
Butyl rubber	10	3.16	12	63
Butyl rubber	15	3.42	10	54

5.1.5 148 mm PUR

Table 13 provides results for 148 mm merged PUR foams. The same test occurs twice with changed orders in how the products were stacked. In Table 8, it is confirmed that 98 mm thick Regufoam allows 27 minutes of driving. Increasing the thickness with 51 % (148 mm) extends the driving time with 7 % (29 minutes). However, in the latter case, this assumes that both Regufoam and Reference are used simultaneously.

Table 13: The table shows values gained from testing 148 mm thick PUR, with seat back rest inclined 20° from the z-axis

Material	Thickness [mm]	a_w [m/s ²]	A(8)_action [min]	A(8)_limit [min]
Regufoam + Reference	98 + 50	2	29	157
Reference + Regufoam	50 + 98	2.13	26	139
Regufoam + Sylomer	98 + 50	2.06	28	149
Sylomer + Regufoam	50 + 98	2.15	25	137

5.1.6 SEAT BACK REST INCLINATION

Table 14 presents the results, which are obtained for varied seat back rest inclination. The angle indicates how much the back support deviates from the z-axis. The outcome for 20° has already been provided in Table 8. As the chart shows, highest drive time is given for 20° inclination.

Table 14: The table shows values gained from testing 50 mm Sylomer, with seat back rest angle altered

Material	Thickness [mm]	Back rest angle	a_w [m/s ²]	A(8)_action [min]	A(8)_limit [min]
Sylomer	50	10°	2.7	16	87
Sylomer	50	20°	2.24	23	126
Sylomer	50	30°	2.67	16	89
Sylomer	50	40°	2.59	14	77

5.2 TEST 2 – FIRST ROW - VIBRATION INSULATION TARGET LEVEL

This subchapter provides transmissibility curves for the materials mentioned in Table 8. Figure 7 in Chapter 2.3 provides frequency-weighted accelerations as a function of time. The transmissibility is here based on frequency level. The translation from decibel to acceleration is also given in Figure 7. In following figures that are presented in this chapter, include two requirements. MIN requirement refers to the daily exposure action value, while MAX requirement regulates the daily exposure limit value. However, the limits assume that the test setup includes a complete seat and not only blocks of material. The damping ratio is derived from the half power bandwidth method, which was introduced in Chapter 2.2.1.

50 mm Reference

Figure 30 illustrates the transmissibility curve for the reference material with a thickness of 50 mm. As the figure shows, resonance occurs at 7.25 Hz, with corresponding transmissibility amplitude equivalent to 6.37 dB. Note that the transmissibility also is given as dimensionless amplitude. Thus, isolation is obtained at 10.88 Hz. Table 15 concludes the parameters, including the calculated damping ratio.

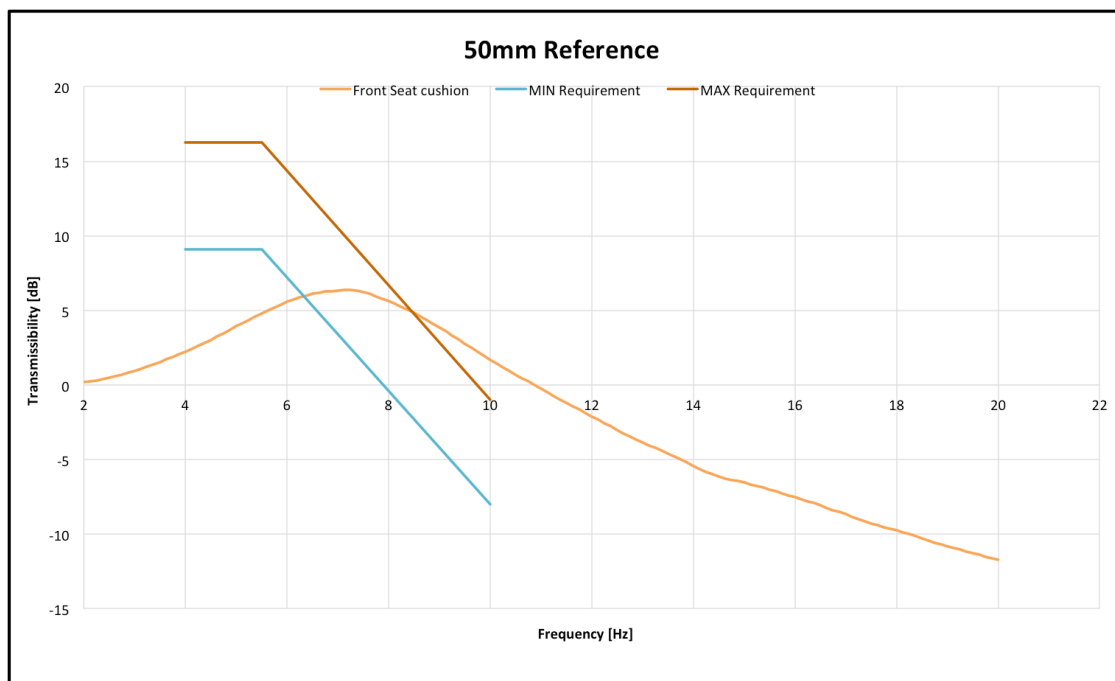


Figure 30: Transmissibility plot for 50 mm Reference

Table 15: The chart provides frequencies and related transmissibility for 50 mm Reference. Damping ratio is also given

Parameter	Resonance	f_2	f_1	Isolation	ζ
Frequency [Hz]	7.25	9.25	4.63	10.88	
Transmissibility [dB]	6.37	3.33	3.33	0	
Transmissibility	2.08	1.47	1.47	1	
Damping ratio	-	-	-	-	0.32

50 mm Reference + Gel oventions pad

In this section, results are shown for 50 mm Reference combined with Gel oventions pad. These are presented in Figure 31. It is concluded that resonance occurs at 6.75 Hz, with related transmissibility measuring 6.25 dB. As it is seen in Table 16, the vibration is isolated at 10.50 Hz. The derived damping ratio is 0.33.

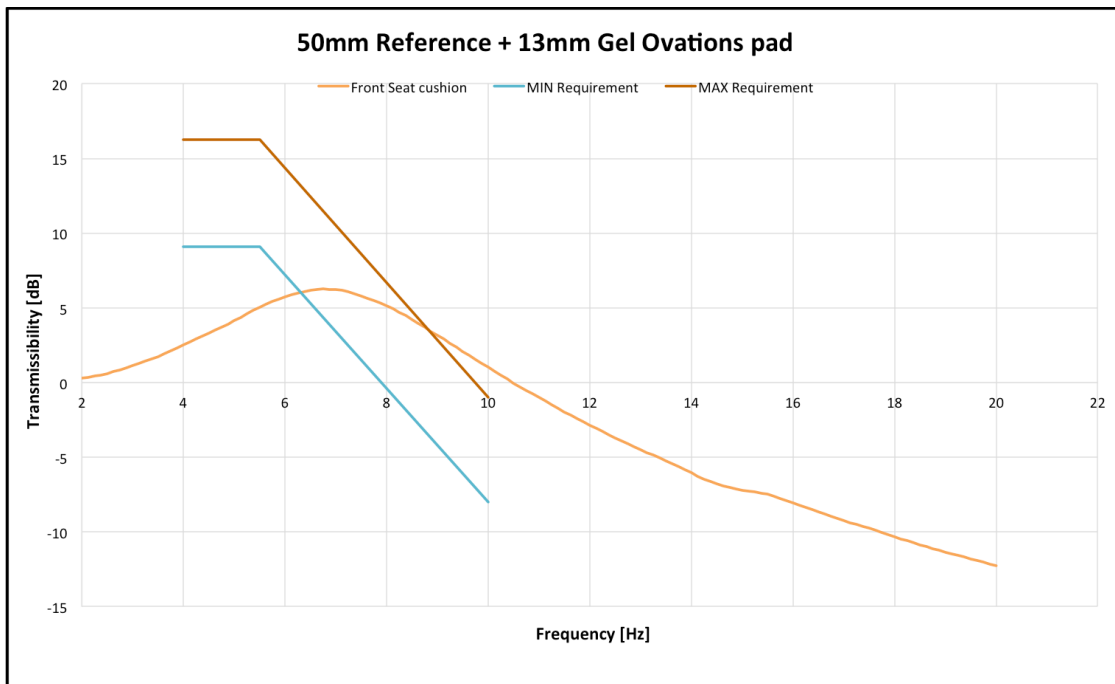


Figure 31: Transmissibility plot for 50 mm Reference combined with Gel oventions pad

Table 16: The chart provides frequencies and related transmissibility for 50 mm Reference combined with Gel oventions pad. Damping ratio is also given

Parameter	Resonance	f_2	f_1	Isolation	ζ
Frequency [Hz]	6.75	8.96	4.46	10.50	
Transmissibility [dB]	6.25	3.25	3.25	0	
Transmissibility	2.05	1.45	1.45	1	
Damping ratio	-	-	-	-	0.33

12 mm Regufoam

The results for 12 mm Regufoam, seen in Figure 32, display a different behavior compared to previous analysis presented in this chapter. The plot shows that the frequency is amplified at 13.00 Hz and thus isolation is obtained at 19.25 Hz. Resulting transmissibility at amplification is 8.58 dB, while the damping ratio is 0.21. The figures are summarized in Table 17.

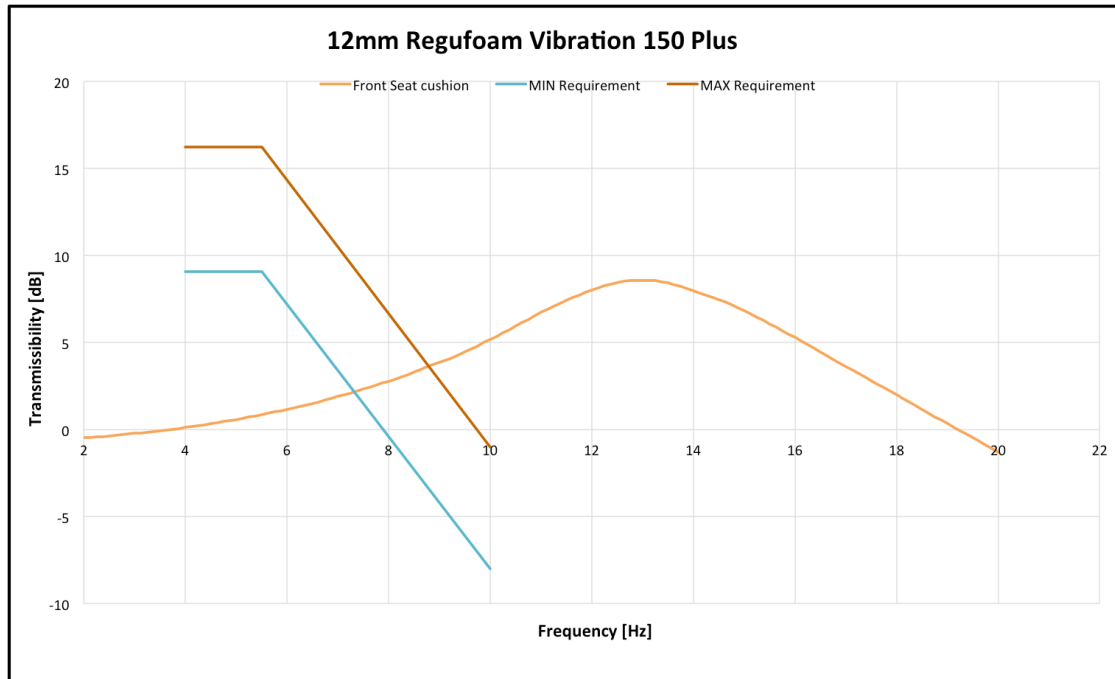


Figure 32: Transmissibility plot for 12 mm Regufoam

Table 17: The chart provides frequencies and related transmissibility for 12 mm Reference. Damping ratio is also given

Parameter	Resonance	f_2	f_1	Isolation	ζ
Frequency [Hz]	13.00	15.80	10.27	19.25	
Transmissibility [dB]	8.59	5.59	5.59	0	
Transmissibility	2.69	1.9	1.9	1	
Damping ratio	-	-	-	-	0.21

50 mm Regufoam

From the graph presented in Figure 33, it is seen that resonance is gained at 8.75 Hz. This means that the oscillation is isolated at 13.38 Hz. Furthermore, the calculated damping ratio is 0.13. This value yields higher transmissibility at amplification. The numbers are presented in Table 18.

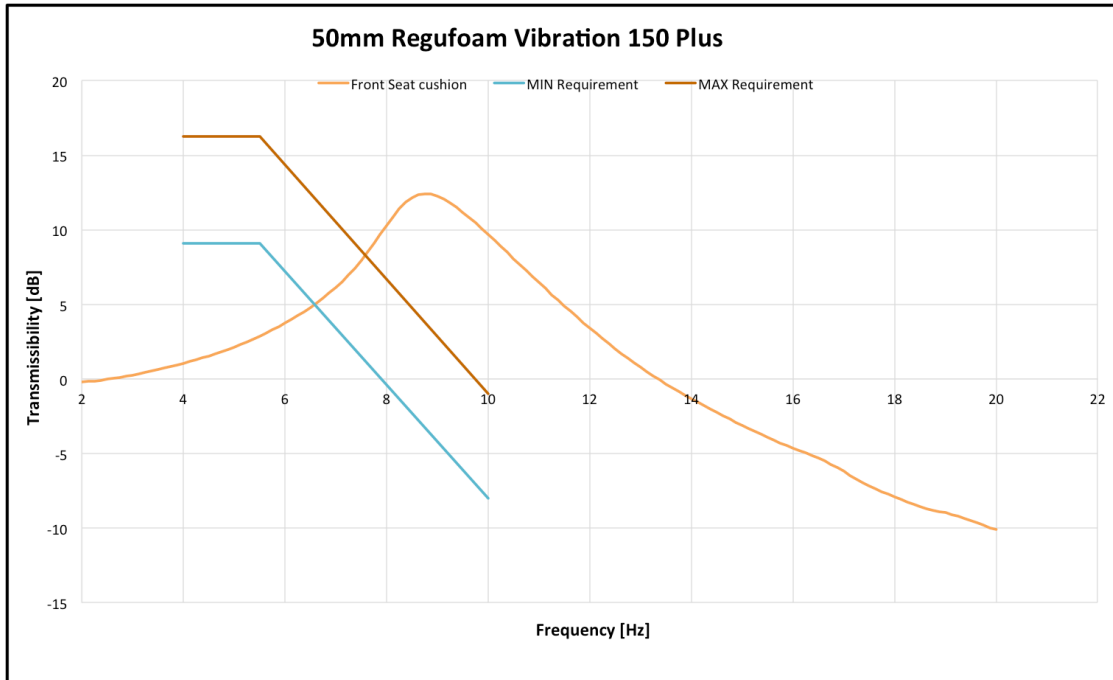


Figure 33: Transmissibility plot for 50 mm Regufoam

Table 18: The chart provides frequencies and related transmissibility for 50 mm Regufoam. Damping ratio is also given

Parameter	Resonance	f_2	f_1	Isolation	ζ
Frequency [Hz]	8.75	10.06	7.82	13.38	
Transmissibility [dB]	12.43	9.43	9.43	0	
Transmissibility	4.18	2.96	2.96	1	
Damping ratio	-	-	-	-	0.13

98 mm Regufoam

In this test, shown in Figure 34, foam thickness is almost doubled compared to the previous one. Even if roughly same transmissibility is attained at resonance, the frequency at which amplification occurs is lowered to 7.5 Hz. Isolation is gained at 11.38 Hz and the damping ratio is 0.13. The numbers are presented in Table 19.

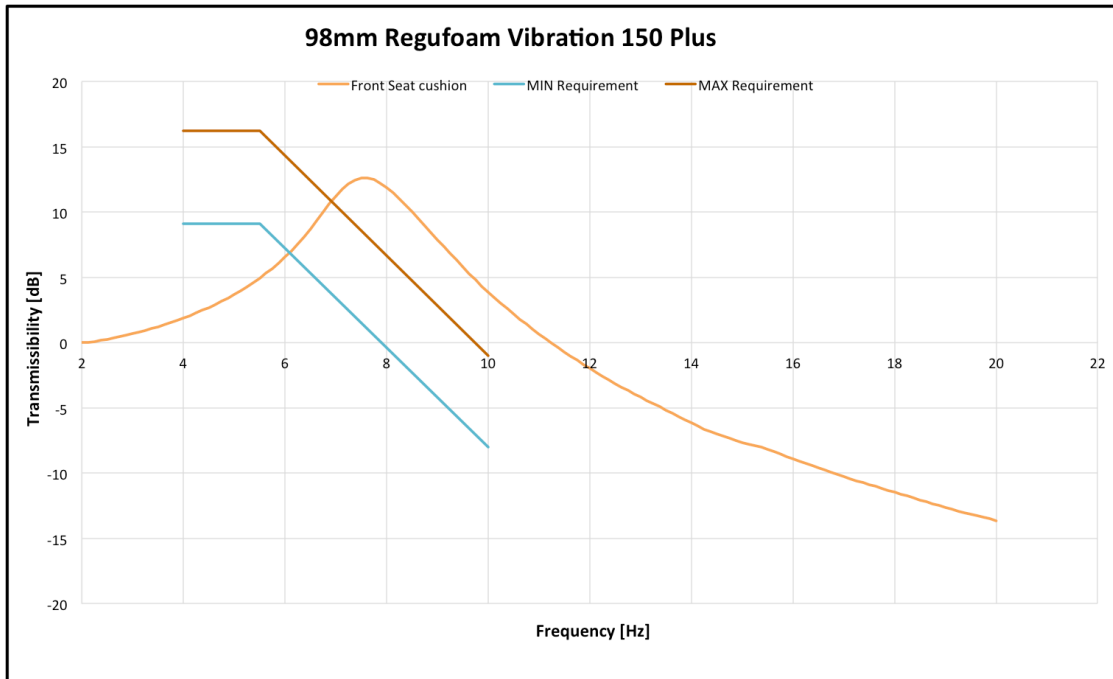


Figure 34: Transmissibility plot for 98 mm Regufoam

Table 19: The chart provides frequencies and related transmissibility for 98 mm Regufoam. Damping ratio is also given

Parameter	Resonance	f_2	f_1	Isolation	ζ
Frequency [Hz]	7.5	8.60	6.66	11.38	
Transmissibility [dB]	12.62	9.62	9.62	0	
Transmissibility	4.28	3.03	3.03	1	
Damping ratio	-	-	-	-	0.13

50 mm Regufoam + Gel ovations pad

Earlier in this chapter, results from transmissibility test on 50 mm were presented. In this study, the effects of Gel ovations pad merged to 50 mm Regufoam are analyzed. Figure 35 illustrates that resonance is given at 9.88 Hz. The resulting transmissibility is 10.11 dB, which gives a damping ratio of 0.17. In addition, isolation is achieved at 14.55 Hz. The results are shown in Table 20.

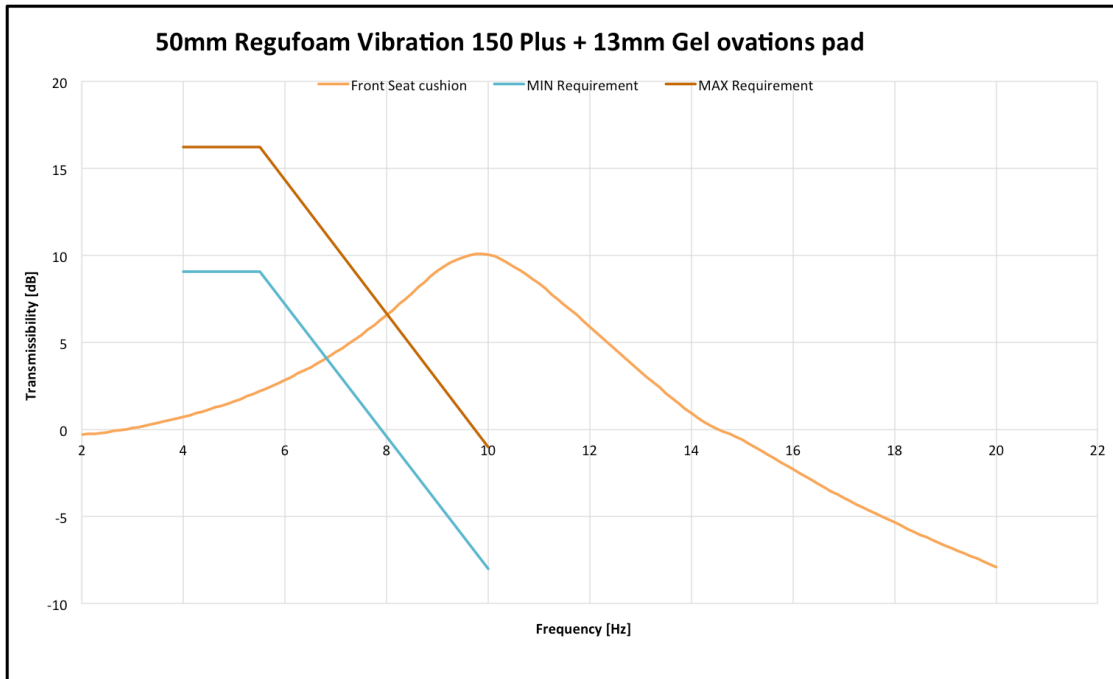


Figure 35: Transmissibility plot for 50 mm Regufoam combined with Gel ovations pad

Table 20: The chart provides frequencies and related transmissibility for 50 mm Regufoam combined with Gel ovations pad. Damping ratio is also given

Parameter	Resonance	f_2	f_1	Isolation	ζ
Frequency [Hz]	9.88	11.54	8.20	14.55	
Transmissibility [dB]	10.11	7.11	7.11	0	
Transmissibility	3.2	2.27	2.27	1	
Damping ratio	-	-	-	-	0.17

Relax Easy

As it has been mentioned, a recovery time of 20 – 25 minutes is needed between each test iteration. However, 45 minutes of recovery was required for this material. Figure 36 shows transmissibility characteristics of Relax Easy. The graph indicates that amplification is obtained at 16.13 Hz. Moreover, same figure demonstrates that isolation region is never achieved. Numbers are given in Table 21.

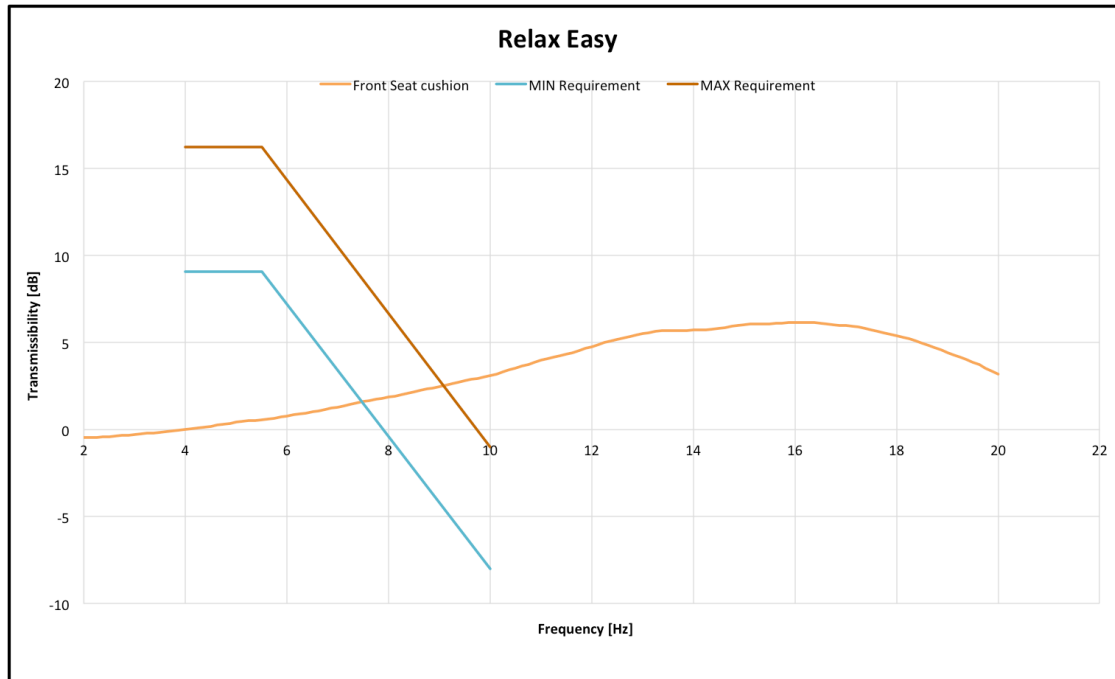


Figure 36: Transmissibility plot for Relax Easy

Table 21: The chart provides frequencies and related transmissibility for Relax Easy. Damping ratio is also given

Parameter	Resonance	f_2	f_1	Isolation	ζ
Frequency [Hz]	16.13	20.00	9.92	-	
Transmissibility [dB]	6.17	3.17	3.17	0	
Transmissibility	2.03	1.44	1.44	1	
Damping ratio	-	-	-	-	0.31

Star Starlock

Figure 37 gives the behavior of Star Starlock men exposed to vibrations in the range 2 – 20 Hz. As the figure shows, resonance occurs 8.63 Hz, with resulting transmissibility of 13.77 dB. Furthermore, isolation is reached at 13.75 Hz and as seen in Table 22, the damping ratio is 0.13.

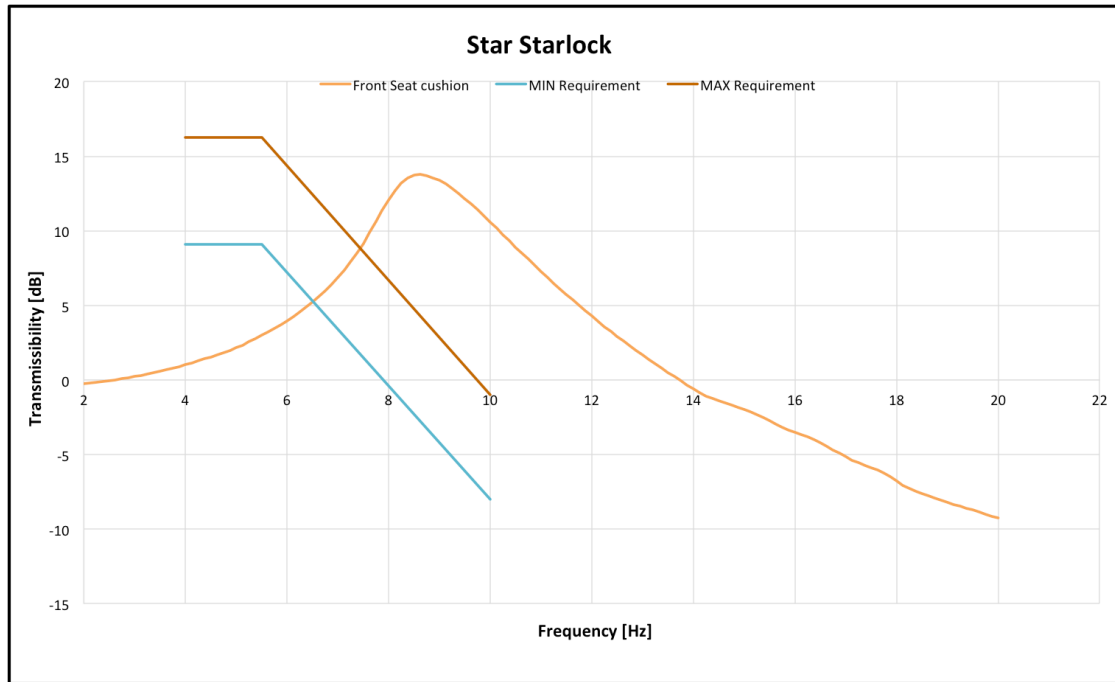


Figure 37: Transmissibility plot for Star Starlock

Table 22: The chart provides frequencies and related transmissibility for Star Starlock. Damping ratio is also given

Parameter	Resonance	f_2	f_1	Isolation	ζ
Frequency [Hz]	8.63	9.81	7.77	13.75	
Transmissibility [dB]	13.77	10.77	10.77	0	
Transmissibility	4.88	3.46	3.46	1	
Damping ratio	-	-	-	-	0.13

12.5 mm Sylomer

Figure 38 illustrates the behavior of 12.5 mm Sylomer. Resonance is gained at 13.88 Hz, with corresponding transmissibility of 9.51 dB. As the graph shows, the isolation region is never reached. In addition, the damping ratio is estimated to 0.19. The values are presented in Table 23.

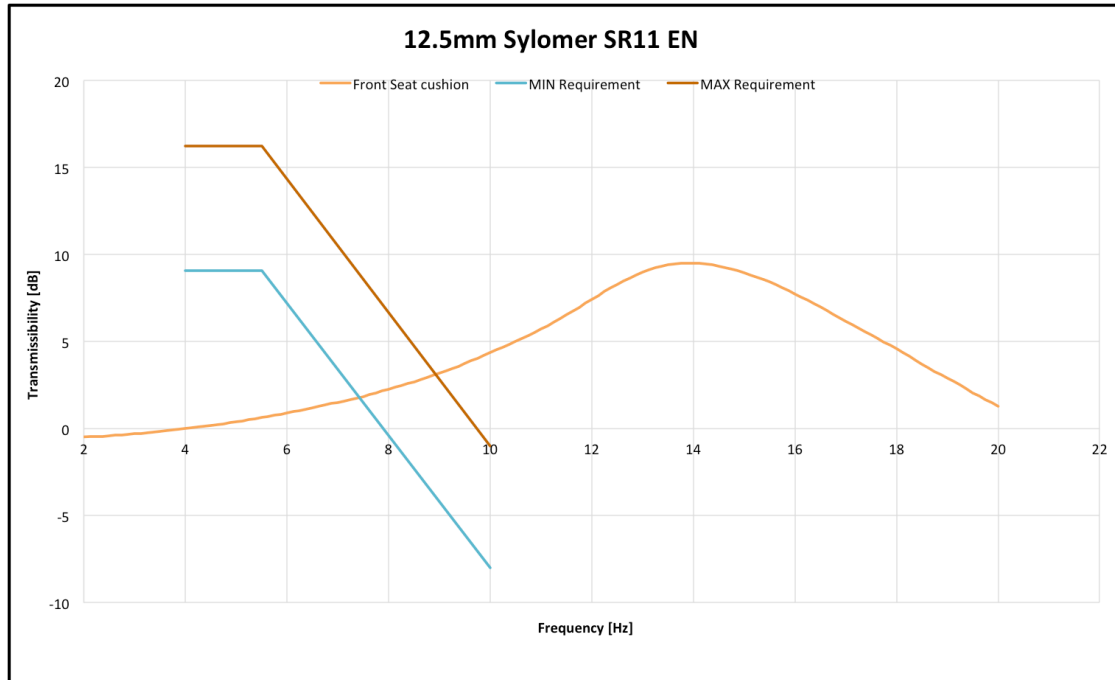


Figure 38: Transmissibility plot for 12.5 mm Sylomer

Table 23: The chart provides frequencies and related transmissibility for 12.5 mm Sylomer. Damping ratio is also given

Parameter	Resonance	f_2	f_1	Isolation	ζ
Frequency [Hz]	13.88	16.81	11.48	-	
Transmissibility [dB]	9.51	6.51	6.51	0	
Transmissibility	2.99	2.12	2.12	1	
Damping ratio	-	-	-	-	0.19

50 mm Sylomer

In Figure 39, transmissibility characteristic of 50 mm Sylomer is seen. The figure confirms that resonance appears at 8.50 Hz and corresponding transmissibility is 9.19 dB. In addition, the oscillations are isolated at 12.62 Hz. The characteristic yields a damping ratio of 0.19. The numbers are summarized in Table 24.

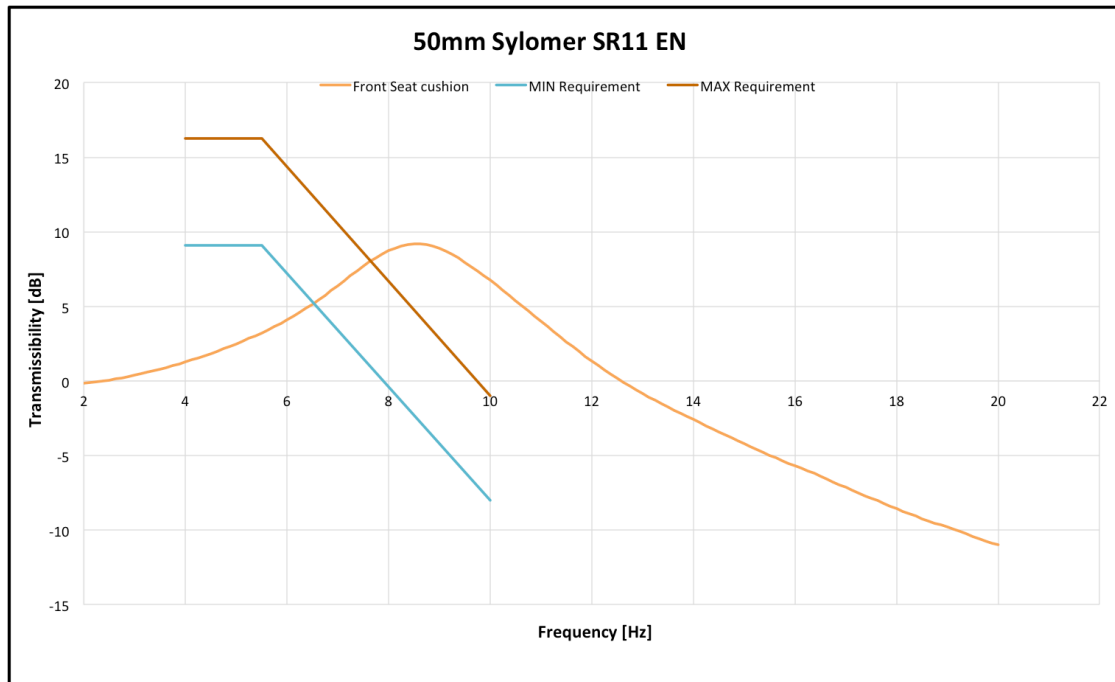


Figure 39: Transmissibility plot for 50 mm Sylomer

Table 24: The chart provides frequencies and related transmissibility for 50 mm Sylomer. Damping ratio is also given

Parameter	Resonance	f_2	f_1	Isolation	ζ
Frequency [Hz]	8.50	10.23	6.94	12.62	
Transmissibility [dB]	9.19	6.19	6.19	0	
Transmissibility	2.88	2.04	2.04	1	
Damping ratio	-	-	-	-	0.19

50 mm Sylomer + Gel ovations pad

In order to understand transmissibility behavior of Gel ovations pad, it was tested with 50 mm Sylomer. Figure 40 can be related to the previous experiment, in which same thickness of Sylomer was tested alone. As Figure 40 shows, the resonance frequency is increased from 8.50 – 9.88 Hz. However, the agreeing transmissibility is reduced from 9.19 – 8.53 dB. Isolation for this setup is given at 14.50 Hz and the damping ratio is 0.21. The chart in Table 25 provides a summary the numbers.

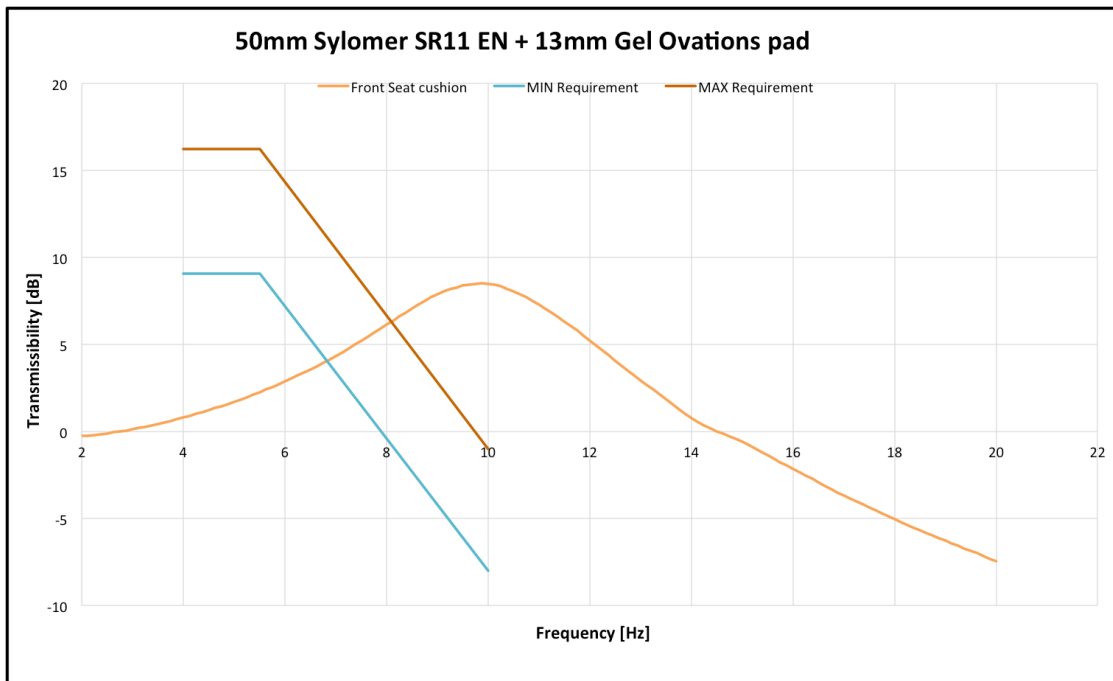


Figure 40: Transmissibility plot for 50 mm Sylomer combined with Gel ovations pad

Table 25: The chart provides frequencies and related transmissibility for 50 mm Sylomer combined with Gel ovations pad. Damping ratio is also given

Parameter	Resonance	f_2	f_1	Isolation	ζ
Frequency [Hz]	9.88	11.88	7.68	14.50	
Transmissibility [dB]	8.53	5.53	5.53	0	
Transmissibility	2.67	1.89	1.89	1	
Damping ratio	-	-	-	-	0.21

50 mm Sylomer + 50 mm Regufoam

Figure 41 studies a case where the foam thickness has been increased significantly. The intention is to gain additional knowledge regarding how this may affect the transmissibility. In this test, the total foam thickness is 100 mm. Seen from Figure 41, amplification is achieved at 7.38 Hz with related transmissibility of 11.79 dB. Thus, isolation occurs at 10.85 Hz. The estimated damping ratio is seen in Table 26.

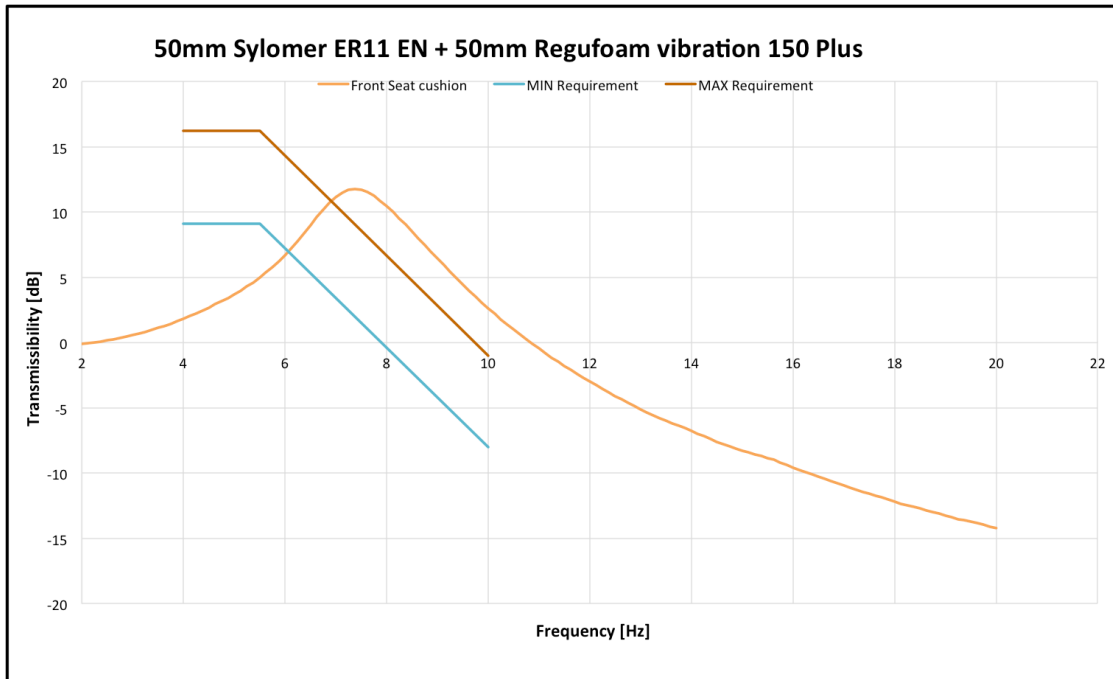


Figure 41: Transmissibility plot for 50 mm Sylomer combined with 50 mm Regufoam

Table 26: The chart provides frequencies and related transmissibility for 50 mm Sylomer combined with 50 mm Regufoam. Damping ratio is also given

Parameter	Resonance	f_2	f_1	Isolation	ζ
Frequency [Hz]	7.38	8.44	6.46	10.85	
Transmissibility [dB]	11.79	8.79	8.79	0	
Transmissibility	3.89	2.75	2.75	1	
Damping ratio	-	-	-	-	0.13

50 mm Sylomer + 98 mm Regufoam

The last experiment performed in TEST 2 shows that the resonance frequency is reduced, with increased foam thickness. On the contrary, the peak transmissibility is increased, which yields a damping ratio of 0.13. In this particular test, amplification occurs at 6.88 Hz and the peak transmissibility is 12.69 dB. In addition, Figure 42 illustrates that isolation is attained 10.17 Hz. The numbers are concluded in Table 27.

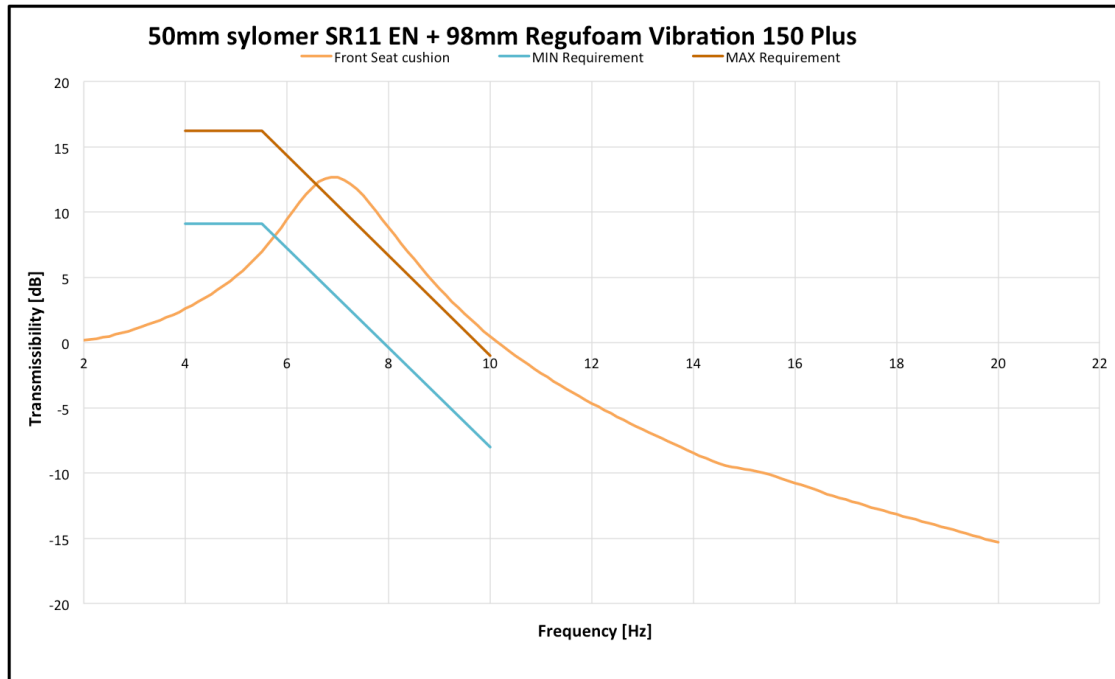


Figure 42: Transmissibility plot for 50 mm Sylomer combined with 98 mm Regufoam

Table 27: The chart provides frequencies and related transmissibility for 50 mm Sylomer combined with 98 mm Regufoam. Damping ratio is also given

Parameter	Resonance	f_2	f_1	Isolation	ζ
Frequency [Hz]	6.88	7.83	6.03	10.17	
Transmissibility [dB]	12.69	9.69	9.69	0	
Transmissibility	4.31	3.05	3.05	1	
Damping ratio	-	-	-	-	0.13

5.2.1 TEST 2 – SUMMARY

A test summary is shown in Table 28. This aim is to simplify the comparison in results from the performed transmissibility experiments. Presented parameters for each material are resonance frequency, corresponding transmissibility, isolation frequency and damping ratio.

Table 28: Summary of results gained from TEST 2

Experiment	Resonance frequency [Hz]	Transmissibility [dB] / [amplitude]	Isolation frequency [Hz]	ζ
50 mm Reference	7.25	6.37 / 2.08	10.88	0.32
50 mm Reference + Gel ovations pad	6.75	6.25 / 2.05	10.50	0.33
12 mm Regufoam	13.00	8.59 / 2.69	19.25	0.21
50 mm Regufoam	8.75	12.43 / 4.18	13.38	0.13
98 mm Regufoam	7.5	12.62 / 4.28	11.38	0.13
50 mm Regufoam + Gel ovations pad	9.88	10.11 / 3.2	14.55	0.17
Relax Easy	16.13	6.17 / 2.03	-	0.31
Star Starlock	8.63	13.77 / 4.88	13.75	0.13
12.5 mm Sylomer	13.88	9.51 / 2.99	-	0.19
50 mm Sylomer	8.50	9.19 / 2.88	12.62	0.19
50 mm Sylomer + Gel ovations pad	9.88	8.53 / 2.67	14.50	0.21
50 mm Sylomer + 50 mm Regufoam	7.38	11.79 / 3.89	10.85	0.13
50 mm Sylomer + 98 mm Regufoam	6.88	12.69 / 4.31	10.17	0.13

5.3 TEST 3 – HÄLLERED PROVING GROUND

The results from the test at HPG are summarized in Table 29. The chart shows that Gel oventions pad provides least drive time before reaching the action value. It is also evident that driving with an addition of Star Starlock or the current pad solution increases the drive time. A comparison between these two pads, confirm similar results. The performance of Star Starlock is reduced compared to TEST 1, since a drive time of 27 minutes is noted for this test.

Table 29: The table shows values gained from testing various additive pads in complete vehicle. The seat back rest is inclined 20° from the z-axis

Material	Thickness [mm]	a_w [m/s ²]	A(8)_action [min]	A(8)_limit [min]
Star Starlock	50	2.23	24	127
Current pad	3 x 19	2.28	23	122
Gel oventions pad	13	2.84	14	78
No pad	-	2.72	16	85

6 DISCUSSION

This chapter will discuss test results based on relevant theory presented in this report.

6.1 INTERPRETATION OF RESULTS

The transmissibility tests yield clear evidence of material behavior when exposed to oscillations between 2 – 20 Hz. Knowledge of material response is essential, since the frequency ranges for different obstacles transmitted to the driver are already known. From the FFT analysis, it is confirmed that frequencies around 11 Hz have highest acceleration magnitude per HZ for Silver creek. Additionally, the same disturbing frequency is found to be most critical for Belgian pave. By theory, this means that if any of the materials succeed to isolate these frequencies, the exposure and thus the A(8) value must be decreased. However, it should be clarified that, even though global maxima are confirmed, the power contain is not gained until a PSD is completed. In addition, these critical frequencies, at which the oscillations occur, are only encountered for the chosen time interval. Another time range may show a different appearance. Unfortunately, due to lack of time, a FFT has not been completed for the Corrugation. Hence, the frequency ranges are therefore unknown. However, as seen in Appendix A4, the time signal is not only shorter, but the acceleration magnitudes are also smaller for the Corrugation, compared to those obtained for Silver creek and Belgian Pave. Hence, applying Equation (11) will yield a lower A(8) for this track sequence.

Observing Table 28, it is seen that four material setups have the ability to isolate the provided disturbances from Silver creek and Belgian Pave, as each material has associated isolation frequency less than 11 Hz. However, it may already have been noticed that the isolation frequencies presented in Table 28 do not comply with the theory explained in Chapter 2.2. The table shows that when resonance occurs, the point at which isolation is reached, is greater than $\sqrt{2}$. This is most likely due to the fact that the signal is filtered. Thus, an average value is yielded, which deviates from the theoretical isolation frequency. Furthermore, the chart verifies a decrease in resonance frequency with increased thickness. However, reduced resonance frequency gives higher transmissibility at amplification. This can probably be explained by material data found in Appendix A5, which confirms that the natural frequency decreases with increased foam thickness. Taking Equation (5) into consideration, it is confirmed that reduction in natural frequency magnifies the transmissibility. In addition, transmissibility is also related to the damping ratio. The results for 12.5 mm Sylomer and 12 mm Regufoam seen in Table 28, illustrate a different behavior. This is most likely due to the fact that the blocks are too thin. Therefore, transmissibility of the aluminum fixture has been measured instead. However, it is not clear how thick each material needs to be in order to eliminate influences from the aluminum plate. Therefore, the plate may have influenced other results in TEST 2 as well. This is also one of the advantages of having a seat attached to the fixture, rather than only foam blocks, since the seat frame most likely eliminates these types of errors.

Increased damping is seen in experiments performed with Gel ovals pad. This is most likely thanks to high viscosity, which appears in the silicon. High rate of viscosity is possibly also found in Relax Easy, since amplification appears at a higher frequency and low transmissibility is obtained. This probably implies that these two viscoelastic materials behave viscously rather than elastically and thus have a higher $\tan \delta$ compared to the PUR blocks. Consequently, extended recovery time is required, as a result of increased hysteresis. This possibly explains why 45 minutes of recovery time was needed between the iterations for Relax Easy. Due to mentioned characteristics of Gel ovals pad and Relax Easy, the products are not preferred for absorbing instant vibrations but rather for shocks, which usually are less immediate.

The intention of combining different fabrics is to create a spring-damper characteristic, including elastic and a viscous material. However, combinations of materials provide did not reduce the drive. However, this only refers to combinations of different material types and merging of PUR foams are excluded from this. It is difficult to conclude why tests including material combinations yield poorer results. One aspect can be that the connections harm the sole properties of each material. Hence it would be interesting to further analyze how vibration characteristics of PUR foam alter, if coir fibers or waste rubber particles are added to the instillation during foam manufacturing. Hypothetically, when fibers are dispersed in the cell walls, the dampening properties of the foam develop, as hysteresis increases.

In addition, it has also been carried out how alternations in seat back angle affect the exposure. Tilting the back rest from $20^\circ - 40^\circ$ shows decrease in the $A(8)$ value, as the angle grows. This is most likely an affect of reduction in mass supported on the seat cushion, as the back support is angled. This is analogous to reducing the mass in the single degree of freedom model that is presented in Figure 1. Furthermore, changing the back support angle does not only result in altered driver occupant posture but also varied mechanical properties of the seat. This should be taken into consideration since applied load and the contact area, between driver and seat affects the dynamic stiffness of the seat cushion.

Uncertainties regarding how mechanical properties affect the transmission of vibration are raised. Added hardness is said to reduce transmissibility at resonance, which can possibly be explained by the fact that less bounce is generated as hardness increases. On the other hand, it is found that higher density is an advantage when resonance occurs. An increase in density seems to lead to that attenuation of the oscillation is quicker after the amplification (Zhang, 2014). Comparing results for 50 mm Reference, 50 mm Regufoam and 50 mm Sylomer presented in the same chart, can provide additional conclusions regarding which mechanical properties that are favorable when WBV reduction is desired. The table shows that lowest resonance and isolation frequency are obtained for the reference foam. From this judgment and considering Table 6, it is concluded that lower density and hardness are wishful. However results from TEST 1, which are presented in Table 9, do not agree with this. The table shows that greater drive time is achieved using the other two foams. A potential motive can be that, since the loads from the hexapod in TEST 1 are greater than the forces given in TEST 2, the dynamic load range of the Reference material is

surpassed. However, additional studies and material data for every product must be provided in order to make reliable conclusions.

Thicker foams appear to increase the A(8) values. Table 13 shows that maximum drive time is obtained when a thickness of 148 mm foam is tested. Data presented in Appendix A5, show that diverse load-deflection characteristics are obtained depending on thickness. An explanation can be that thicker foams behave as being less stiff, which allows the material to compress more during loading and thus more energy can be stored. However, even if a continuous grow in drive time with increased foam thickness is seen, results from TEST 1 show that the rate is highest for thicknesses up to approximately 80 mm. Table 13 does also show that different results for the same configuration are obtained depending on which order the blocks are stacked. However, this is probably an effect of the materials still being in recovery mode, rather than the arrangement. This statement is also enhanced by the fact that a decrease in A(8) value is seen for the second iteration, in all configurations that include material order changes.

Even though implementing thicker foams in seat cushions seem to be promising, some limiting aspects must be discussed. One of the main issues is the restricted cab space. As it has been mentioned, adding material on top of the current cushion disfavors the drivers. An optional solution is to add more foam towards the cab floor. Let's assume that desired foam thickness is 148 mm. Consequently, this would imply removal and repositioning of some components that are found in or under the seat. The most important ones include the electric length adjuster, cables and the seat frame springs mentioned in Chapter 3.1. Since this thesis work is aimed to solve an internal problem for VCG, not all regulations need to be considered. Internal in this sentence refers to the fact that the solution will not be implemented in cars, which are currently sold on the market. A mechanical adjuster can easily replace the electric length adjuster. The bended shape of the seat frame springs when installed, reminds of a hammock. Since the foam is placed on the springs, increasing the bend of the springs will allow more foam to be put between the driver and the springs. This can be done without reducing the distance between the driver's head and the cab roof. However, since the spring depth is increased, the distance to the floor needs to be reflected. In Chapter 3.1, it is also mentioned that the current vertical distance between lowest point on the springs and the floor is 135 mm. As it is mentioned in Chapter 3.2, the current foam thickness measures 86 mm. The increase in thickness from 86 mm to 148 mm, is equivalent to 49 mm, which means that there is 86 mm to spare. It is also desired that this solution is applicable in all car models. Removing the 40 mm seat raiser reduces the number to 46 mm. This is still within the limits. However, static deflection and dynamic displacements of the seat is yet not taken into account. Another point to mention is that vibration reduction thanks to increased foam thickness is in this study evident while temperature is constant. TEST 1 and TEST 2 are performed in two different laboratory rooms. The temperature in these rooms were fluctuating between 20 – 23°C. The temperature in a vehicle can alter between –30 – 80°C, depending on weather conditions. This diversity in temperature may therefore have an influence on foam performance. However, this is most likely an issue only in the initial state of the complete vehicle testing, as the temperature condition in the car stabilizes during driving.

Lastly, results presented in Table 29 show that, while operating with Star Starlock as an additive pad on the seat, the drive time is improved compared to no pad. The figures are similar than those obtained for the current foam pad, but the height is reduced. The advantage of using Star Starlock as an optional product enables individual mass tuning. Therefore, the product can perform equally regardless driver mass. On the contrary, the PUR foam's ability to isolate oscillations is partly dependent on static and dynamic deflection.

6.2 SOURCES OF ERROR

The results gained in TEST 1 should be critically used due to several simplifications. The experiments exclude many essential factors, amongst material shape, covering trim, attachment to the seat, usage of manikin instead of human etc. Properly molded foam may show different dynamic characteristic. In addition, cover trims made of various fabrics have probably an impact on the results, as the area of which the foam can deform is limited. Furthermore, laying blocks of foam directly on the seat frame springs may affect the outcomes. Additionally, it is not evident that stacking layers of blocks to increase the thickness yield same performance as having one piece of equal height. Hence, material properties can be harmed due to internal friction and change in natural frequency. The experiments in TEST 2 involve recovery time between the iterations, which is especially important for the viscoelastic materials. This is however not applied in TEST 1 and since same material or material combination are tested continuously, the results are most likely not definite. Furthermore, conclusions regarding possible health risks cannot be taken. Using a manikin does not provide the same body response due to internal damping and other biomechanical fundamentals. In contrast to TEST 2, each experiment is only made once in TEST 1. Therefore, the results may not be conservative.

The methodology applied in TEST 2 has never been investigated before. Hence, the reliability in results is not confirmed. The usual test setup involves testing of a complete seat. The MAX and MIN requirements are therefore derived for the original experiment.

6.3 WBV EXPOSURE

The importance of protecting the employee from being exposed to WBV cannot be stressed enough. It has been confirmed that extensive transmission of WBV can develop LBP and permanent deformities of the spinal column. Chapter 2.4.1 presents health status reviews among 72 test drivers. The study shows that LBP experience among the operators has increased from 45/81 (56 %) in 2010 – 2011 to 49/72 (68 %) in 2014 – 2015. Statistics performed on the Swedish population in 2014 – 2015 verify that 33.9 % (± 2.3 %) in ages 35 – 44 experience back pain, while 36.1 % (± 2.3 %) confirmed pain in shoulders and neck (Statistiska Centralbyrån, 2014). From this, it can be concluded that the prevalence is greater among the employees at HPG. Thus, complete vehicle testing most likely has a negative affect on presented figures. However, a fact that should be added to this discussion is the employment

time as test driver at HPG. The latest health examination from 2014 – 2015 confirmed that, even though 10/72 (14 %) participants have been employed for three or less years, LBP among these drivers is co-occurrence. Based on the fact that VCG has introduced an action plan for reducing WBV since 2006, earlier work experience should be taken into consideration. In Chapter 2.4, different factors for developing LBP are introduced. However, even if there are doubts about whether experienced back pain among the drivers is an affect of WBV or not, Table 2 confirms that the disturbing frequencies and the natural frequencies in studied body parts coincide.

7 CONCLUSION

The objective of this thesis work is to suggest a solution for reducing WBV transmitted to operating drivers performing complete vehicle testing at HPG. Evident results from practical tests confirm that there is dependency seen between increased foam thickness and extended drive time before the daily exposure values are reached. Increased foam thickness appears to reduce the frequency at which resonance occurs, but yields higher transmissibility. New implementations are commonly a trade-off between economy and results. In this case, also the health aspects must be accounted for. From TEST 1, increasing the foam thickness to 148 mm increases the drive time from 20 minutes to 29 minutes, which is an improvement of 45 %. This is compared to results gained for Reference. Average results from complete vehicle testing at HPG shows that the daily exposure action value is achieved after 87 min, if the additive foam pad is not used. Assuming that one cycle takes 30 minutes to complete, it gives 2.9 cycles. Corresponding calculation, declare that 4.2 cycles can be performed with 148 mm foam.

Raise in foam thickness appear to be superior to changes in mechanical properties, as density and or hardness. However, this conclusion is fairly doubtful and not fully confirmed. Thus, further studies are required. Materials indicating viscous characteristic seem to be less suitable to be applied in environments, where frequencies in ranges 2 – 20 Hz happen. This is based on practical experiments, showing that material recovery time due to hysteresis is too long.

Even though a link between WBV and LBP is confirmed, many other aspects must be examined as well. These factors include previous work conditions, overall health status, age etc. but also the fact that the human body is a unique creation and persistency to WBV varies importantly among individuals.

8 FUTURE WORK

With the intention of confirming the accuracy of obtained results, additional tests must be completed. Most importantly, a replication of TEST 1 and TEST 2 including molded PUR foam, to verify whether exposure is reduced with increased foam thickness or not. In addition, TEST 2 should be performed according to original setup, i.e. complete seat tested and not only foam.

Even though improvements on WBV reduction are presented, complete removal of vibrations transmitted to the body is hardly achieved in terms of passive means. This is based on the fact that no isolating material, suitable for this type of application has been found. Something that has not been mentioned yet is a possible solution that involves change in how the seat frame is attached to the chassis floor. The idea is to add spring-damper arrangement between the seat frame and the chassis instead of having it rigidly bolted. However, all possible springs that were studied during this solution were not low enough in natural frequency and thus not suitable.

Further investigations on active damping are needed. From TEST 2 various damping ratios are generated. Applying this ratio in Equation (5) can derive values for stiffness and viscous damping. In addition, considering the quarter car model that is introduced in Chapter 2.6, a model for active damping can be created using state-space model.

In contemporary engineering, the development of autonomous cars is highly ranked. Its potential for reducing WBV is discussable also here. For instance, Belgian Pave is a perfect example of an obstacle, which can be driven autonomously. Thus, there will be no vibration transmitted to a human. In addition, it will also be a common goal towards Vision 2020.

BIBLIOGRAPHY

Council Directive 2002/44/EC of 22 June on the minimum health and safety requirements regarding the exposure of workers to the risks arising from physical agents (vibration).

Adient, (2016). *Johnson Controls contributes to maximum seating comfort in 'Truck of the Year' Volvo XC90*, [online] Available at: <<http://www.adient.com/media/image-galleries>> [Accessed 2 June 2017].

Arbetsmiljöverket, (2005). *Vibrationer (AFS 2005:15) föreskrifter*. Stockholm: Arbetsmiljöverket.

Albin, M. and Bohgard, M., (2015). *Arbete och teknik på människans villkor*. Stockholm: Prevent.

Andersson, G.B., (1981). Epidemiologic aspects on low-back pain in industry. *Spine (Phila Pa 1976)*, 6(1).

Barry Controls, (1999). Engineered Solutions for Controlling, Shock, Vibration & Noise. [online] Available at: <http://vibrona.ru/upload/BARRY_CONTROLS.pdf> [Accessed 5 March 2017].

Biering-Sørensen, F., Hansen, F., Schroll, M. and Runeborg, O., (1985). The relation of spinal x-ray to low-back pain and physical activity among 60-year-old men and women. *Spine (Phila Pa 1976)*, 10(5).

Bressler, H.B., Keyes, W.J., Rochon, P.A. and Badley, E., (1999). The Prevalence of Low Back Pain in the Elderly. *Spine (Phila Pa 1976)*, 24(17).

Christian Berner, (2017). Sylomer SR11 EN, [online] Available at: <[http://christianberner.se/\\$-1/file/sylomer-product-datasheet-sr-11.pdf](http://christianberner.se/$-1/file/sylomer-product-datasheet-sr-11.pdf)> [Accessed 6 March 2017]

Curry, B.D., Bain, J.L., Yan, J.G., Zhang, L.L., Yamaguchi, M., Matloub, H.S. and Riley, D.A., (2002). Vibration injury damages arterial endothelial cells. *Muscle Nerve*, 25(4).

German National Standard, (1990). *DIN 53513 Determination of the viscoelastic properties of elastomers on exposure to forced vibration at non-resonant frequencies*. Berlin: DIN.

Dowds, P. and Dwyer, A.O., (2005). *Modelling and control of a suspension system for vehicle applications. Proceedings of the 4th Wismarer Automatisierungssymposium*. Wismar, Germany, 22-23 Sept 2005. Dublin. Ireland.

Eklundh, U., (2015b). *Slutrapport 2014/2015 års medicinska kontroll av helkroppsvibrationer på testförare*. Hällered: Volvo Car Group.

Govindaraju, S.R., Curry, B.D., Bain, J.L. and Riley, D.A., (2006). Comparison of continuous and intermittent vibration effects on rat-tail artery and nerve. *Muscle Nerve*, 34(2).

Grahn, R. and Jansson, P.-Å., (1997). *Mekanik*. 2nd ed. Lund: Studentlitteratur AB.

Hansen, A., Hopperstad, O., Langseth, M. and Ilstad, H., (2002). Validation of constitutive models applicable to aluminium foams. *International Journal of Mechanical Sciences*, 44(2).

Hägglund, C. and Danielsson, A., (2015). *Vibration Insulation, front seat cushion*. Gothenburg: Volvo Car Group.

International Organization for Standardization, (1997). *ISO 2631-1:1997 Mechanical vibration and shock -- Evaluation of human exposure to whole-body vibration -- Part 1: General requirements*. Geneva: ISO.

International Organization for Standardization, (2011). *ISO 6721-1:2011 Plastics -- Determination of dynamic mechanical properties -- Part 1: General principles*. Geneva: ISO.

International Organization for Standardization, (2005). *ISO 8041:2005 Human response to vibration -- Measuring instrumentation*. Geneva: ISO.

Klooster, S.J., (2004). *Vibration Suppression and Safety Seat Motion Design of a Hyper-Active Seat*. MSc. Georgia Institute of Technology.

Maeda, S. and Mansfield, N., (2005). Comparison of the apparent mass during exposure to whole-body vertical vibration between Japanese subjects and ISO 5982 standard. *Industrial Health*, 43(3).

Magnusson, S., (2015). *Dynor som hjälpmedel för reducering av helkroppsvibrationer*. Hällered: Volvo Car Corporation.

Makhsous, M., Hendrix, R., Crowther, Z., Nam, E. and Lin, F., (2005). Reducing whole-body vibration and musculoskeletal injury with a new car seat design. *Ergonomics*, 48(9).

Mansfield, N., (2005). Impedance methods (apparent mass, driving point mechanical impedance and absorbed power) for assessment of the biomechanical response of the seated person to whole-body vibration. *Ind Health*, 43(3).

Mellin, G., (1987). Correlations of spinal mobility with degree of chronic low back pain after correction for age and anthropometric factors. *Spine (Phila Pa 1976)*, 12(5).

Nandini, V.V., Venkatesh, K.V. and Nair, K.C., (2008). Basic Elasticity and Viscoelasticity. *Journal of conservative dentistry*, 11(1).

Noren, R., Trafimow, J., Andersson, G. and Huckman, M., (1991). The role of facet joint tropism and facet angle in disc degeneration. *Spine (Phila pa 1976)*, 16(5).

Panjabi, M.M., (1992). The stabilizing system of the spine. Part I. Function, dysfunction, adaptation, and enhancement. *J Spinal Disord*, 5(4).

Papagiannopoulos, G.A. and Hatzigeorgiou, G.D., (2011). On the use of the half-power bandwidth method to estimate damping in building structures. *Soil Dynamics and Earthquake Engineering*, 31(7).

Patten, W.N., Sha, S. and Mo, C., (1998). a Vibrational Model of Open Celled Polyurethane Foam Automotive Seat Cushions. *Journal of Sound and Vibration*, 217(1).

Pauschke, J.M. and Krishnamurty, S., (1985). *PEAK VS. ROOT-MEAN-SQUARE (RMS) ACCELERATION AS A RESPONSE PARAMETER*, [online] Available at: <http://www.iitk.ac.in/nicee/wcee/article/8_vol4_45.pdf> [Accessed 14 April 2017].

Rasa, A., (2014). *Applying dynamic mechanical analysis to research & development for viscoelastic damping materials, Internoise 2014*. Melbourne, Australia, 16-19 November 2014.

Rubin, D., (2007). Epidemiology and risk factors for spine pain. *Neurol Clin*, 25(2).

Salubrious AB, (2016). Gel Oventions, [online] Available at: <<http://www.salubrious.se/sv/component/virtuemart/alla-produkter/gel-ovations-detail?Itemid=0>> [Accessed 16 April 2017].

Salubrious AB, (2016). Relax Easy, [online] Available at: <<http://www.salubrious.se/sv/component/virtuemart/alla-produkter/relax-easy-detail?Itemid=0>> [Accessed 16 April 2017].

Salubrious AB, (2016). Star Starlock, [online] Available at: <<http://www.salubrious.se/sv/component/virtuemart/rehab/star-starlock-detail?Itemid=0>> [Accessed 16 April 2017].

Sharma, A. and Peel, L., (2004). *Vibration damping of flexible and rigid polyurethane composites, SAMPE 2004*. Long Beach, California, May 2004.

Siddha Y, U. and Kumbhar B, S., (2013). *Natural Frequency Analysis of Automotive Seating System by using FEM Software*, [online] Available at: <http://www.academia.edu/15316458/Natural_Frequency_Analysis_of_Automotive_Seating_System_by_using_FEM_Software> [Accessed 23 April 2017].

Slota, G.P., (2008). *Effects of Seated Whole-Body Vibration on Spinal Stability Control*. Ph. D. Virginia Polytechnic Institute and State University.

Statistiska Centralbyrån, (2014). *Undersökningarna av levnadsförhållanden (ULF/SILC)*, [online] Available at: <http://www.sverigeisiffror.scb.se/contentassets/9608d268fa9c40178e30131f03776b76/halsa_tabell_2014-2015.xlsx> [Accessed 24 May 2017].

Trelleborg Elastomer Laminates, (2015). *Butyl rubber sheeting - IIR*, [online] Available at: <<http://www.trelleborg.com/en/Elastomer-Laminates/Rubber-Sheeting/Butyl/>> [Accessed 2 May 2017].

Vibratec® akustikprodukter, (2014). *Regufoam® Vibration 150 Plus*, [online] Available at: <<http://en.vibratec.se/wp-content/uploads/sites/6/2016/02/regufoam-vibration-150-plus.pdf>> [Accessed 1 May 2017].

Volvo Car Group, (2012). *VPT-TEST, FULL VEHICLE ENDURANCE*. Hällered: Volvo Car Group.

Volvo Car Group, (2016). *Master mätningar*. Hällered: Volvo Car Group.

Webb, R., Brammah, T., Lunt, M., Urwin, M., Allison, T. and Symmons, D., (2003). Prevalence and predictors of intense, chronic, and disabling neck and back pain in the UK general population. *Spine (Phila Pa 1976)*, 28(11).

Wilder, D.G., Pope, M.H. and Frymoyer, J.W., (1988). The biomechanics of lumbar disc herniation and the effect of overload and instability. *J Spinal Disord*, 1(1).

Zhang, X., (2014). *MEASUREMENT AND MODELLING OF SEATING DYNAMICS TO PREDICT SEAT TRANSMISSIBILITY*. Ph. D. University of Southampton.

Özkaya, N., Leger, D., Goldsheyder, D. and Nordin, M., (1991). *Mechanical Properties of Biological Tissues*, [online] Available at: <<http://courses.washington.edu/bioen520/notes/Viscoelasticity.pdf>> [Accessed 29 March 2019].

APPENDIX

A1 – From RMS to peak acceleration

$$a_{RMS} = \sqrt{\frac{1}{T} \int_0^T a(t)^2 dt} \quad (1)$$

The time dependent sine wave is given by

$$a(t) = A \sin(\omega t) \quad (2)$$

(2) \rightarrow (1) and the RMS value squared gives

$$a_{RMS}^2 = \frac{1}{T} \int_0^T x(t)^2 dt = \frac{A^2}{T} \int_0^T [\sin(\omega t)]^2 dt \quad (3)$$

From trigonometry, it is known that

$$[\sin(\omega t)]^2 = \frac{1}{2} - \frac{\cos(2\omega t)}{2} \quad (4)$$

Hence (3) can now be written as

$$a_{RMS}^2 = \frac{1}{T} \int_0^T \frac{A^2}{2} (1 - \cos(2\omega t)) dt \quad (5)$$

$$a_{RMS}^2 = \frac{A^2}{2T} \left[t - \frac{\sin(2\omega t)}{2\omega} \right]_0^T$$

$$a_{RMS}^2 = \frac{A^2}{2T} \left[T - \frac{\sin(2\omega T)}{2\omega} \right]$$

$$a_{RMS} = \sqrt{\frac{A^2}{2} - \frac{A^2 \sin(2\omega T)}{4\omega T}} \quad (6)$$

As $T \rightarrow \infty$, the oscillatory term given by equation (6) goes towards zero. Hence following relation is obtained

$$a_{RMS} = \frac{a_{peak}}{\sqrt{2}} \quad (7)$$

A2 – Frequency based weighting factors W_d and W_k

Frequency [Hz]	W_d (x- and y-directions) [dB]	W_k (z-direction) [dB]
2	0.890	0.531
2.5	0.776	0.631
3.15	0.642	0.804
4	0.512	0.967
5	0.409	1.039
6.3	0.323	1.054
8	0.253	1.036
10	0.212	0.988
12.5	0.161	0.902
16	0.125	0.768
20	0.100	0.636

The table presents frequency based weighing factors in dB (Albin and Bohgard, 2015).

A3 – A(8) calculation example

Assume that following frequencies were obtained from measured data:

$$f_1 = 2 \text{ Hz}, f_2 = 3.15 \text{ Hz}$$

The frequency-weighted accelerations are calculated from table data given in Appendix A2 (z-direction). Equation (9) now gives:

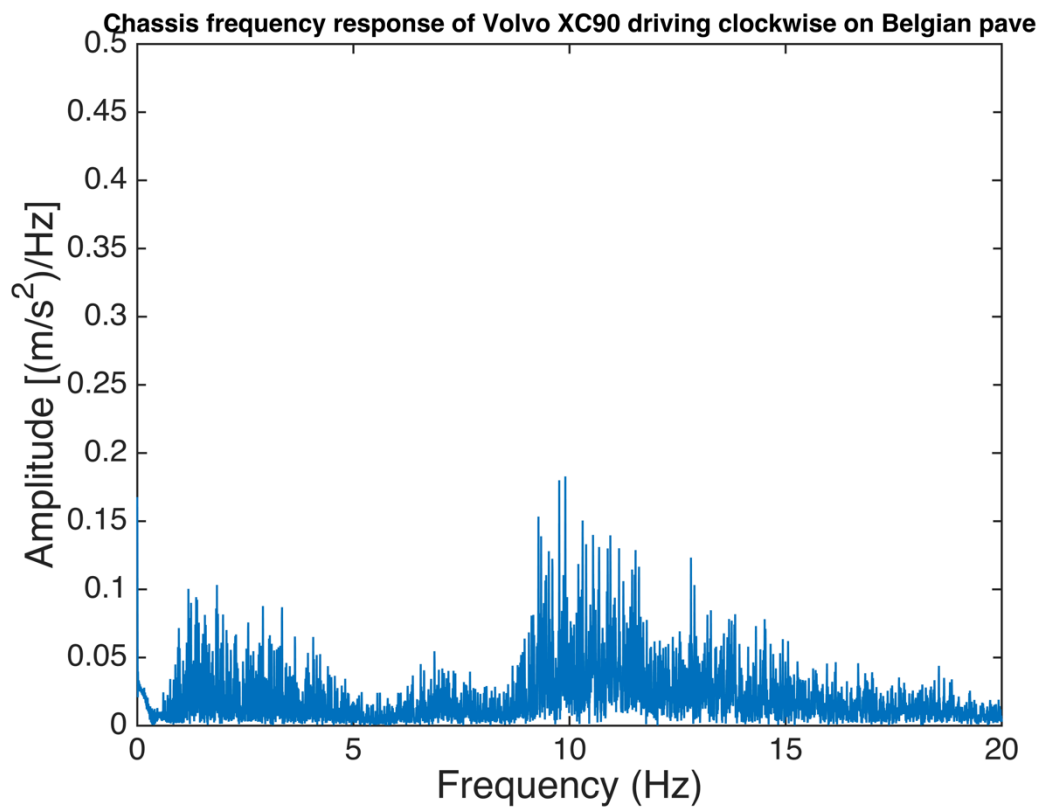
$$a_{wz} = \sqrt{2 \cdot 0.531 + 3.15 \cdot 0.804} = 1.896 \text{ m/s}^2$$

The A(8) value is thereafter calculated by applying Equation (11). Assume $T = 2$

$$A_z(8) = 1.896 \sqrt{\frac{2}{8}} = 0.948 \text{ m/s}^2$$

As it can be seen from Table 1, the value exceeds the daily exposure action value.

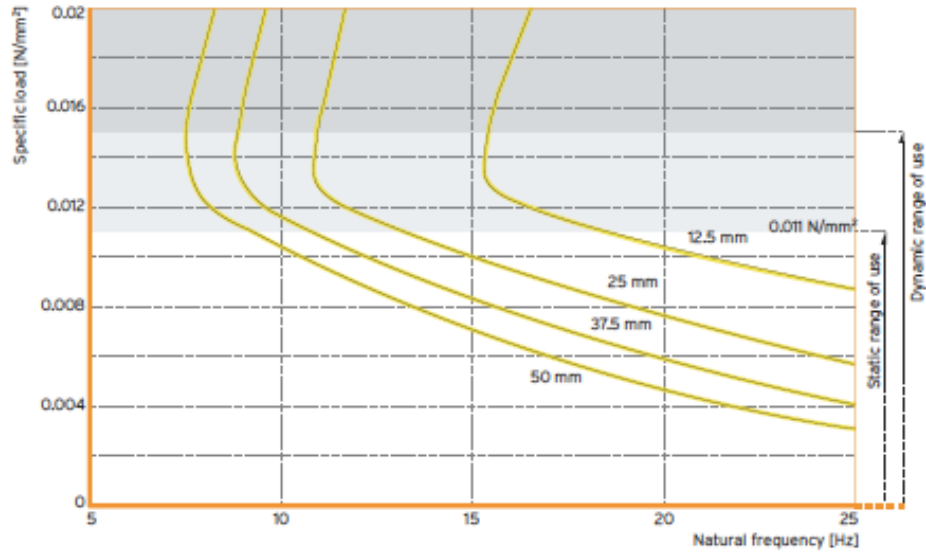
A4 – FFT on chassis response while driving on Belgian pave (clockwise)



A5 – Material data Sylomer SR11 EN and Regufoam Vibration 150 Plus

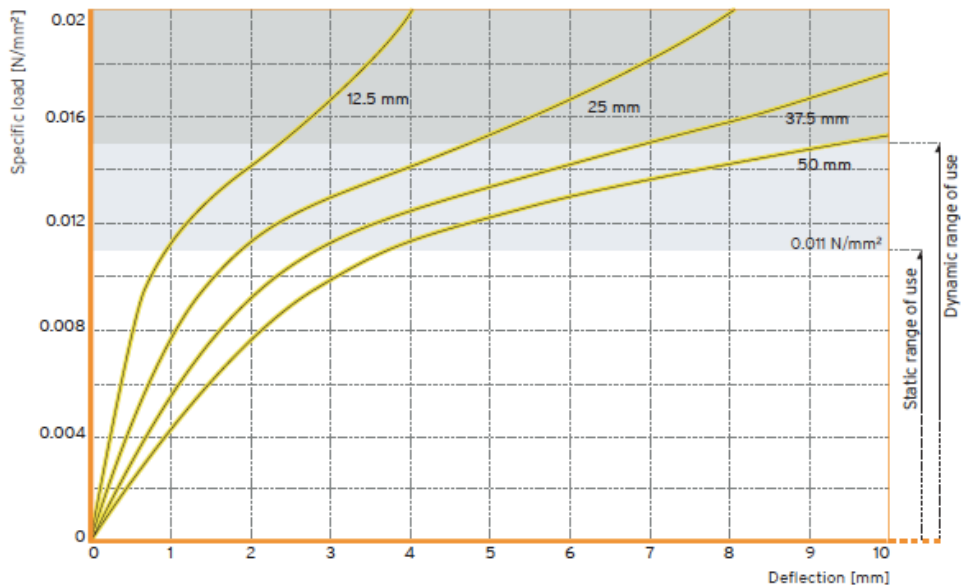
Sylomer SR11 EN

Natural frequency



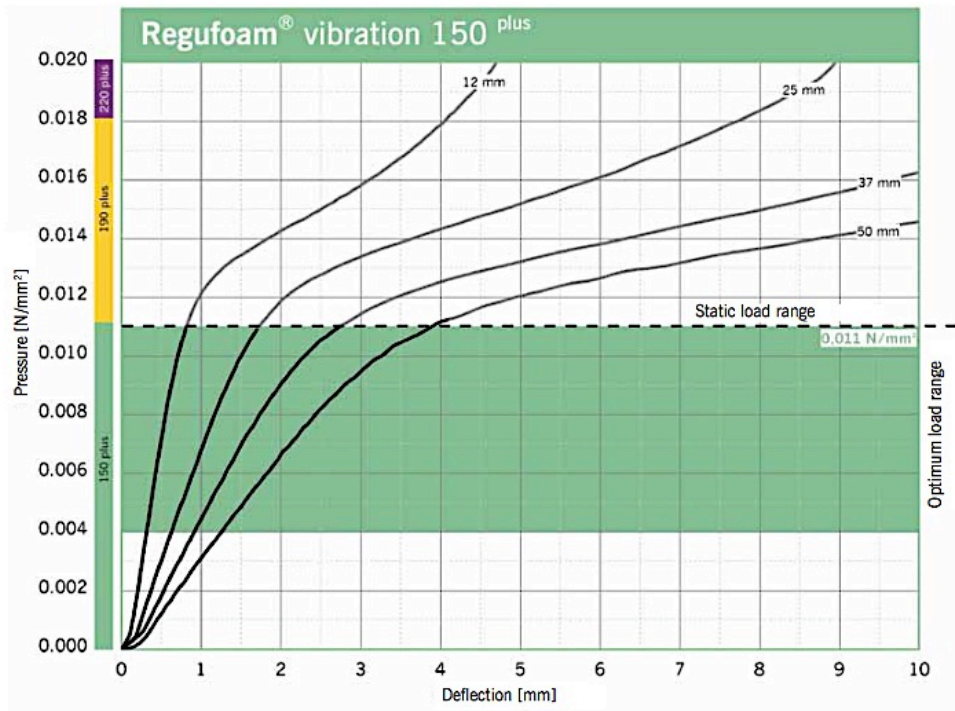
Load-deflection curve as a function of thickness (Christian Berner, 2017)

Load deflection curve

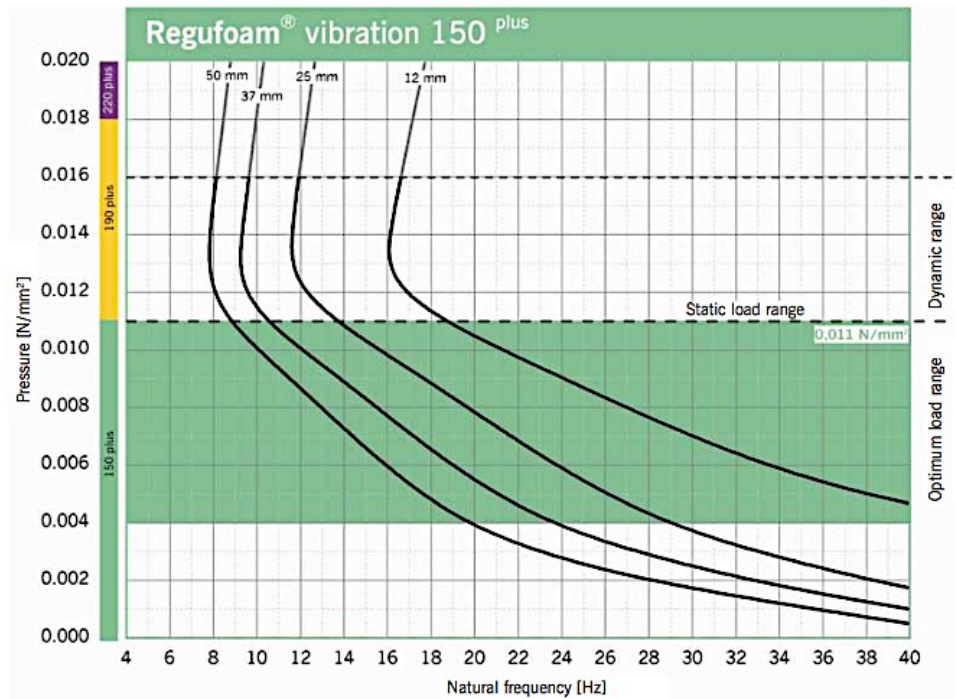


Change in natural frequency as a function of thickness and load (Christian Berner, 2017)

Regufoam® Vibration 150 Plus

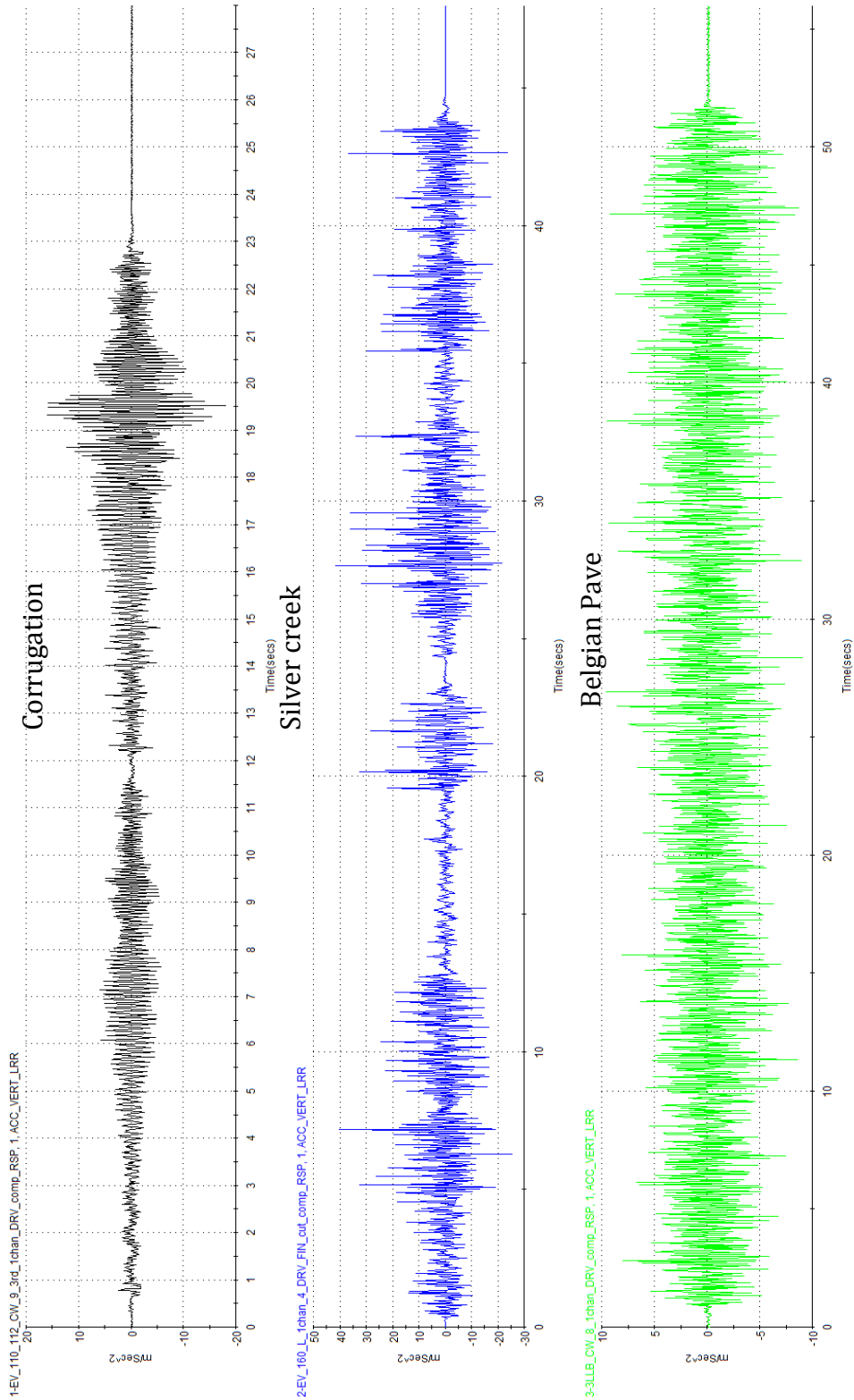


Load-deflection curve as a function of thickness (Vibratec® akustikprodukter, 2014)



Change in natural frequency as a function of thickness and load (Vibratec® akustikprodukter, 2014)

A5 – Input signals for Corrugation, Silver creek and Belgian pave, which are used during TEST 1



A6 – Test plan and results from TEST 1 and TEST 3

Equipment	Load case	Material	Thickness	Seat back support angle	Z _{a_w} m/s ²	A8 _{action} (min)	A8 _{lim} (min)
Hexapod	Manikin	Reference V526	37,5mm	20 degrees from vertical plane	2,689	16	87
Hexapod	Manikin	Reference V526	50mm	20 degrees from vertical plane	2,982	13	71
Hexapod	Manikin	Reference V526	86mm	20 degrees from vertical plane	2,435	20	106
Hexapod	Manikin	Sylomer SR11 EN	12,5mm	20 degrees from vertical plane	2,59	17	94
Hexapod	Manikin	Sylomer SR11 EN	25mm	20 degrees from vertical plane	2,588	17	94
Hexapod	Manikin	Sylomer SR11 EN	37,5mm	20 degrees from vertical plane	2,28	23	122
Hexapod	Manikin	Sylomer SR11 EN	50mm	20 degrees from vertical plane	2,242	23	126
Hexapod	Manikin	Regufoam Vibration 150 Plus	12mm	20 degrees from vertical plane	2,843	14	78
Hexapod	Manikin	Regufoam Vibration 150 Plus	24mm	20 degrees from vertical plane	2,637	17	91
Hexapod	Manikin	Regufoam Vibration 150 Plus	36mm	20 degrees from vertical plane	2,386	21	111
Hexapod	Manikin	Regufoam Vibration 150 Plus	50mm	20 degrees from vertical plane	2,317	22	118
Hexapod	Manikin	Regufoam Vibration 150 Plus	86mm	20 degrees from vertical plane	2,097	27	143
Hexapod	Manikin	Regufoam Vibration 150 Plus	98mm	20 degrees from vertical plane	2,108	27	142
Hexapod	Manikin	Reference V526 + Salubrious Gel pad Gel Ovations	37,5mm + 13mm	20 degrees from vertical plane	2,802	15	80
Hexapod	Manikin	Reference V526 + Salubrious Gel pad Gel Ovations	50mm + 13mm	20 degrees from vertical plane	2,609	17	92
Hexapod	Manikin	Sylomer SR11 EN + Salubrious Gel pad Gel Ovations	12,5mm + 13mm	20 degrees from vertical plane	2,664	16	89
Hexapod	Manikin	Sylomer SR11 EN + Salubrious Gel pad Gel Ovations	25mm + 13mm	20 degrees from vertical plane	2,74	15	84
Hexapod	Manikin	Sylomer SR11 EN + Salubrious Gel pad Gel Ovations	37,5mm + 13mm	20 degrees from vertical plane	2,471	19	103
Hexapod	Manikin	Sylomer SR11 EN + Salubrious Gel pad Gel Ovations	50mm + 13mm	20 degrees from vertical plane	2,36	21	113
Hexapod	Manikin	Regufoam Vibration 150 Plus + Salubrious Gel pad Gel Ovations	12mm + 13mm	20 degrees from vertical plane	2,791	15	81
Hexapod	Manikin	Regufoam Vibration 150 Plus + Salubrious Gel pad Gel Ovations	24mm + 13mm	20 degrees from vertical plane	2,64	17	91
Hexapod	Manikin	Regufoam Vibration 150 Plus + Salubrious Gel pad Gel Ovations	36mm + 13mm	20 degrees from vertical plane	2,638	17	91
Hexapod	Manikin	Regufoam Vibration 150 Plus + Salubrious Gel pad Gel Ovations	50mm + 13mm	20 degrees from vertical plane	2,322	22	117
Hexapod	Manikin	Regufoam Vibration 150 Plus + Salubrious Gel pad Gel Ovations	98mm + 13mm	20 degrees from vertical plane	2,285	22	121
Hexapod	Manikin	Salubrious Relax Easy	60mm	20 degrees from vertical plane	2,534	18	98
Hexapod	Manikin	Salubrious Star Starlock	50mm	20 degrees from vertical plane	2,084	27	146
Hexapod	Manikin	Trelleborg natural rubber	5mm	20 degrees from vertical plane	3,102	12	65
Hexapod	Manikin	Trelleborg natural rubber	10mm	20 degrees from vertical plane	3,113	12	65
Hexapod	Manikin	Trelleborg natural rubber	15mm	20 degrees from vertical plane	3,186	11	62
Hexapod	Manikin	Trelleborg natural rubber + Sylomer 11 SR EN	5mm + 12,5mm	20 degrees from vertical plane	2,911	14	74
Hexapod	Manikin	Trelleborg natural rubber + Sylomer 11 SR EN	5mm + 25mm	20 degrees from vertical plane	2,577	18	95
Hexapod	Manikin	Trelleborg natural rubber + Sylomer 11 SR EN	5mm + 37,5mm	20 degrees from vertical plane	2,508	19	100
Hexapod	Manikin	Trelleborg natural rubber + Sylomer 11 SR EN	5mm + 50mm	20 degrees from vertical plane	2,214	24	129
Hexapod	Manikin	Trelleborg natural rubber + Sylomer 11 SR EN	10mm + 12,5mm	20 degrees from vertical plane	2,834	14	79
Hexapod	Manikin	Trelleborg natural rubber + Sylomer 11 SR EN	10mm + 25mm	20 degrees from vertical plane	2,571	15	83
Hexapod	Manikin	Trelleborg natural rubber + Sylomer 11 SR EN	10mm + 37,5mm	20 degrees from vertical plane	2,529	18	99
Hexapod	Manikin	Trelleborg natural rubber + Sylomer 11 SR EN	10mm + 50mm	20 degrees from vertical plane	2,358	21	114
Hexapod	Manikin	Trelleborg natural rubber + Sylomer 11 SR EN	15mm + 12,5mm	20 degrees from vertical plane	3,109	12	65
Hexapod	Manikin	Trelleborg natural rubber + Sylomer 11 SR EN	15mm + 25mm	20 degrees from vertical plane	2,723	16	85
Hexapod	Manikin	Trelleborg natural rubber + Sylomer 11 SR EN	15mm + 37,5mm	20 degrees from vertical plane	2,636	17	91
Hexapod	Manikin	Trelleborg natural rubber + Sylomer 11 SR EN	15mm + 50mm	20 degrees from vertical plane	2,636	17	91
Hexapod	Manikin	Trelleborg natural rubber + Regufoam Vibration 150 plus	5mm + 12mm	20 degrees from vertical plane	3,092	12	66
Hexapod	Manikin	Trelleborg natural rubber + Regufoam Vibration 150 plus	5mm + 24mm	20 degrees from vertical plane	2,927	14	74
Hexapod	Manikin	Trelleborg natural rubber + Regufoam Vibration 150 plus	5mm + 36mm	20 degrees from vertical plane	2,683	16	88
Hexapod	Manikin	Trelleborg natural rubber + Regufoam Vibration 150 plus	5mm + 50mm	20 degrees from vertical plane	2,411	20	109
Hexapod	Manikin	Trelleborg natural rubber + Regufoam Vibration 150 plus	5mm + 98mm	20 degrees from vertical plane	2,318	22	118
Hexapod	Manikin	Trelleborg natural rubber + Regufoam Vibration 150 plus	10mm + 12mm	20 degrees from vertical plane	3,218	11	61
Hexapod	Manikin	Trelleborg natural rubber + Regufoam Vibration 150 plus	10mm + 24mm	20 degrees from vertical plane	3,002	13	70
Hexapod	Manikin	Trelleborg natural rubber + Regufoam Vibration 150 plus	10mm + 36mm	20 degrees from vertical plane	2,566	18	96
Hexapod	Manikin	Trelleborg natural rubber + Regufoam Vibration 150 plus	10mm + 50mm	20 degrees from vertical plane	2,577	18	95
Hexapod	Manikin	Trelleborg natural rubber + Regufoam Vibration 150 plus	10mm + 98mm	20 degrees from vertical plane	2,464	19	104
Hexapod	Manikin	Trelleborg natural rubber + Regufoam Vibration 150 plus	15mm + 12mm	20 degrees from vertical plane	3,256	11	59
Hexapod	Manikin	Trelleborg natural rubber + Regufoam Vibration 150 plus	15mm + 24mm	20 degrees from vertical plane	2,974	13	71
Hexapod	Manikin	Trelleborg natural rubber + Regufoam Vibration 150 plus	15mm + 36mm	20 degrees from vertical plane	2,741	15	84
Hexapod	Manikin	Trelleborg natural rubber + Regufoam Vibration 150 plus	15mm + 50mm	20 degrees from vertical plane	2,906	14	75
Hexapod	Manikin	Trelleborg natural rubber + Regufoam Vibration 150 plus	15mm + 98mm	20 degrees from vertical plane	2,666	16	89
Hexapod	Manikin	Trelleborg butyl rubber	5mm	20 degrees from vertical plane	3,333	10	57
Hexapod	Manikin	Trelleborg butyl rubber	10mm	20 degrees from vertical plane	3,161	12	63
Hexapod	Manikin	Trelleborg butyl rubber	15mm	20 degrees from vertical plane	3,424	10	54
Hexapod	Manikin	Trelleborg butyl rubber + Sylomer 11 SR EN	5mm + 12,5mm	20 degrees from vertical plane	3,214	11	61
Hexapod	Manikin	Trelleborg butyl rubber + Sylomer 11 SR EN	5mm + 25mm	20 degrees from vertical plane	3,075	12	67
Hexapod	Manikin	Trelleborg butyl rubber + Sylomer 11 SR EN	5mm + 37,5mm	20 degrees from vertical plane	2,884	14	76
Hexapod	Manikin	Trelleborg butyl rubber + Sylomer 11 SR EN	5mm + 50mm	20 degrees from vertical plane	2,728	16	85
Hexapod	Manikin	Trelleborg butyl rubber + Sylomer 11 SR EN	10mm + 12,5mm	20 degrees from vertical plane	3,035	13	68
Hexapod	Manikin	Trelleborg butyl rubber + Sylomer 11 SR EN	10mm + 25mm	20 degrees from vertical plane	3,11	12	65
Hexapod	Manikin	Trelleborg butyl rubber + Sylomer 11 SR EN	10mm + 37,5mm	20 degrees from vertical plane	2,529	18	99
Hexapod	Manikin	Trelleborg butyl rubber + Sylomer 11 SR EN	10mm + 50mm	20 degrees from vertical plane	2,787	15	81
Hexapod	Manikin	Trelleborg butyl rubber + Sylomer 11 SR EN	15mm + 12,5mm	20 degrees from vertical plane	3,107	12	65
Hexapod	Manikin	Trelleborg butyl rubber + Sylomer 11 SR EN	15mm + 25mm	20 degrees from vertical plane	3,138	12	64
Hexapod	Manikin	Trelleborg butyl rubber + Sylomer 11 SR EN	15mm + 37,5mm	20 degrees from vertical plane	2,951	13	72
Hexapod	Manikin	Trelleborg butyl rubber + Sylomer 11 SR EN	15mm + 50mm	20 degrees from vertical plane	2,902	14	75
Hexapod	Manikin	Trelleborg butyl rubber + Regufoam Vibration 150 plus	5mm + 12mm	20 degrees from vertical plane	3,096	12	66
Hexapod	Manikin	Trelleborg butyl rubber + Regufoam Vibration 150 plus	5mm + 24mm	20 degrees from vertical plane	3,194	11	62
Hexapod	Manikin	Trelleborg butyl rubber + Regufoam Vibration 150 plus	5mm + 36mm	20 degrees from vertical plane	2,872	14	76
Hexapod	Manikin	Trelleborg butyl rubber + Regufoam Vibration 150 plus	5mm + 50mm	20 degrees from vertical plane	2,673	16	88
Hexapod	Manikin	Trelleborg butyl rubber + Regufoam Vibration 150 plus	5mm + 98mm	20 degrees from vertical plane	2,707	16	86
Hexapod	Manikin	Trelleborg butyl rubber + Regufoam Vibration 150 plus	10mm + 12mm	20 degrees from vertical plane	3,052	12	68
Hexapod	Manikin	Trelleborg butyl rubber + Regufoam Vibration 150 plus	10mm + 24mm	20 degrees from vertical plane	2,991	13	70
Hexapod	Manikin	Trelleborg butyl rubber + Regufoam Vibration 150 plus	10mm + 36mm	20 degrees from vertical plane	2,539	18	98
Hexapod	Manikin	Trelleborg butyl rubber + Regufoam Vibration 150 plus	10mm + 50mm	20 degrees from vertical plane	2,621	17	92
Hexapod	Manikin	Trelleborg butyl rubber + Regufoam Vibration 150 plus	10mm + 98mm	20 degrees from vertical plane	2,714	16	86
Hexapod	Manikin	Trelleborg butyl rubber + Regufoam Vibration 150 plus	15mm + 12mm	20 degrees from vertical plane	2,699	16	87
Hexapod	Manikin	Trelleborg butyl rubber + Regufoam Vibration 150 plus	15mm + 24mm	20 degrees from vertical plane	3,224	11	61
Hexapod	Manikin	Trelleborg butyl rubber + Regufoam Vibration 150 plus	15mm + 36mm	20 degrees from vertical plane	2,662	16	89
Hexapod	Manikin	Trelleborg butyl rubber + Regufoam Vibration 150 plus	15mm + 50mm	20 degrees from vertical plane	2,552	18	97
Hexapod	Manikin	Trelleborg butyl rubber + Regufoam Vibration 150 plus	15mm + 98mm	20 degrees from vertical plane	2,532	18	99
Hexapod	Manikin	Regufoam Vibration 150 plus + Sylomer 11 SR EN	50mm + 37,5mm	20 degrees from vertical plane	2,224	24	127
Hexapod	Manikin	Regufoam Vibration 150 plus + Sylomer 11 SR EN	98mm + 50mm	20 degrees from vertical plane	2,064	28	149
Hexapod	Manikin	Regufoam Vibration 150 plus + Reference V526	98mm + 50mm	20 degrees from vertical plane	2	29	157
Hexapod	Manikin	Sylomer 11 SR EN + Regufoam Vibration 150 plus	50mm + 98mm	20 degrees from vertical plane	2,15	25	137

Hexapod	Manikin	Sylomer 11 SR EN + Salubrious Star Starlock	25mm + 50mm	20 degrees from vertical plane	2,44	20	106
Hexapod	Manikin	Sylomer 11 SR EN + Salubrious Star Starlock	37,5mm + 50mm	20 degrees from vertical plane	2,404	20	109
Hexapod	Manikin	Sylomer 11 SR EN + Salubrious Star Starlock	50mm + 50mm	20 degrees from vertical plane	2,45	20	105
Hexapod	Manikin	Sylomer 11 SR EN + Salubrious Gel pad Gel Ovations + Salubrious Star Starlock	12,5mm + 13mm + 50mm	20 degrees from vertical plane	2,228	24	127
Hexapod	Manikin	Sylomer 11 SR EN + Salubrious Gel pad Gel Ovations + Salubrious Star Starlock	25mm + 13mm + 50mm	20 degrees from vertical plane	2,3	22	119
Hexapod	Manikin	Sylomer 11 SR EN + Salubrious Gel pad Gel Ovations + Salubrious Star Starlock	37,5mm + 13mm + 50mm	20 degrees from vertical plane	2,479	19	103
Hexapod	Manikin	Sylomer 11 SR EN + Salubrious Gel pad Gel Ovations + Salubrious Star Starlock	50mm + 13mm + 50mm	20 degrees from vertical plane	2,263	23	124
Hexapod	Manikin	Reference V526 + Salubrious Star Starlock	37,5mm + 50mm	20 degrees from vertical plane	2,295	22	119
Hexapod	Manikin	Reference V526 + Salubrious Star Starlock	50mm + 50mm	20 degrees from vertical plane	2,192	24	131
Hexapod	Manikin	Reference V526 + Salubrious Gel pad Gel Ovations + Salubrious Star Starlock	37,5mm + 13mm + 50mm	20 degrees from vertical plane	2,262	23	123
Hexapod	Manikin	Reference V526 + Salubrious Gel pad Gel Ovations + Salubrious Star Starlock	50mm + 13mm + 50mm	20 degrees from vertical plane	2,125	26	139
Hexapod	Manikin	Sylomer 11 SR EN	50mm	30 degrees from vertical plane	2,665	16	89
Hexapod	Manikin	Sylomer 11 SR EN	50mm	40 degrees from vertical plane	2,587	14	77
Hexapod	Manikin	Sylomer 11 SR EN	50mm	10 degrees from vertical plane	2,697	16	87
Hällered	Test driver	Salubrious Star Starlock	50mm	20 degrees from vertical plane	2,229	24	127
Hällered	Test driver	Current extra pad	3x19mm	20 degrees from vertical plane	2,276	23	122
Hällered	Test driver	Salubrious Gel pad Gel Ovations	13mm	20 degrees from vertical plane	2,841	14	78
Hällered	Test driver	Referense without pad		20 degrees from vertical plane	2,718	16	85

For tests showing a combination of different materials, the order in which the materials are put is decided by the test name. For instance, test name "Sylomer SR11 EN + Regufoam Vibration 150 Plus" implies that Sylomer is placed first and Regufoam is placed second.

A7 – Hardware and software used during TEST 2

Hardware	Version
MTS four poster KSK2	Rig-441:1
Measurement computer	Dell Precision 390
Measuring equipment	IST 8800
Signal amplifiers	Dewe-30-16 / MR-588:1
Sensor accelerometers	Entran 10G

Software	Version
Rig control software 2	IST Project Manager 2.4.53 SP1
Analysis software	Matlab R2011b
Rig amplifier software	Dewesoft 7.1.1

Others	
Sample frequency	512 Hz
Filter	Butterworth, cutoff frequency 100 Hz, 6 poles